Title
Stem Cells in Tissue Regeneration and Diseases

Author
Huang, Wen-Chin

Publication Date
2016

Peer reviewed|Thesis/dissertation

Stem Cells in Tissue Regeneration and Diseases

by

Wen-Chin Huang

A dissertation submitted in partial satisfaction of the

requirements for the degree of

Joint Doctor of Philosophy
with the University of California, San Francisco

in

Bioengineering

in the

Graduate Division

of the

University of California, Berkeley

Committee in charge:

Professor Song Li, Chair
Professor Jeffrey C. Lotz
Professor John Ngai

Fall 2016

Abstract

Stem Cells in Tissue Regeneration and Diseases

by

Wen-Chin Huang

Joint Doctor of Philosophy
with the University of California, San Francisco

in Bioengineering

University of California, Berkeley

Professor Song Li, Chair

The thesis includes two parts: (1) the role of stem cells in nerve regeneration, and (2) the role of stem cells in the development of vascular diseases.

The use of stem cells has promising potential for the fields of tissue engineering and regenerative medicine, which relies on precise control of cell proliferation and differentiation by cellular, biochemical and biophysical cues. For cell therapy in tissue regenerative applications, the specific differentiation state of implanted cells must be optimized to control cell fate, viability, potency and safety *in vivo*. In this dissertation, we investigate the therapeutic effect of induced pluripotent stem cell-derived neural crest stem cells (iPSC-NCSCs) at various differentiation stages and mesenchymal progenitor cells (MPCs) on peripheral nerve regeneration. Transplantation of NCSCs has better outcomes of motor nerve recovery and muscle reinnervation by Schwann cell differentiation *in vivo* and paracrine signaling, whereas transplantation of MPCs fails to promote functional nerve regeneration. This study provides an insight into the selection of stem cells during tissue regeneration, and has broad impact on the strategic design of cell therapy for tissue engineering.

It is generally accepted that the phenotypical de-differentiation of smooth muscle cells (SMCs) has an important role in the development of vascular diseases. Here we identify a population of SOX10+ vascular stem cells (VSCs) that can be isolated from human blood vessel wall and are able to differentiate into cell types of neural lineages and mesenchymal lineages *in vitro*. SOX10+ cells can be identified in both normal and diseased blood vessels, and some of these cells are positive for osteogenic and adipogenic markers, suggesting that the differentiation of VSCs in blood vessel *in vivo* can contribute to vascular diseases. In addition, *in situ* polymerase chain reaction proximity ligation assay (ISPCR-PLA) shows that some of the SOX10+ cells are derived from SMCs. Further investigation of these cells will help us understand the mechanism of vascular pathogenesis and potential therapeutic target of vascular diseases.

The work in this dissertation demonstrates the important role of stem cells in tissue regeneration and diseases, which may lead to wide applications in stem cell biology, tissue engineering and regenerative medicine.

Table of Contents

Chapter 4: SOX10+ Cells Contribute to Vascular Diseases

Chapter 5: Conclusion

References

List of Figures

Chapter 1

Chapter 2

Chapter 3

Chapter 4

List of Tables

Chapter 4

Acknowledgments

First and foremost, I would like to thank my warm family, especially my lovely mom and older sister Vivian, for all of your support, love, encouragement and cheer at all times. I truly want to thank my mom for raising my sister and me, and teaching us with good education and positive attitude toward our lives. Next, I want to thank my older sister, Vivian, you always take care of me, share your treasure with me and set yourself as a good example. Without all your support, I definitely would not be able to achieve my dream of studying in the U.S. and not be who I am today. I want to say that all of my accomplishments are the results of all you have done for me, and you all really mean the world to me. I would also like to thank my PhD advisor and mentor, Dr. Song Li. I truly appreciate him giving me the most flexible freedom to do my research and giving me helpful suggestion and valuable advice in my career and life. I would like to thank my qualifying exam committee (led by Dr. Amy Herr, Dr. John Ngai, Dr. Lin He, and Dr. C. Anthony Hunt) and my dissertation committee (led by Dr. Song Li, Dr. Jeffrey C. Lotz, and Dr. John Ngai) for their guidance and advice in my research throughout my PhD career. I would also like to thank the past and present members in the Song Li Laboratory; Zoey Huang, Sze Yue Wong and Helen Huang (we shared happy and sad, enjoyed delicious food and traveled through California, and thanks for always helping me not only in experiments but also in life), Junren Sia, Weixi Zhong, Tiffany Dai and Angela Hsieh (thanks for working together and always sharing interesting stories), Dr. Ben Lee, Jennifer Soto, Doug Kelkhoff and Elaine Su (thanks for being awesome labmates and offering me useful advice), Dr. Zhenyu Tang (thanks for teaching me a lot of experimental techniques and protocols in stem cell biology and vascular biology), Dr. Aijun Wang (thanks for offering me scientific guidance and advice, and providing the important samples for my research), Dr. Dong Wang and Dr. Xuefeng Qiu (thanks for teaching me the techniques and knowledges in animal surgery and *in vivo* analysis), Dr. Shyam Patel (thanks for providing me the materials and techniques for tissue engineering and your careful mentorship in everything), Julia Chu (thanks for handling everything in lab, offering your experienced assistant in my experiments, and being a great lab manager), Jeffrey Henry, An-Chi Tsou, Timothy Downing, and Julia Chang (thanks for being good labmates and bring the lab happiness and joy). I would also like to thank my graduate program student affairs officer at Berkeley and UCSF, Kristin Olson and SarahJane Taylor, for taking care of me, dealing with the financial and administrative issues, and giving me helpful suggestions as well as mental support. In addition, I am also grateful for all of my close friends and roommates who have shared laughter and tears with me and make my life more enjoyable; Ping-Hung Hsieh, Yi-Pei Li, William Huang, Cian-Cian Hsieh, Joyce Yang, Irena Chen, Wei-Cheng Chang, Shang-Lin Hsu, Ya-Fang Cheng, Yi-An Lin, Renay Su, and Betty Yang. Your friendships and memories are greatly appreciated and will never be forgotten in my lifetime. Finally, I would like to thank all of the funding sources that have helped support me during my PhD study at the University of California, Berkeley, including the California Institute of Regenerative Medicine (CIRM), the Siebel Scholars Foundation, the University of California, San Francisco and the University of California, Berkeley. All of them provided me with valuable financial and academic support, which I hope will help me make significant contributions and implications to the world.

Chapter 1: Introduction

1.1 Dissertation Introduction

Tissue regeneration is the ultimate goal of the research on stem cells, biomaterials and tissue engineering, which relies on accurate control of cell differentiation, proliferation and cellular communication. Each of these factors can dramatically affect cell behavior and the extent of tissue repair. Under normal conditions, stem cells can be guided to proliferate and differentiate into desired cell types to replenish body tissues by microenvironmental cues, cell-cell interactions and secreted growth factors. Both internal and external factors may influence the behavior of stem cells, however, which in some cases leads to aberrant cell proliferation, migration and differentiation, eventually resulting in stem cell-derived diseases and various types of cancers. To obtain better control of the stem cell, it is therefore important to obtain a fundamental understanding of how these external and internal factors can influence cellular behavior *in vitro* and *in vivo*. This dissertation unravels the mechanisms of how stem cells are involved in the nerve regeneration and the contribution of stem cells to the development of vascular diseases. This work can provide a powerful and novel model to investigate the therapeutic effects of stem cell therapy for regenerative medicine, as well as having important implications in the study of disease pathogenesis.

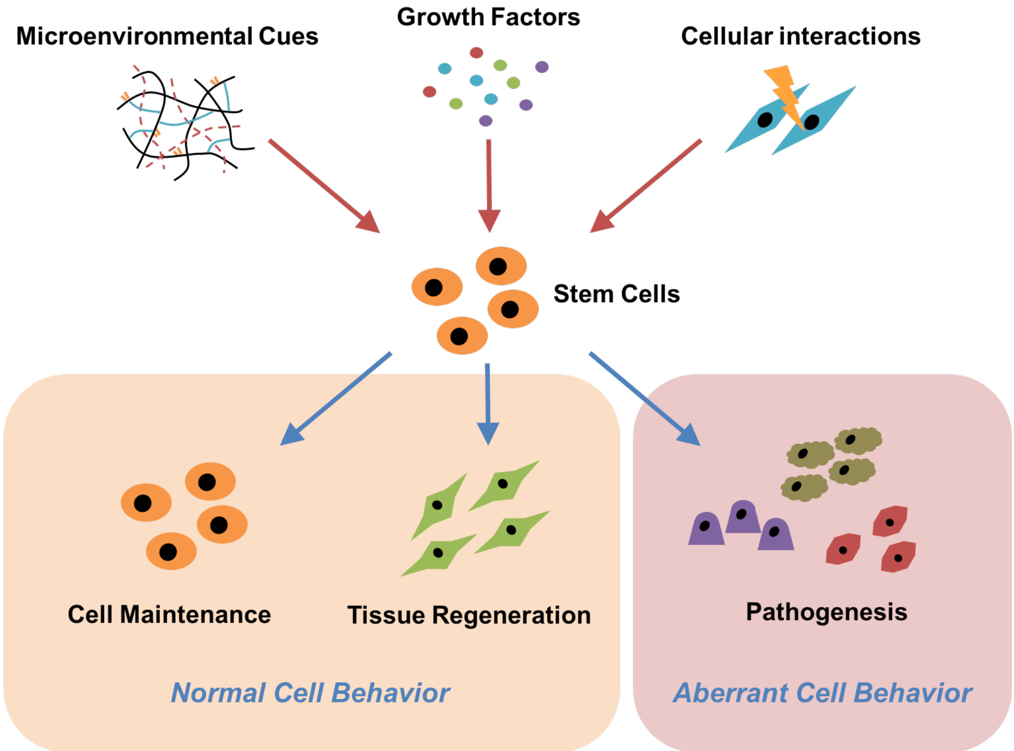

Figure 1.1. Illustration of stem cell behavior under normal and pathological conditions. This illustration demonstrates that the role of stem cells in tissue maintenance, tissue regeneration and the development of diseases in response to various cellular, biochemical and biophysical factors.

1.2 Dissertation Outline

In **Chapter 2**, we generate human integration-free induced pluripotent stem cells (iPSCs) via the electroporation technique, and then differentiate them into neural crest stem cells (NCSCs) and Schwann cells (NCSC-SCs). Nanofibrous poly(L-lactide-co-caprolactone) (PLCL) nerve conduits and NCSCs/NCSC-SCs are utilized for peripheral nerve tissue engineering to compare the therapeutic effects of cells at various differentiation stages. This study shows that transplantation of NCSCs causes better motor nerve recovery in early-stage and long-term muscle recovery than that of NCSC-SCs. Overall, this work has important implications in the selection of appropriate stem cells for cell therapies in regeneration of nerves and other tissues.

In **Chapter 3**, we combine mesenchymal progenitor cells (MPCs) with nanofibrous PLCL nerve conduits to bridge a transected sciatic nerve in a peripheral nerve regeneration model. In this report, we observe that stem cells may have different behaviors and differentiation abilities *in vitro* and *in vivo*. The results show that transplantation of MPCs with Matrigel in a nerve conduit is not able to regenerate peripheral nerves in early and long-term stages. This information is critical to the field of regenerative medicine, as it reveals that *in vivo* differentiation and paracrine effects of stem cells are the crucial factors affecting nerve recovery and may result in significant differences in peripheral nerve regeneration.

In **Chapter 4**, I demonstrate a successful method which can isolate vascular stem cells (VSCs) from human blood vessels and then characterize these cells in explant culture. In addition, I also identify the existence of VSCs in both normal and diseased blood vessels. Importantly, my results provide strong evidence that VSCs can indeed differentiate into multiple cell types and contribute to atherosclerotic lesions *in vivo*. Notably, a part of the vascular cells accumulated within lesions are identified via the *in situ* polymerase chain reaction proximity ligation assay (ISPCR-PLA) lineage tracing method. In summary, these findings show that VSCs can contribute to vascular diseases and provide a promising model by which to elucidate the mechanisms of vascular pathogenesis.

Chapter 2: Neural Crest Stem Cells for Peripheral Nerve Regeneration

2.1 Introduction

2.1.1 Cell Source for Nerve Regeneration – Neural Crest Stem Cells

Induced pluripotent stem cells (iPSCs) are derived from somatic cells that have been reprogrammed back into an embryonic-like pluripotent state. The generation of iPSCs [1-7], especially iPSCs without integration of reprogramming factors into the host genome [8-16], makes it possible for patient-specific cell therapies, which may bypass immune rejection issues and ethical concerns for the usage of embryonic stem cells (ESCs). For therapeutic use in tissue regenerative applications, the specific differentiation state of implanted iPSCs must be optimized to control cell fate, viability, potency and safety *in vivo*. Therefore, it is important to use the appropriate differentiation stage of the cells for a specific cell therapy, as well as understanding the mechanism of stem cell differentiation and the functional activities during the regeneration of specific tissue. To address these critical issues of stem cell therapies, in this study we specifically investigated the impact of different differentiation stages of iPSC-derived neural lineage cells on peripheral nerve regeneration in a rat sciatic nerve transection model.

Peripheral nerve injuries following traumatic injuries and tumor removal surgeries often requires surgical repair. Disadvantages of using nerve autograft [17, 18] include morbidity at the donor site and the unavailability of autograft. There is evidence that Schwann cells can enhance axon growth and myelination [19-22]. However, harvesting adult Schwann cells is difficult and causes morbidity at the donor site.

Neural crest stem cells (NCSCs), a source of Schwann cells [23-25], are multipotent stem cells that can be isolated from ESCs and embryonic neural crest but have relative low abundance in adult tissues [23, 26, 27]. We and others have shown that NCSCs can be differentiated from iPSCs [28, 29], and further differentiate into cell types of all three germ layers, e.g., neurons, Schwann cells, vascular smooth muscle cells (SMCs), bone cells, cartilage cells, melanocytes and endocrine cells, which makes NCSCs a valuable stem cell source for tissue regeneration and an ideal model system to study the lineage commitment and therapeutic potential of stem cells. Previous studies have shown that transplantation of iPSC-derived NCSCs in berve conduits promotes nerve regeneration at 1 month [30], but those iPSCs are not integration-free and the underlying mechanisms are not clear.

2.1.2 Tissue-engineered Nerve Graft

For peripheral nerve repair, autologous nerve grafting remains the gold standard, with a high rate of success, and is currently the primary method used for such situations. The use of an autologous nerve graft requires that a comparable nerve be taken from somewhere else on the patient’s body, however, where there is the risk that functionality will be lost. In addition, there are a limited number of nerves that can be removed and used as a donor site, as the selected nerve should have a similar structure to the nerve that was injured. In some cases, there is the possibility of death of donor site tissue because of unsuccessful regeneration of the damaged site, resulting in two damaged locations and no restoration of function in the original location [31].

Because of the drawbacks of autologous nerve grafting, alternative methods, including acellular nerve conduits and tissue-engineered nerve conduits, are currently being explored to replace autologous nerve grafting as the primary method for peripheral nerve regeneration. Synthetic nerve conduits with aligned nanofibers have shown great potential in guiding axon growth [32, 33]; however, the functional recovery of transected nerves across a 1-cm gap takes two to three months and the regeneration across a gap > 3 cm is difficult, which may result in the degeneration and dysfunction of muscle and tissue, and lack of innervation. Furthermore, the lack of Schwann cells or neurotrophic factors in the nerve conduit also causes the efficiency of nerve repair to be relatively low or to possess an unpredictable success rate.

To address this issue, the use of acellular nerve conduits and stem cells may provide a promising approach to promote nerve repair without the drawbacks associated with autologous nerve grafting and acellular nerve conduit grafting. In this study, we generated human integration-free iPSCs from human adult dermal fibroblasts via an electroporation technique, and then differentiated the iPSCs into NCSCs and finally into Schwann cells (NCSC-SCs). The therapeutic effects of the cells at various differentiation stages were investigated and compared in a rat sciatic nerve transection model wherein the nerve injury was bridged with a poly(L-lactide-co-caprolactone) (PLCL) nanofibrous nerve conduit. The mechanisms of transplanted cell-promoted nerve regeneration, including *in vivo* differentiation and paracrine signaling, were further studied.

2.2 Materials and Methods

2.2.1 Reprogramming of Fibroblasts into Induced Pluripotent Stem Cells

Establishment of human integration-free iPS cell lines.

Human dermal fibroblasts (HDFa, Life Technologies) were reprogrammed with episomal vectors containing Oct4, Sox2, Klf4 and c-Myc genes by using electroporation technique. Electroporation was performed with Human iPS Cell Reprogramming Episomal Kit (RF202, ALSTEM Bio) according to the manufacturer's protocol. In brief, the four episomal vectors were electroporated into HDFa cells which were then reseeded onto gelatin-coated plate to culture on day 0 (Fig. 1.1A). Puromycin selection was performed from day 1 to day 6 by using Fibroblast Medium supplemented with 0.5 μg/mL of Puromycin. After day 6, the transfected cells were trypsinized, reseeded onto 6-well plate pre-coated with Matrigel (354234, Corning Life Sciences), and then cultured and maintained in mTeSR^{TM}1 medium (05850, STEMCELL Technologies). About two weeks after transfection, small cell colonies became visible. After three-week culturing, pluripotent stem cell-like colonies were picked up from transfected cells and replated onto Matrigel-coating culture plates. Established iPS cell lines were identified with typical pluripotent stem cell morphology such as clear colony border and big nuclei and positive AP staining (SCR004, Millipore). To characterize the integration-free iPS cell lines, immunostaining was performed to examine typical pluripotent stem cell markers OCT4 (sc-5279, Santa Cruz Biotechnology), SOX2 (AB5603, Millipore), SSEA4 (sc-21704, Santa Cruz Biotechnology), TRA-1-60 (MAB4360, Millipore) and TRA-1-81 (MAB4381, Millipore). Nuclei were stained by Hoechst 33342 (H3570, Molecular Probes).

2.2.2 Derivation of Neural Crest Stem Cells from Induced Pluripotent Stem Cells

Derivation of neural crest stem cells (NCSCs) from integration-free iPSCs.

To obtain human integration-free iPSC-derived NCSCs, the iPSCs were detached and formed embryoid bodies (EBs) in suspension cultures for 6 days using NCSC medium (A10509-01, Life Technologies) (Fig. 1.1B). After suspension culture, EBs were plated on Matrigel-coating culture plates and kept cultured with NCSC medium for up to 2 weeks. After rosette-like structures were appeared, cells were dissociated into single cells and cultured as monolayer. To obtain homogeneous NCSC populations, magnetic-activated cell sorting (MACS, Miltenyi Biotec) was used to select p75 positive cells (130-097-127, Miltenyi Biotec). All NCSC lines were further purified by fluorescence-activated cell sorting (FACS, BD Influx) for HNK1 positive (C6680, Sigma-Aldrich) and SSEA4 negative (sc-21704, Santa Cruz Biotechnology) cells to harvest homogeneous and stable NCSC lines.

NCSC characterization and derivation of NCSC-Schwann cells.

To characterize iPSC-derived NCSCs, NCSC differentiation towards neural lineage (peripheral neurons and Schwann cells) and mesenchymal lineage (osteogenic and adipogenic cells) was carried out using the protocol described previously [30]. For NCSC differentiation into peripheral neurons, NCSCs were cultured in N2 medium supplemented with 10 ng/mL brain-derived neurotrophic factor

(BDNF, 248-BD, R&D Systems), 10 ng/mL nerve growth factor (NGF, 256-GF, R&D Systems), 10 ng/mL glial cell-derived neurotrophic factor (GDNF, 212-GD, R&D Systems) and 500 μg/mL dbcAMP (D0260, Sigma-Aldrich) for 2 weeks. The differentiated cells were immunostained for peripheral neuron markers TUJ1 and Peripherin. For osteogenic differentiation, NCSCs were seeded at a low density (10^3 cells/cm^2) and grown for 4 weeks in the presence of 10 mM β-glycerol phosphate, 0.1 μm dexamethasone and 200 μm ascorbic acid. Then cells were fixed in 4% paraformaldehyde and stained with Alizarin Red (A5533, Sigma-Aldrich) for calcified matrix. For adipogenic differentiation, confluent NCSCs were treated with 10 μg/mL insulin, 1 μM dexamethasone and 0.5 mM isobutylmethylxanthine for 3 weeks, and cells were stained with Oil Red (O0625, Sigma-Aldrich) for lipid and fat deposited by the cells.

To obtain NCSC-derived Schwann cells, iPSC-NCSCs were cultured in N2 medium supplemented with 10 ng/mL ciliary neurotrophic factor (CNTF, 257-NT, R&D Systems), 10 ng/mL basic Fibroblast Growth Factor (bFGF, 100-18B, Peprotech), 500 μg/mL dbcAMP and 20 ng/mL neuregulin (NRG, 377-HB, R&D Systems). The cells were immunostained periodically with Schwann cell markers GFAP and S100β to monitor the differentiation stage (Figure 2.3). Schwann cells obtained after 3-week differentiation were used for *in vivo* transplantation.

2.2.3 Implantation of Neural Crest Stem Cell-Embedded Nerve Graft

Fabrication of nerve conduit.

Electrospinning technique was used to produce nanofibrous nerve conduits. Aligned nanofibrous nerve conduits composed of poly(L-lactide-co-caprolactone) (70:30, Purac Biomaterials), poly(propylene glycol) (Acros Organics) and sodium acetate (Sigma-Aldrich) were fabricated by using a customized electrospinning process. To make tubular scaffolds with aligned nanofibers in the longitudinal direction on luminal surface, a rotating mandrel assembly with two electrically conductive ends and a central non-conductive section was used. The jet stream of polymer solution from the spinneret whipped between the two conductive ends, resulting in longitudinally aligned nanofibers forming a tubular scaffold on the non-conductive portion of the mandrel. To enhance the mechanical strength of the scaffolds, outer layers of random nanofibers were deposited on this layer of longitudinally aligned fibers [30].

Fabrication of hydrogel matrix.

Hyaluronic acid (HA) crosslinker MMP peptides (GCREG-PQGIWGQ-ERCG) were purchased from GenScript. Sodium Hyaluronate (60 kDa) was purchased from Lifecore Biomedical (HA60k-1), rat tail collagen I from Corning (354249), divinyl sulfone from Sigma-Aldrich (V3700), Ellman's reagent from Fisher Scientific (PI22582). Vinyl sulfone modified HA (HA-VS) was prepared using one-step synthesis [34]. In brief, sodium hyaluronate (240 mg, 0.2 mmol, 60 kD) was reacted with divinyl sulfone (602 μL, 1.3 mol) in 0.1 N NaOH solution for 26 minutes at room temperature. The reaction was stopped by 600 μL 4 N HCl, and the product was purified through dialysis (10 kD MWCO) against 0.15 M NaCl solution overnight and then against DI water overnight. The purified intermediate HA-VS was lyophilized and stored at 4°C until use. The vinyl sulfone content at modified HA polymer was determined by quantitating sulfhydryl (thiol) groups using Ellman's reagent and a cysteine standard. Based on the assay, 20.1% of the hydroxyl groups were modified with vinyl sulfone. The HA-VS polymers can then be crosslinked with bis-cysteine containing peptide crosslinkers to form hydrogel.

Preparation of tissue-engineered nerve conduit.

The cells were embedded in collagen-HA hydrogel carrier and injected into the lumen of the PLCL nerve conduit. The PLCL conduits and modified HA powder were sterilized by ethylene oxide gas sterilization before use. HA-VS was dissolved in 0.3 M triethanolamine (TEA) buffer and pre-mixed with collagen I solution, 10X PBS, and 1 N NaOH. NCSCs were detached and re-suspended in the serum-free NCSC maintenance medium in the concentration of 4×10^4 cells/μL. The cell suspension was then mixed with HA and collagen solution. The lyophilized MMP peptides were dissolved in 0.3 M TEA buffer and immediately mixed with the hydrogel-cell mixture. The final concentration of HA was 4 mg/mL and collagen I was 4 mg/mL, the final pH value of the hydrogel was 7, and the crosslinking density of HA-VS was 0.7 (moles of –SH from the crosslinkers over moles of –VSs from the HA-VSs). The hydrogel precursor solution was injected into the nanofibrous nerve conduits (25 μL hydrogel with 0.5 million cells per conduit). The tissue-engineered constructs were kept in the incubator at 37°C for 1 hour for gelation, and cell culture media were then added to cover the constructs. The tissue-engineered nerve conduit was maintained in the incubator overnight before transplantation.

In vivo transplantation of stem cells and nerve conduits.

In this study xenogenic transplantation was performed since there is no allogenic model available for human cells due to ethical reasons. All experimental procedures with animals were approved by the ACUC committee at UC Berkeley and were carried out according to the institutional guidelines. Adult female athymic nude rats (Charles River) weighing 200-250 g were used in all experiments, and 12 animals were used in each group. Three experimental groups included: (1) conduits filled with collagen-HA hydrogel without cells (control group), (2) conduits seeded with NCSCs (experimental NCSC group), and (3) conduits seeded with NCSC-SCs (experimental NCSC-SC group). For nerve conduit implantation, an incision was made over the skin of the hip joint with a sterile scalpel. Under a surgical microscope, the sciatic nerve was severed with a scalpel at two spots to make a 1-cm gap. Then a tissue-engineered nerve conduit (11 mm in length, 1.5 mm in diameter) was inserted between the two nerve stumps and sutured with 8-0 nylon monofilament sutures. The overlying muscle layers and skin were sutured with 4-0 absorbable sutures to close the surgery site. After 2 weeks, 6 animals of each group were euthanized and the nerve conduits were harvested. Three nerve conduits per group were snap-frozen with liquid nitrogen for ELISA test, the other three nerve conduits were fixed in 4% paraformaldehyde for immunohistological analysis. After 1-month and 5-month transplantation, nerve regeneration was assessed by electrophysiology testing, and muscle recovery was assessed by wet gastrocnemius muscle weight.

2.2.4 *In Vivo* Electrophysiology Testing

Electrophysiology testing.

Electrophysiology testing was performed following the previous methods [30, 35]. In brief, the rat sciatic nerve was re-exposed and the electrical stimuli (single-pulse shocks, 1 mA, 0.1 ms) were applied to the native sciatic nerve trunk at the point 5 mm proximal to the graft suturing point. CMAPs were recorded on the gastrocnemius belly from 1V to 12V or until a supramaximal CMAP was reached. Normal CMAPs from the un-operated contralateral side of sciatic nerve were also recorded for comparison. Grass Tech S88X Stimulator (Astro-Med, Inc) was used for the test and PolyVIEW16 data acquisition software (Astro-Med, Inc) was used for recording CMAPs. Recovery rate is the ratio of injured hindlimb's CMAP to contralateral normal hindlimb's CMAP of a rat.

2.2.5 Histological Analysis and Immunohistochemistry

Histological analysis and immunostaining.

The nerve conduits were harvested and fixed in 4% paraformaldehyde at 4°C for 2 hours. After been washed with PBS, tissues were cryoprotected with 30% sucrose in PBS at 4°C overnight, and were then embedded in optimum cutting temperature (OCT) compound and were frozen in -80°C. The frozen samples were cryosectioned longitudinally and transversely in -20°C in the thickness of 10 μm. The slices were placed onto Superfrost Plus slides and stored in -20°C.

Immunostaining was performed for histological analysis. Slices were permeabilized with 0.5% Triton X-100 in PBS for 30 minutes, blocked with 4% normal goat serum in PBS for 1 hour, and then incubated overnight at 4°C with primary antibodies. Slides were then washed with PBS and incubated with secondary antibodies for 1 hour at room temperature. After further PBS washing, coverslips were mounted and viewed with Zeiss fluorescence microscope. The primary antibodies used for immunohistochemistry in this study were: NFM (ab7794, Abcam), S100β (ab4066, Abcam), NuMA (ab84680, Abcam), FSP1 (ab27957, Abcam), HNK1 (C6680, Sigma-Aldrich), human Lamin A/C (MAB1281, Millipore), CD31 (ab28364, Abcam). Besides, Abcam goat anti-mouse and goat anti-rabbit secondary antibodies were used. Cell nuclei were stained by Hoechst 33342.

2.2.6 Paracrine and Biochemical Analysis

Enzyme-linked immunosorbent assay (ELISA).

Solid phase sandwich ELISA was performed to detect neurotrophic factors in nerve conduits. The snap-frozen 2-week nerve conduits were thawed on ice. The tissue inside nerve conduit was then collected, soaked in 500 μL tissue lysis buffer (786-180, Mammalian Cell PE LB, G-Biosciences) supplemented with protease inhibitors (1 mM PMSF, 1 mM Na_3VO_4, and 10 μg/mL Leupeptin), and then homogenized with GentleMACS dissociator. The tissue lysate was centrifuged under 14000 xg for 15 minutes at 4°C to remove debris, and the supernatant was collected for ELISA test. Human BDNF Quantikine ELISA kit (DBD00, R&D Systems), human

CNTF Quantikine ELISA kit (DNT00, R&D Systems), and human β-NGF DuoSet ELISA kit (DY256-05, R&D Systems) were used for the tests according to the manufacturer's instruction. The amount of growth factor was normalized by total protein concentration of tissue lysate for comparison. Total protein concentration of tissue lysate was determined by DC™ Protein Assay (BioRad) prior to ELISA.

2.3 Results

2.3.1 Characterization of Human Integration-free iPSC Lines and iPSC-derived NCSCs and Schwann Cells

Human dermal fibroblasts were reprogrammed with episomal vectors of Yamanaka factors delivered by electroporation to generate integration-free human iPSCs, and the fully characterized iPSC lines were used to derive NCSCs by using an optimized protocol (Figure 2.1A). Established human integration-free iPS cell lines showed typical pluripotent stem cell morphology, positive alkaline phosphatase (AP) staining, and positive expression of iPSC markers, such as OCT4, SSEA4, and TRA-1-60 (Figure 2.2A). The iPSC-NCSC lines were stained and positive for NCSC markers SOX10, HNK1, and AP2, and negative for iPSC marker SSEA4 (Figure 2.2B). *In vitro* differentiation showed that the iPSC-NCSCs were able to differentiate into peripheral neural lineages and mesenchymal lineages (Figure 2.2C). Positive expression of neuron marker TUJ1 (peripheral neuron differentiation) and Schwann cell marker S100β (Schwann cell differentiation) was observed after 2-week NCSC differentiation upon differentiation media. Mesenchymal lineage differentiation was verified by positive Alizarin red staining for calcium precipitation and positive Oil red lipid staining in NCSC-derived osteoblast and adipocyte cultures, respectively, following a 4-week differentiation protocol. To obtain Schwann cells from NCSCs (NCSC-SCs), we compared the expression of Schwann cell markers at day 10 and day 21 of NCSC-SC differentiation. At day 21, majority of the cells showed positive S100β and GFAP staining (Figure 2.3). We then used NCSC-SCs at day 21 for the *in vivo* studies to compare the therapeutic effects with undifferentiated NCSCs.

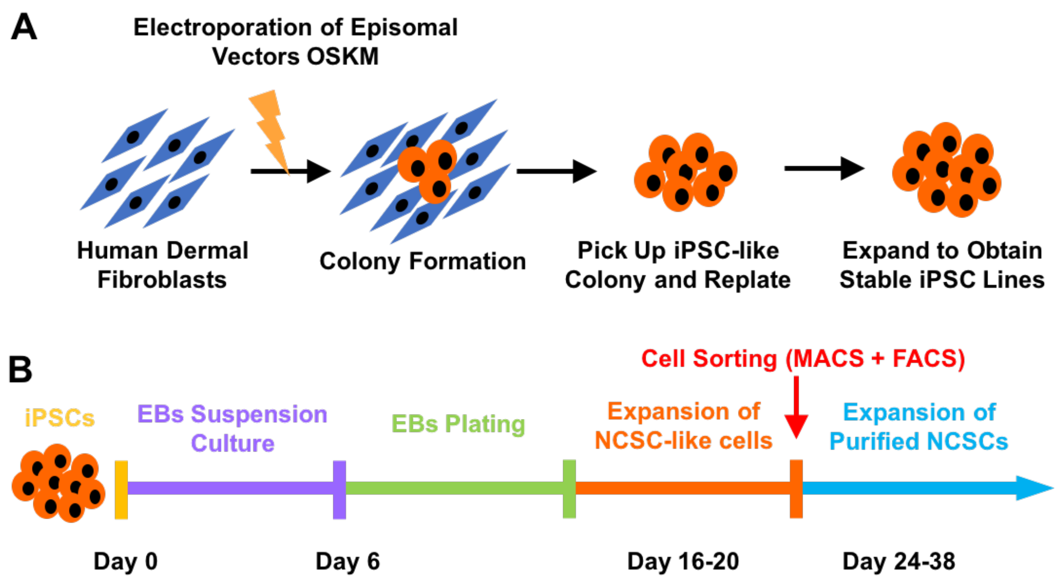

Figure 2.1. Reprogramming and establishment of human integration-free iPSC lines and iPSC-derived NCSCs. (A) Schematic outline demonstrated that human adult dermal fibroblasts were reprogrammed with episomal vectors containing Oct4, Sox2, Klf4, and c-Myc genes by using electroporation method. Pluripotent stem

cell-like colonies were picked up and expanded to obtain stable iPSC lines. **(B)** To establish NCSC lines, iPSCs were detached and formed embryoid bodies (EBs) in suspension cultures. EBs were then plated on Matrigel-coating culture plates for up to 2 weeks. Subsequently, cells were dissociated into single cells and cultured as monolayer. To obtain homogeneous NCSC populations, magnetic-activated cell sorting (MACS) were used to select p75+ cells. Expanded p75+NCSCs were further purified by fluorescence-activated cell sorting (FACS) for HNK1+ and SSEA4- cells to obtain more homogeneous and stable NCSC lines.

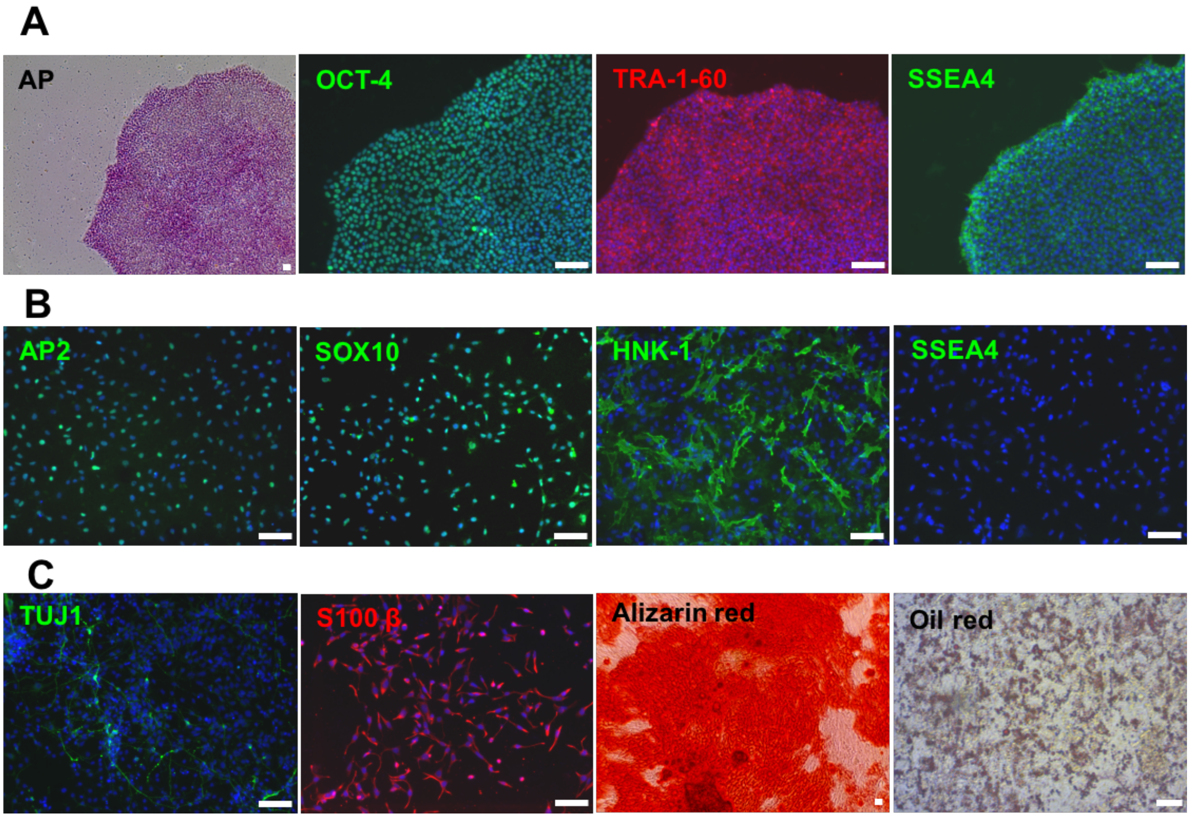

Figure 2.2. Characterization and differentiation of human integration-free iPSC lines and iPSC-derived NCSCs. (A) Established iPSC lines showed typical pluripotent stem cell morphology, positive AP staining, and iPSC markers OCT-4, SSEA4, and TRA-1-60. **(B)** The iPSC-derived NCSC lines showed positive NCSC markers SOX10, HNK1, and AP2 and negative iPSC marker SSEA4. **(C)** *In vitro* differentiation of iPSC-derived NCSCs into peripheral neural lineages (peripheral neurons, TUJ1; Schwann cells, S100β) and mesenchymal lineages (osteoblasts, Alizarin red; adipocytes, Oil red). Nuclei were stained by Hoechst 33342. Scale bar = 50 μm.

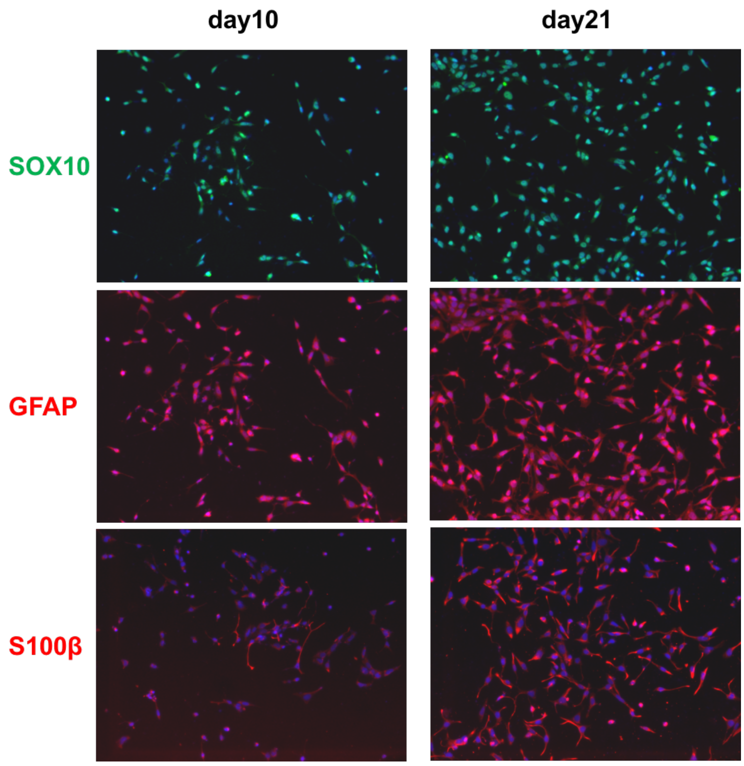

Figure 2.3. Schwann cell differentiation of iPSC-NCSCs at day 10 and day 21 in Schwann cell differentiation medium. iPSC-NCSCs expressed NCSC marker SOX10 as well as Schwann cell markers GFAP and S100β after 21 days of induction.

2.3.2 *In Vivo* Evaluation of Nerve Functional Recovery

Nerve conduits containing human iPSC-derived NCSCs or NCSC-SCs, PLCL polymer tubes, and hydrogel matrix were prepared in the tissue culture hood and then transplanted into nude rats to bridge the transected sciatic nerves in the right hindlimbs (Figure 2.4). To assess nerve functional recovery following nerve conduit implantation, electrophysiology testing was performed *in vivo* 1 month after surgery. Compound muscle action potentials (CMAPs) of the injured sciatic nerve and the contralateral intact sciatic nerve were measured and compared (Figure 2.5A). After 1-month recovery, CMAPs were detected in 83% of the animals in all groups (5 out of 6 rats for each group). For the rats with detectable CMAPs, the recovery rate of each rat was calculated as a percentage of the measured values from the normal contralateral sciatic nerve. The recovery rate of NCSC-engrafted group, NCSC-SC-engrafted group, and acellular group at 1 month were 30.4±3.9%, 23.3±2.9%, and 12.9±3.4%, respectively. Significant difference was observed between NCSC group and acellular group ($p<0.01$), but not between NCSC-SC group and acellular group (Figure 2.5B). Additionally, all three groups showed over 75% recovery of response latency with no significant difference detectable between groups.

At 5 months after surgery, neuromuscular function recovery was determined by gastrocnemius muscle wet weight measurement and electrophysiology (Figure 2.5C). Muscle mass outcomes were reported as proportions between operated sciatic nerve side and contralateral sciatic nerve side. The wet gastrocnemius muscle weight ratio in NCSC-engrafted group was significant higher than the acellular group ($p<0.01$) (Figure 2.5D), implying that the accelerated recovery of nerve function might help maintain muscle mass. On the other hand, electrophysiology tests showed that all the tested rats had detectable CMAPs, and there were no significant differences among the three groups for both CMAP and latency recovery, suggesting that nerve function in all groups had recovered at 5 months (Figure 2.6).

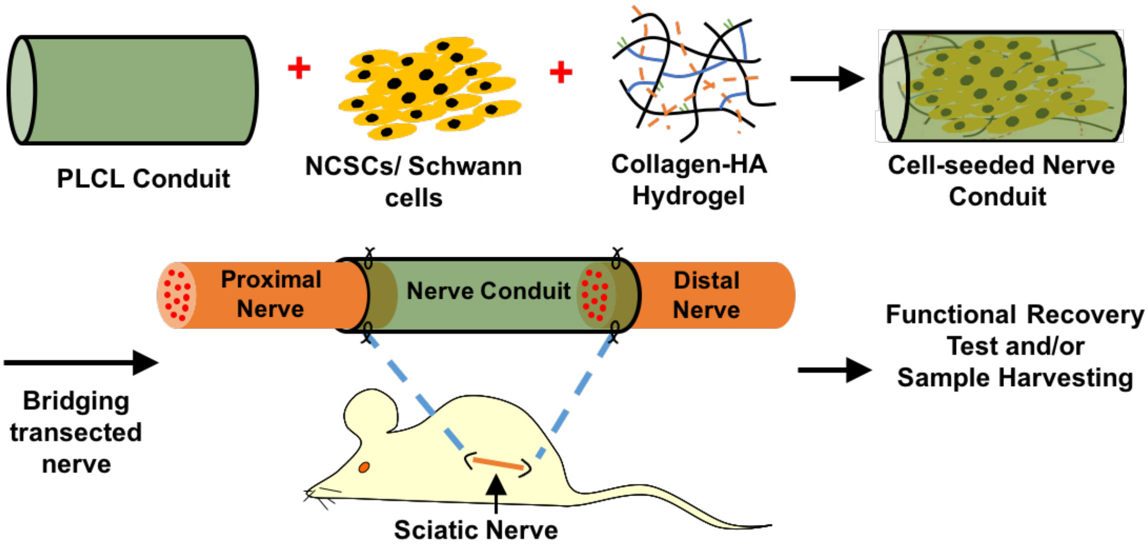

Figure 2.4. Transplantation of NCSCs and NCSC-SCs for peripheral nerve repair. Schematic outline of tissue engineering approach by combining NCSCs/NCSC-SCs, collage/HA hydrogel, and a PLCL nerve conduit. The NCSCs/NCSC-SCs were mixed with collagen-hyaluronic acid hydrogel, injected into the nerve conduits, and incubated overnight *in vitro*. The nerve conduits were then used to connect the transected sciatic nerves in a nude rat model.

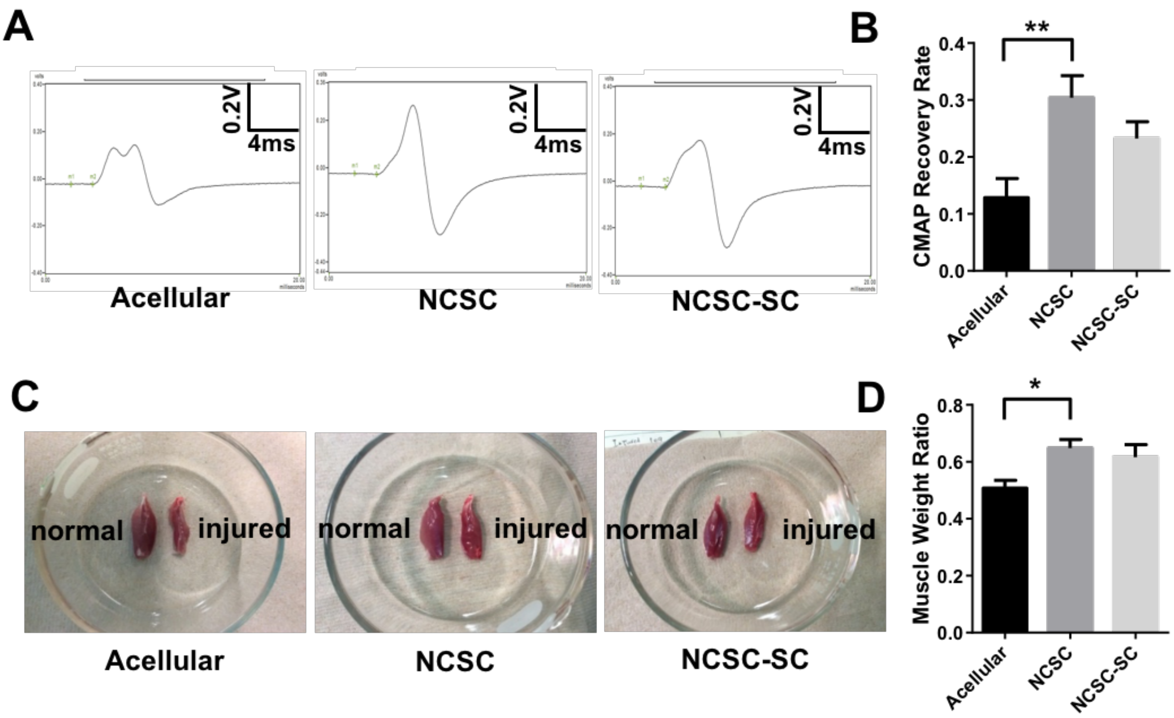

Figure 2.5. *In vivo* evaluation of functional recovery. (A) Compound muscle action potentials (CMAPs) were measured *in vivo* at 1-month after surgery. Representative CMAP curves of acellular, NCSC, and NCSC-SC groups are shown. Recovery rate is the ratio of injured hindlimb's CMAP to contralateral normal hindlimb's CMAP of a rat. **(B)** Bars represent mean ± SEM. ** indicates significant difference (p<0.01; n=6). **(C)** 5-month after surgery, gastrocnemius muscle wet weight was measured and compared between injured hindlimb and contralateral normal hindlimb of a rat. Representative images of gastrocnemius muscle are shown for acellular, NCSC, and NCSC-SC groups. **(D)** Bars represent mean ± SEM. * indicates significant difference (p<0.05; n=5 for acellular group and NCSC group, and n=6 for NCSC-SC group).

2.3.3 Cell Fate of Transplanted Cells in Nerve Conduits

To understand the mechanisms of nerve regeneration, the distribution and differentiation stage of transplanted cells were examined two weeks after surgery. Transplanted NCSCs and NCSC-SCs were identified by immunostaining of human nuclei mitotic apparatus (NuMA). Positive human NuMA staining was observed in both NCSC and NCSC-SC nerve conduits but not in acellular nerve conduits. Transplanted NCSCs were observed throughout the entire length of the nerve conduits (Figure 2.7A). However, the transplanted NCSC-SCs were only found at the proximal end of the nerve conduit (Figure 2.7A). Co-staining with axonal marker NFM and human NuMA showed that both NCSCs and NCSC-SCs integrated into newly growing host axons after 2-week transplantation near the proximal end. On the other hand, no obvious difference in leading edge length was observed between the acellular, NCSC, and NCSC-SC groups, which was about 3.5-4 mm from the proximal nerve stump.

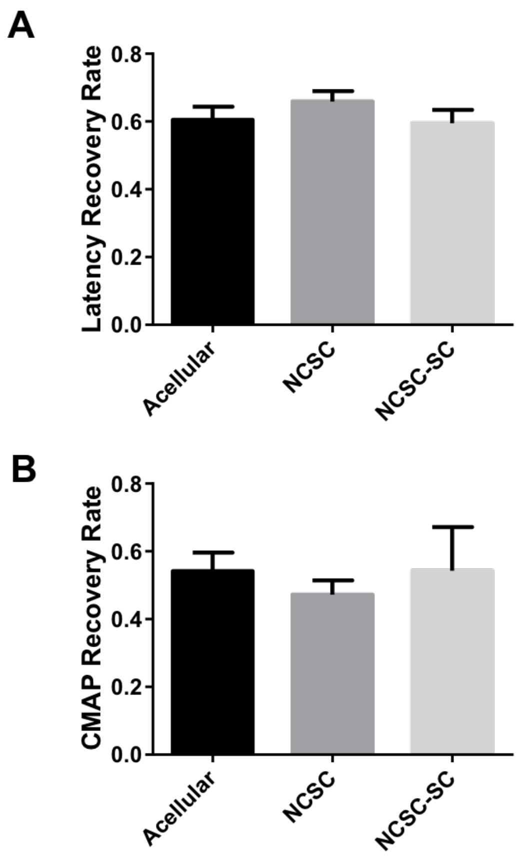

Figure 2.6. Electrophysiology testing of 5-month recovered sciatic nerves. (A) Recovery rate of response latency in acellular, NCSC, and NCSC-SC groups. **(B)** CMAP recovery rate of acellular, NCSC, and NCSC-SC groups. There were no significant differences between all groups for latency and CMAPs.

The fate of implanted NCSCs was determined by immunohistochemical staining for Schwann cell marker S100β, fibroblast marker FSP1, NCSC marker HNK1, and endothelial cell marker CD31 with double staining of human NuMA or human Lamin A/C in longitudinal sections of 2-week NCSC-engrafted nerve conduits (Figure 2.7B). Quantification of co-localized lineage specific cell markers and human cell markers showed that a majority of the transplanted NCSCs expressed Schwann cell marker S100β (Figure 2.7B. S100β+/human NuMA+, 71.1% in proximal end, 75.4% in middle conduit, 75.6% in distal end). The remaining cells expressed fibroblast marker FSP1 (FSP1+/human Lamin A/C+, 12.8% in proximal end, 14.4% in middle conduit, 13.7% in distal end) or NCSC marker HNK1 (HNK1+/human NuMA+, 7.5% in proximal end, 9.2% in middle conduit, 9.4% in distal end). Some transplanted NCSCs were also found to be associated with growing host microvessels (CD31+/human NuMA+) in the proximal end of the nerve conduit.

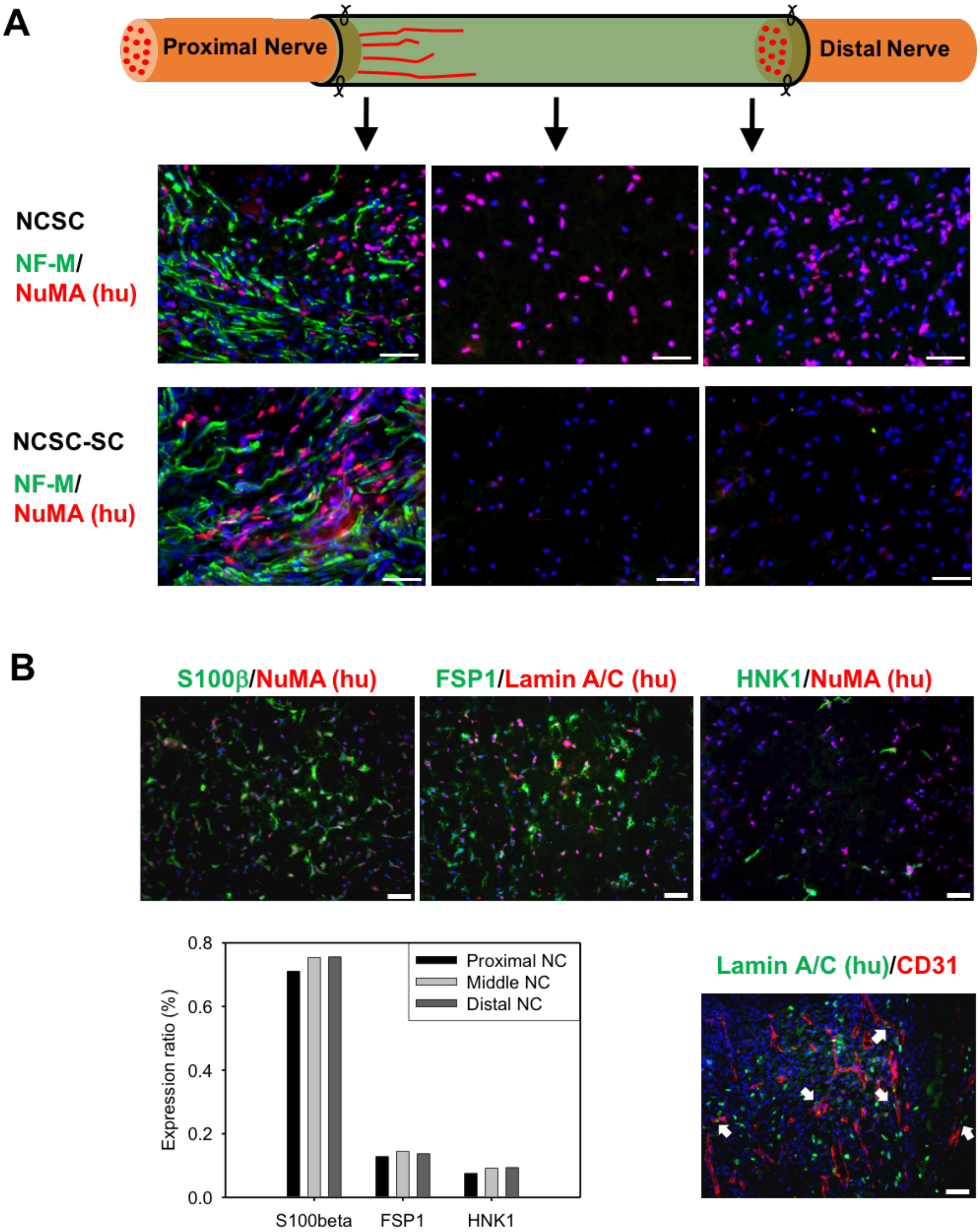

Figure 2.7. Distribution and behavior of transplanted NCSCs/NCSC-SCs in nerve conduit and NCSC differentiation *in vivo*. (A) Immunofluorescence staining of axon marker NFM and human nuclei antigen NuMA was performed in longitudinally cryosectioned nerve conduits of the NCSC group and the NCSC-SC group at 2-week after surgery. **(B)** Immunofluorescence staining of Schwann cell marker S100β (green), fibroblast marker FSP1 (green), NCSC marker HNK1 (green), and endothelial marker CD31 (red) was performed with double staining of human nuclei antigen (NuMA or Lamin A/C). White arrows pointed the transplanted NCSCs co-localized with the newly growing blood vessels (CD31+). Scale bar = 50 μm.

2.3.4 Paracrine Signaling of Transplanted Cells

To determine whether transplanted NCSC and NCSC-SC expressed neurotrophic factors *in vivo*, ELISA was performed in tissue samples collected from within the nerve conduits that were explanted after 2-week transplantation. The expression of secreted human BDNF, NGF, and CNTF was quantified by ELISA. As shown in Figure 2.8, the amount of human NGF per 1 mg total protein was 1.4±1.1 pg, 8.6±1.3 pg, and 2.2±1.5 pg in acellular group, NCSC group, and NCSC-SC group, respectively (Figure 2.8A). The amount of human BDNF per 1 mg total protein was 89.2±23.0 pg, 199.7±8.1 pg, and 75.0±13.9 pg in acellular group, NCSC group, and NCSC-SC group, respectively (Figure 2.8B). Significant differences in the amount of human NGF (p<0.05) and BDNF (p<0.01) were observed between acellular group and NCSC group, as well as between NCSC group and NCSC-SC group. The detection of NGF and BDNF in acellular group may due to the non-specific binding of ELISA kit antibodies to endogenous rat BDNF. The amount of human CNTF did not have significant difference in all three groups (Figure 2.8C).

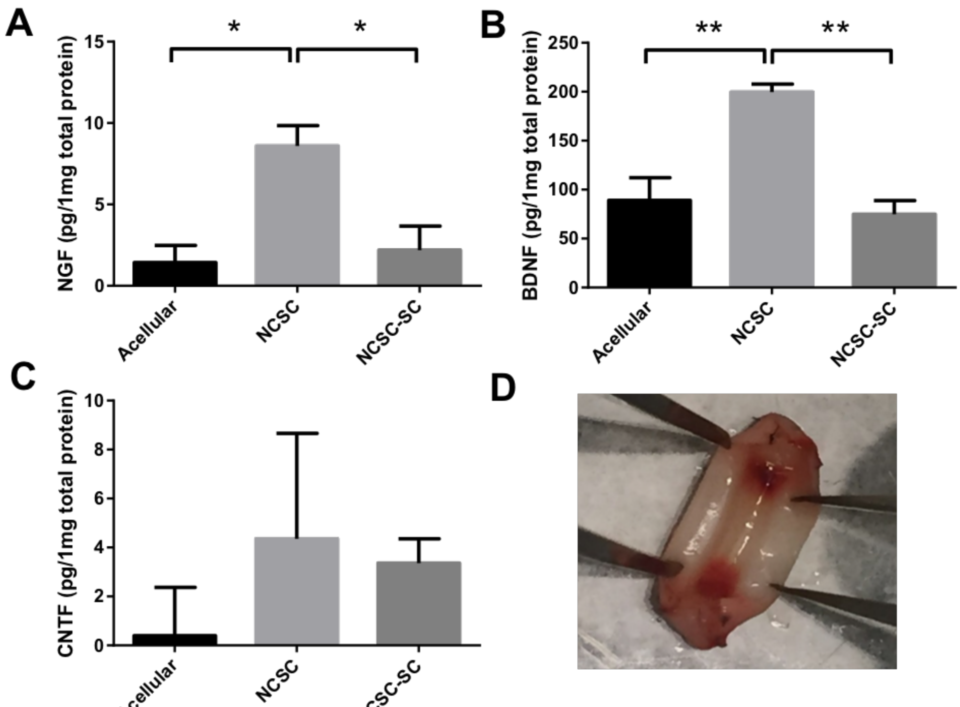

Figure 2.8. Neurotrophic factors secreted by transplanted NCSCs/NCSC-SCs. (A) The expression of nerve growth factor (NGF), **(B)** brain-derived neurotrophic factor (BDNF), and **(C)** ciliary neurotrophic factor (CNTF) were examined by using ELISA for the tissue inside nerve conduit at 2-week after transplantation. Bars represent mean ± SEM. * and ** indicate significant differences; p<0.05 and p<0.01, respectively. n=3 for each group. **(D)** Nerve conduit was shown during transplantation surgery.

2.4 Discussion

Functional recovery after segmental peripheral nerve injuries continues to be a challenging clinical problem. Stem cell transplantation has the potential to enhance nerve regeneration, particularly across long injury gaps (>3 cm). However, the differentiation stage of transplanted stem cells could dramatically impact therapeutic safety and efficacy. In this study, we investigated whether the differentiation stage of transplanted iPSC-derived neural lineage cells could impact functional nerve recovery *in vivo*. Since adult Schwann cell has been well studied to help nerve regeneration and NCSC is a potential source of Schwann cell, we differentiated the human iPSCs into NCSCs and subsequently into Schwann cells before transplantation to compare the differentiation stage of transplanted cells in their potency to repair injured nerve tissues. The cells were transplanted within a nanofibrous nerve conduit and embedded in a composite collagen/hyaluronic acid hydrogel, both of which have previously been shown to support nerve regeneration *in vivo* [36, 37].

After 2-week transplantation, we noticed that more human cells were in NCSC-engrafted conduits than that in NCSC-SC-engrafted conduits, indicating a distinct survival advantage for NCSCs over NCSC-SCs after transplantation. In the proximal end of the conduit, the transplanted NCSCs and NCSC-SCs mostly distributed around the newly growing axons, implying their involvement in axon regrowth. In the injured sciatic nerve microenvironment, over 70% of the transplanted NCSCs expressed Schwann cell marker S100β after 2-week differentiation *in vivo*. About 13% of the transplanted NCSCs in nerve conduit expressed fibroblast marker FSP1. Fibroblasts are known to play a key role in bridging the injured stumps and inducing the Schwann cells to migrate through the bridge during the early stage of peripheral nerve regeneration [38, 39], which is then followed by axon extension. A smaller amount of the transplanted NCSCs still expressed NCSC marker HNK1, suggesting that they remained on undifferentiated status. Interestingly, some transplanted NCSCs were observed to co-localize with newly growing microvessels in the proximal end, thereby suggesting that the transplanted NCSCs may also be involved in angiogenesis within regenerating nerve tissues.

It has been reported that transplantation of rat bone marrow mesenchymal stem cells (BMSCs) in a rat sciatic nerve injury model leads to the increased expression of BDNF and NGF at the injured site [40]. To investigate whether the engrafted iPSC-derived NCSCs and Schwann cells secrete neurotrophic factors (NFs) and participate in paracrine signaling in nerve regeneration, ELISA analysis of human neurotrophic factors NGF, BDNF and CNTF were performed in the tissues within the implanted nerve conduits. The results showed that BDNF and NGF concentration were higher in the NCSC-engrafted nerve conduits after 2-week transplantation than that in acellular and NCSC-SC-engrafted nerve conduits. The results showed that the NCSC group had significantly higher BDNF and NGF expression than the NCSC-SC group, suggesting that transplanted NCSCs were able to secrete essential NFs for nerve regeneration and a better NF-secreting source than NCSC-SCs. On the other hand, both NCSC and NCSC-SC groups did not show meaningful expression in human CNTF secretion. It was noticed that BDNF level in acellular was detectable and high, implying that the ELISA kit had cross-reactivity to rat BDNF. Thus, it is possible that the source of the BDNF expressed in NCSC group could be from endogenous rat cells which were stimulated by the transplanted human NCSCs.

BDNF has been demonstrated to possess a wide variety of biological effects on survival, soma size, cholinergic enzymes, and axonal outgrowth of adult motor neurons. In rat spinal root avulsion model, BDNF treatment protects motor neurons from axotomy-induced cell death, and it induced axonal outgrowth of severely damaged motor neurons [41]. BDNF can be secreted by Schwann cells. It plays an essential role in promoting axonal regeneration and re-myelination when Schwann cells were transplanted into nerve injury lesions [42]. There are at least two preferred receptors for mature BDNF, tropomyosin-receptor kinase B (TrkB) and neurotrophin receptor p75 (p75NTR) [43]. p75NTR may serve as a retrograde transport molecule in neurons, promote Schwann cell migration near injury site, and/or modulate TrkB activity in those cells that co-express both p75NTR and TrkB [44, 45]. Since human and rat TrkBs exhibit over 90% identity in amino acid sequence [46], the human BDNF secreted by Schwann cells differentiated from transplanted NCSCs may interact with the host tissues and improve nerve regeneration.

The better integration of NCSCs and the paracrine effects may explain the improved nerve functional recovery in the early stages of regeneration (1 month), and more muscle mass at 5-month post-implantation. The amplitude and response latency of the action potential were used to quantify the functional recovery of the regenerated peripheral nerve. The value of CMAP amplitude reflects the number of motor axons activated in the gastrocnemius muscle. The response latency is the time between the onset of the stimulus signal and the beginning of CMAP. Decreased latency may be related to the enhanced action potential conduction and a better myelination of the regenerated motor axons. The gastrocnemius muscle undergoes significant atrophy in a rat sciatic nerve transection model. Thus, wet gastrocnemius muscle mass measurements reflect the recovery of gastrocnemius muscle innervation and overall neuromuscular function recovery. The significantly higher CMAP recovery at 1 month and muscle mass recovery at 5 months in NCSC group as compared to acellular group suggests that the NCSC promoted rapid nerve growth across the injury gap in the early stages of nerve regeneration thereby enhancing muscle innervation and reducing atrophy.

To sum up, this study demonstrates that the cell fate and paracrine signaling are related to the stage of NCSC differentiation, which may result in the difference in peripheral nerve regeneration. Transplantation of human iPSC-derived NCSCs has better motor nerve recovery in early stage and long-term muscle recovery than that of mature Schwann cells derived from iPSC-NCSCs for the cell therapy of peripheral nerve injury. These findings have important implications in the selection of appropriate stem cells and their derivatives for stem cell therapies in the regeneration of nerves and other tissues.

Chapter 3: Mesenchymal Progenitor Cells for Peripheral Nerve Regeneration

3.1 Introduction

3.1.1 Cell Source for Nerve Regeneration – Mesenchymal Progenitor Cells

Peripheral nerve injuries affect millions of people in this country. Approximately 800,000 cases of peripheral nerve injuries (e.g., following traumatic injuries and tumor removal surgeries) occur in the United States every year, which often requires surgical repair. Disadvantages of using a nerve autograft include morbidity at the donor site and the unavailability of autograft [47]. There is evidence that the transplantation of Schwann cells or stem cells derived from skin or other adult tissues can facilitate nerve regeneration [48, 49]. Harvesting adult Schwann cells is difficult, and the viability of transplanted Schwann cells remains relatively low, making these cells unsuitable for cell therapies and tissue engineering applications.

The success of peripheral nerve repair depends on the speed of axonal growth and the myelination of Schwann cells to bridge the damaged region and to decrease the time to complete organ re-innervation [50]. Previous study has shown that the rate of nerve regeneration processes can be enhanced by neurotrophic factors that are normally secreted by Schwann cells near the injured sites [51]. One useful clinical strategy for peripheral nerve regeneration could therefore be to develop methods to promote or modulate the expression of neurotrophic factors by delivery of neurotrophic factor-secreting cells into the damaged nerve region.

Cell source is a major issue for tissue engineering and regenerative medicine. Mesenchymal progenitor cells (MPCs) were harvested from traumatized muscle tissue during orthopaedic reconstructive surgery and exhibit similar characterization to mesenchymal stem cells (MSCs) as described in previous studies [52-56]. In addition, MPCs possess multilineage differentiation potential, and are capable of modulating inflammatory responses and participate in specific mechanisms of angiogenesis and vascular maintenance [56]. Furthermore, MPCs have shown the ability to express neurotrophic factors including nerve growth factor (NGF), brain-derived growth factor (BDNF), ciliary neurotrophic factor (CNTF) and neurotrophin 3 (NT-3) [52], all of which have important roles in peripheral nerve regeneration to promote the growth of axons and migration of Schwann cells into the injured site [57-59]. Culturing the MPCs in a defined medium for neurotrophic induction can also enhance the expression and production of these factors [52], while co-culturing MPCs with dorsal root ganglia appeared to increase the expression of neurotrophic factors via cellular communication and to enhance *in vitro* axon growth in a chick embryo model [53]. In combination, MPCs can be expandable, differentiate into cell types of neural lineages and mesenchymal lineages *in vitro*, and secrete necessary neurotrophic factors to improve functional nerve regeneration, which makes MPCs a valuable stem cell source for tissue engineering and an ideal model system for studying the lineage commitment. In this study, we expanded MPCs, combined with Matrigel and PLCL nanofibrous nerve conduits, and took advantage of the established model of peripheral nerve regeneration in order to investigate the differentiation ability and therapeutic potential of MPCs *in vivo*.

3.2 Materials and Methods

3.2.1 Maintenance and Characterization of Mesenchymal Progenitor Cells

Maintenance and characterization of human MPCs.

Human mesenchymal progenitor cells (MPCs) were generously provided by Dr. Youngmi Ji (Cartilage Biology and Orthopaedic Branch, Department of Health and Human Services, National Institutes of Health). MPCs were harvested and maintained from traumatized muscle as previously described [52-56]. In brief, traumatized muscle tissue was obtained from healthy wound margin, then minced and digested with digestion medium. The cells were pelleted and plated in tissue culture flask in DMEM supplemented with 10% fetal bovine serum (FBS) and 1% penicillin and streptomycin (P/S). Subsequent subcultures were maintained in growth medium (DMEM supplemented with 10% FBS and 1% P/S) until cell marker characterization and *in vivo* cell transplantation. To characterize the MPCs, immunostaining was performed to examine stem cell markers SOX10 (MAB2864, R&D Systems), SOX17 (MAB1924, R&D Systems), AP2 (05-634, Millipore), p75 (ab8874, Abcam) and SOX2 (AB5603, Millipore), and smooth muscle cell markers ACTA2 (ab21027, Abcam), CNN1 (ab46794, Abcam) and SM-MHC (MC-352, Kamiya Biomedical). Nuclei were stained by Hoechst 33342.

Lineage-specific differentiation of human MPCs

To assess differentiation ability of MPCs, multipotent differentiation towards neural lineage (peripheral neurons and Schwann cells) and mesenchymal lineage (osteogenic, adipogenic cells and smooth muscle cells) was performed according to the protocol described previously [30, 60]. For peripheral neuron differentiation, MPCs were cultured in N2 medium supplemented with 10 ng/mL BDNF, 10 ng/mL NGF, 10 ng/mL GDNF, and 500 μg/mL dbcAMP for 2 weeks. The differentiated cells were then immunostained with peripheral neuron markers TUJ1 and Peripherin. For Schwann cell differentiation, MPCs were cultured in N2 medium supplemented with 10 ng/mL CNTF, 10 ng/mL bFGF, 500 μg/mL dbcAMP and 20 ng/mL NRG for 2 weeks. The cells were then fixed and immunostained with Schwann cell markers GFAP and S100β. For osteogenic differentiation, MPCs were seeded at a low density (10^3 cells/cm^2) and grown for 4 weeks in the presence of 10 mM β-glycerol phosphate, 0.1 μm dexamethasone and 200 μm ascorbic acid. Then cells were fixed in 4% paraformaldehyde and stained with Alizarin Red for calcified matrix. For adipogenic differentiation, confluent MPCs were treated with 10 μg/mL insulin, 1 μM dexamethasone and 0.5 mM isobutylmethylxanthine for 4 weeks, and cells were stained with Oil Red for lipid and fat deposited by the cells. For smooth muscle cell differentiation, confluent MPCs were cultured in the presence of 10 ng/mL transforming growth factor β1 (TGFβ1, 8915, Cell Signaling) for 3 weeks, and cells were then immunostained with smooth muscle cell markers ACTA2 and CNN1. Nuclei were stained with Hoechst 33342.

3.2.2 Implantation of Mesenchymal Progenitor Cell-Embedded Nerve Graft

Fabrication of nerve conduit.

Electrospinning technique was performed to fabricate nanofibrous nerve conduits. The electrospinning process was allowed to proceed until a desired wall thickness (200~250 μm) was achieved based on measurements with a thickness gauge. Polymer solution used in this study is poly(L-lactide-co-caprolactone) (70 wt% L-lactide and 30 wt% ε-Caprolactone), and PLCL nerve conduits were fabricated by using a customized electrospinning process as previously described [30]. Nerve conduits were sterilized by ethylene oxide gas sterilization before use.

Preparation of tissue-engineered nerve conduit.

MPCs were detached and re-suspended in the 10% FBS growth medium. The cell suspension (5×10^5 cells per nerve conduit) was mixed with an ice-cold Growth Factor Reduced Matrigel at a 1:1 ratio (volume to volume), and injected into the PLCL nanofibrous nerve conduits. The tissue-engineered nerve conduits were incubated at 37°C for 1 hour for gelation. Cell culture medium was added to cover the nerve conduits, and then maintained in the incubator overnight before transplantation.

In vivo transplantation of stem cells and nerve conduits.

All experimental procedures with animals were approved by the ACUC committee at UC Berkeley and were carried out according to the institutional guidelines. All efforts were made to minimize the number of animals used and their suffering. Adult female athymic nude rats (Charles River) weighing 200-250 g were used in all experiments, and 6 animals were used in each group. Three experimental groups included: (1) autologous sciatic nerve (autograft) (2) conduits filled with Growth Factor Reduced Matrigel without cells (control group), and (3) conduits filled with mixture of Growth Factor Reduced Matrigel and MPCs (experimental group).

For nerve conduit implantation, an incision was made over the skin of the hip joint with a sterile scalpel. Under a surgical microscope, the sciatic nerve was severed with a scalpel to make a 1-cm gap. Then a tissue-engineered nerve conduit (11 mm in length, 1.5 mm in diameter) was inserted between the two nerve stumps and bridged by suturing with 8-0 nylon monofilament sutures. The overlying muscle layers and skin were sutured with 4-0 absorbable sutures to close the surgery site. After 2 months, 6 animals of each group were euthanized and the nerve conduits were harvested. All nerve conduits were fixed in 4% paraformaldehyde for further immunofluorescence staining. After 2-week, 1-month and 2-month of transplantation, nerve regeneration and muscle innervation were assessed by electrophysiology testing and muscle weight measurement.

3.2.3 *In Vivo* Electrophysiology Testing

Electrophysiology testing.

Electrophysiology testing was performed following the previous methods [30, 35]. Briefly, the electrical stimuli (single-pulse shocks, 1 mA, 0.1 ms) were applied to the native sciatic nerve trunk at the point 5 mm proximal to the graft suturing point. Compound muscle action potentials (CMAPs) were recorded on the gastrocnemius belly from 1V to 12V or until a supramaximal CMAP was reached. Normal CMAPs from the contralateral side of sciatic nerve were also recorded for comparison. Grass Tech S88X Stimulator (Astro-Med, Inc) and PolyVIEW16 data acquisition software (Astro-Med, Inc) were used for recording CMAPs. Recovery rate is the ratio of injured hindlimb's CMAP to contralateral normal hindlimb's CMAP of a rat.

3.2.4 Histological Analysis and Immunohistochemistry

Histological analysis and immunostaining.

The nerve conduits were collected and fixed in 4% paraformaldehyde at 4°C for 2 hours, followed by multiple washes with PBS, tissues were then cryoprotected with 30% sucrose in PBS at 4°C overnight. Tissue samples were embedded in OCT compound and frozen at -80°C until ready for cryosectioning. The frozen OCT blocks were cryosectioned longitudinally in the thickness of 10 μm, and the slices were placed onto Superfrost Plus slides and stored at -20°C. Frozen sections were used for immunohistochemistry to evaluate nerve regeneration in this study.

For Immunostaining, slides were fixed with 4% paraformaldehyde for 10 minutes, permeabilized with 0.5% Triton X-100 in PBS for 30 minutes and blocked with 4% normal goat serum in PBS for 1 hour. Then samples were incubated with primary antibodies overnight at 4°C, followed by incubation with secondary antibodies for 1 hour at room temperature. After multiple washes with PBST, coverslips and mounting medium were used to mount slides. The primary antibodies used for immunohistochemistry in this study were: NFM (ab7794, Abcam), S100β (ab4066, Abcam), NuMA (ab84680, Abcam), and ACTA2 (ab21027, Abcam). Secondary antibodies included Alexa Fluor 488 goat anti-mouse and Alexa Fluor 546 goat anti-rabbit.Nuclei were stained with Hoechst 33342. Fluorescence images were collected by a Zeiss Axio Observer.A1 microscope. All image analysis was performed with Zeiss ZEN or Photoshop software.

Statistical analysis.

The data were reported as mean ± S.D., unless otherwise described. Comparisons among values for groups greater than two were performed by one-way analysis of variance (ANOVA), and differences between groups were then determined using a Tukey's *post hoc* test. For two groups analysis, a two-tailed, unpaired Student's *t*-test was used for the analysis of differences. For all experiments, a value of $p < 0.05$ was considered statistically significant. GraphPad Prism and SigmaPlot software were used for all statistical analyses.

3.3 Results

3.3.1 Characterization and Differentiation of Mesenchymal Progenitor Cells

MPCs were harvested from human traumatized muscle tissue and maintained in MPC growth medium (DMEM supplemented with 10% FBS) as described previously [52-56]. During cell maintenance and expansion, MPCs showed spindle-shaped cell morphology (Figure 3.1A) and homogeneous populations as shown by the expression of NCSC markers SOX10, AP2, p75, Twist and Vimentin (Figure 3.1B, E, F, H) and early neural stem cell marker SOX2 (Figure 3.1D), but no expression of smooth muscle cell (SMC) markers CNN1 and SM-MHC (Figure 3.1J, K). MPCs expressed the early SMC marker ACTA2 with diffused staining, however, rather than typical filamentous structures (Figure 3.1I). The homogeneous MPCs were selected for further studies such as *in vitro* cell differentiation and *in vivo* cell transplantation.

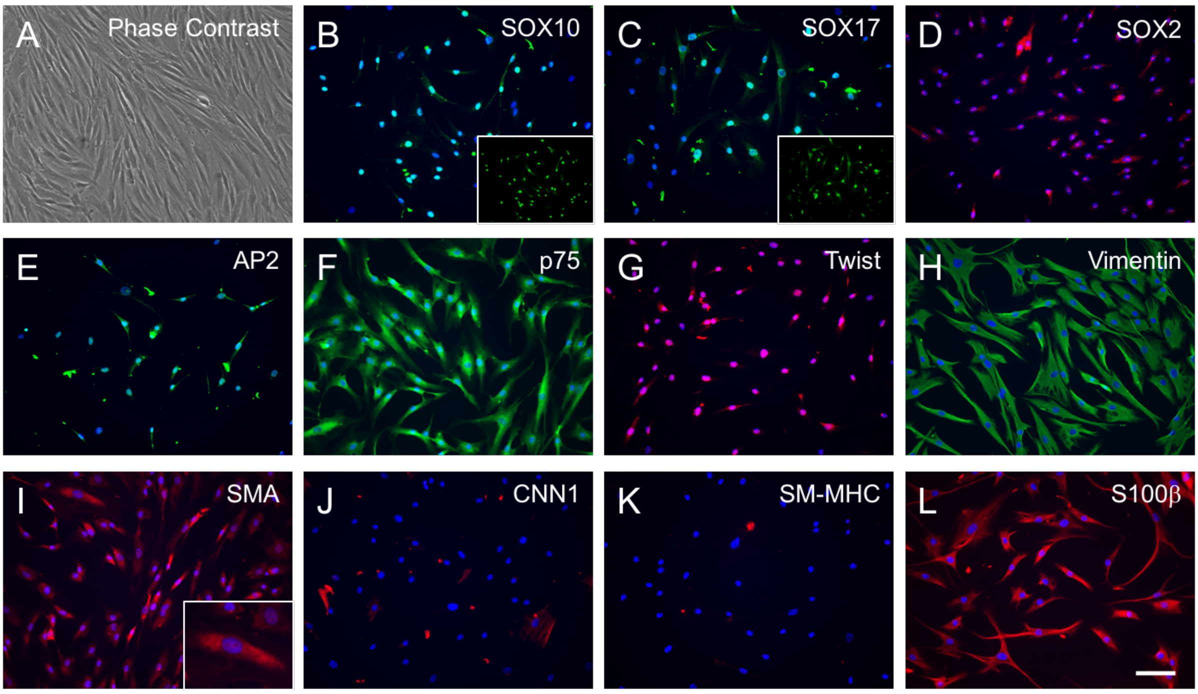

Figure 3.1. Characterization of human MPCs derived from traumatized muscle. (A) Cultured MPCs showed spindle-shaped cell morphology as typical morphology of MSC. MPCs expressed the NCSC markers **(B)** SOX10, **(E)** AP2, **(F)** p75 and **(H)** Vimentin, MVSC marker **(C)** SOX17 and **(L)** S100β, and early neural stem cell marker **(D)** SOX2, but not express SMC marker **(J)** CNN1 and **(K)** SM-MHC. MPCs show positive expression of early SMC marker **(I)** ACTA2 with diffused staining. Scale bar = 100 μm.

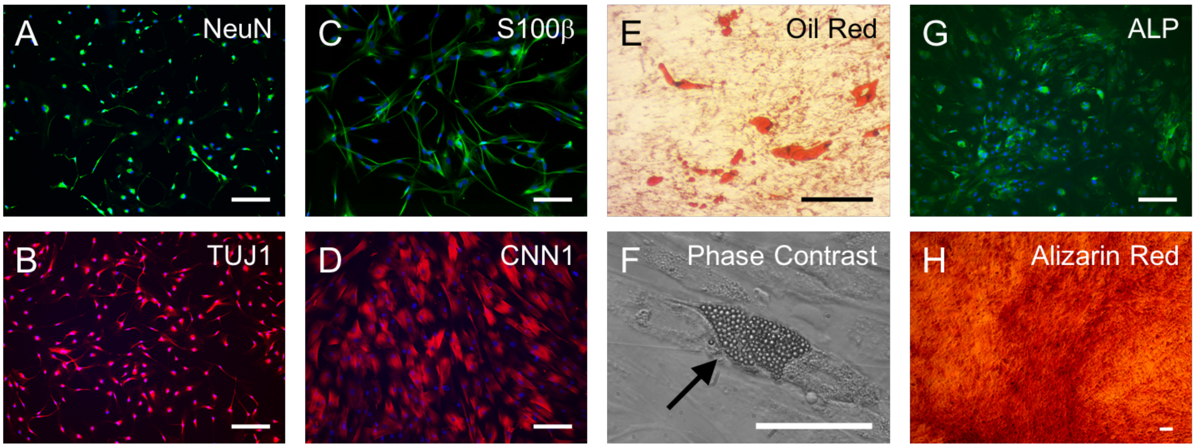

Figure 3.2. Differentiation of MPCs into neural and mesenchymal lineages. (A) Human MPCs were capable of differentiating into neural lineages such as peripheral neurons (NeuN and TUJ1) and **(C)** Schwann cells (S100β), and mesenchymal lineages including **(D)** SMCs (CNN1), **(E)** adipocytes (Oil red) and **(G)** osteoblasts (ALP and Alizarin red). Black arrow pointed lipid droplets produced by differentiated adipocyte. Nuclei were stained by Hoechst 33342. Scale bar = 100 μm.

In vitro differentiation showed that the MPCs were able to differentiate into peripheral neural lineages and mesenchymal lineages. Neuronal differentiation was induced by a combination of BDNF, GDNF, NGF and dbcAMP. Positive expression of neuronal markers TUJ1 and NeuN (Figure 3.2A, B), and multiple neurites from differentiated neurons were observed after two weeks of differentiation in conditioned medium. For Schwann cell differentiation, MPCs could be induced by a combination of CNTF, bFGF, NRG and dbcAMP, and expressed Schwann cell marker S100β after two weeks of induction (Figure 3.2C). These neurons and Schwann cells derived from MPCs were not expandable, easily detached from culture plates, and had a low survival rate in culture, however, which makes them not suitable for direct use in cell therapies. In addition to neural lineages differentiation, MPCs were also able to differentiate into several mesenchymal lineages under specific conditions. Mesenchymal lineage differentiation was verified by positive Alizarin red staining for calcium precipitation in osteogenic cultures (Figure 3.2H), positive Oil red staining for lipid deposits in adipogenic cultures (Figure 3.2E) and positive SMC marker expression (Figure 3.2D) in SMC cultures, following an optimized protocol as previously described [30]. These results demonstrated that MPCs possessed multipotent differentiation ability and may be a suitable cell source for therapeutic applications in nerve regeneration.

3.3.2 Transplantation of Mesenchymal Stem Cells for Nerve Repair

To explore the potential of MPCs for tissue engineering applications, tissue-engineered nerve conduits containing human MPCs, PLCL nanofibrous tube, and Growth Factor Reduced Matrigel were prepared in a tissue culture hood and transplanted into nude rats to connect the transected sciatic nerves in their right hindlimbs. The tissue engineering approach is schematically outlined in Figure 3.3.

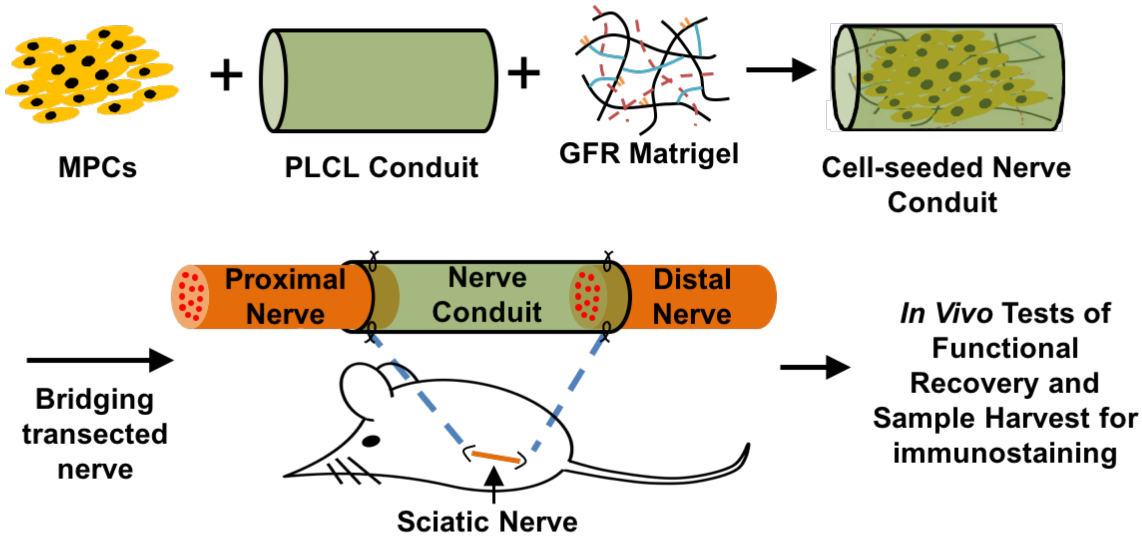

Figure 3.3. Transplantation of MPCs for peripheral nerve regeneration. Schematic outline of tissue engineering approach by combining MPCs, Growth Factor Reduced Matrigel, and a PLCL nerve conduit. The MPCs were mixed with Matrigel, injected into the nanofibrous nerve conduits, and incubated overnight *in vitro*. The tissue-engineered nerve conduits were then used to bridge the transected sciatic nerve in a nude rat model.

We engineered the electrospinning system to fabricate nanofibrous nerve conduits by using the biodegradable polymer PLCL with randomly aligned nanofibers on both the luminal side and outer surface side (Figure 3.4). MPCs (passage 4) were mixed with ice-cold Growth Factor Reduced Matrigel and injected into the lumen of the nerve conduits. These tissue-engineered nerve conduits were maintained in a cell culture incubator at 37°C overnight before being used for transplantation.

3.3.3 *In Vivo* Functional Recovery of Sciatic Nerve

To evaluate nerve functional recovery following transplantation, electrophysiology testing was performing *in vivo* two weeks, one month and two months after surgery. CMAPs of the injured sciatic nerve and normal contralateral sciatic nerve were measured and compared for each animal. After 2-week recovery, CMAPs were detected in 33.33%, 42.86% and 83.33% of the animals in the autograft (2 out of 6 rats), control (3 out of 7 rats) and experimental groups (5 out of 6 rats), respectively. The recovery rate of each rat was recorded as a percentage of its operated side in comparison to its normal contralateral side. The mean recovery rates of the autograft, Matrigel-engrafted, and MPC-engrafted groups at 2 weeks were 1.10±1.84%, 3.97±5.86%, and 3.46±5.11%, respectively (Figure 3.5A). Significant differences were not observed among all groups after two weeks of recovery. At 1-month time point of nerve recovery, CMAPs were only detected in 33.33% of animals in both the control (2 out of 6 rats) and experimental groups (2 out of 6 rats), whereas CMAPs were detected in100% of animals in the autograft group (6 out of 6 rats). The mean recovery rate of the autograft, Matrigel-engrafted, and MPC-engrafted groups at 1 month were 6.35±7.17%, 4.59±8.57%, and 3.10±5.45%, respectively (Figure 3.5B), and significant differences were not observed among all groups. For long-term nerve recovery, 2-month electrophysiology testing was performed to detect CMAPs within all groups. CMAPs were detected in all the animals in the autograft and Matrigel-engrafted groups (5 out of 5 rats in autograft and 6 out of 6 rats in control group), whereas CMAPs were only detected in 66.66% of animals in the MPC-engrafted group (4 out of 6 rats). The mean recovery rate of the autograft, Matrigel-engrafted, and MPC-engrafted groups at 2 months were 35.54±10.93%, 5.17±6.21%, and 5.33±7.02%, respectively (Figure 3.5C). Significant differences were observed between the autograft and control groups, and between the autograft and experimental groups, but not between the control and experimental groups. The magnitude of CMAPs in the autograft group at 2 months was approximately one-third that of normal sciatic nerves (Figure 3.5C). These findings suggested that MPCs were capable of accelerating and improving peripheral nerve regeneration in the early stage, but not for long-term nerve recovery.

In addition to electrophysiological testing, neuromuscular function recovery was determined by gastrocnemius muscle wet weight measurement. Muscle mass outcomes were reported as proportions between operated and contralateral sides. Two months after surgery, the mean muscle mass ratios in the autograft, Matrigel-engrafted, and MPC-engrafted groups were 0.42±0.10, 0.35±0.10, and 0.35±0.08, respectively. There were no significant differences among the three groups in respect to muscle mass measurement (Figure 3.5D).

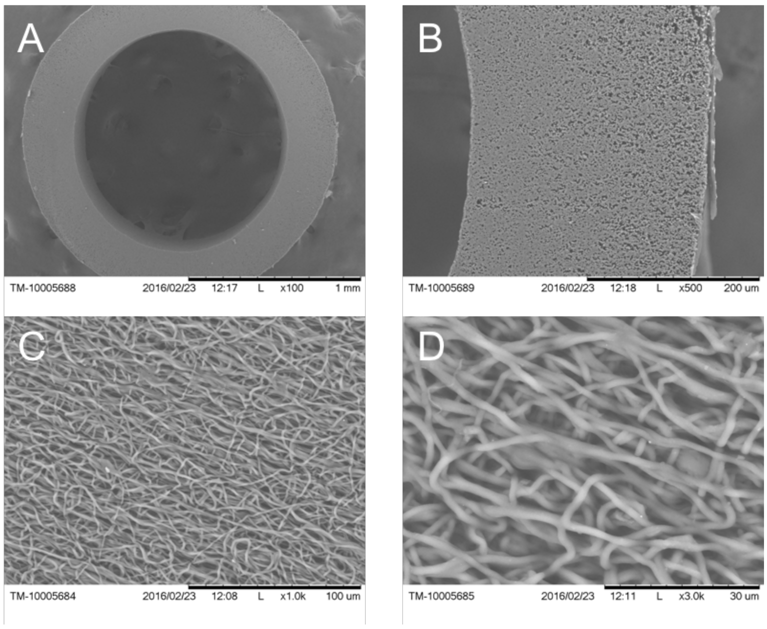

Figure 3.4. Scanning electron microscope images of the PLCL nanofibrous nerve conduits. SEM micrographs of PLCL nerve conduit with different sections in various magnifications; **(A)** cross-section, 100x, **(B)** cross-section, 500x, **(C)** inner surface, 1000x, and **(D)** inner surface, 3000x.

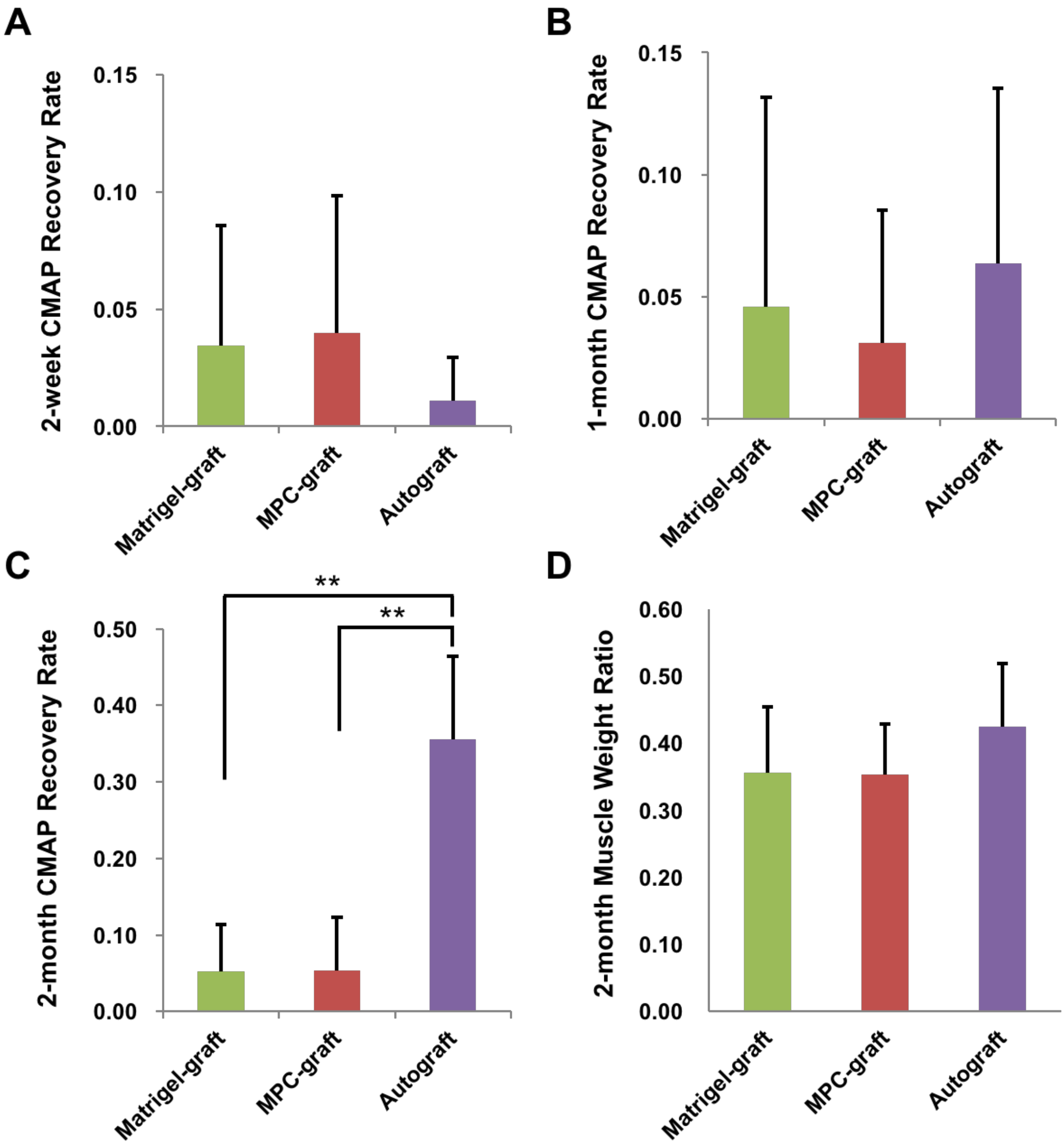

Figure 3.5. *In vivo* evaluation of functional recovery. Compound muscle action potentials (CMAPs) were measured *in vivo* at **(A)** 2 weeks, **(B)** 1 month and **(C)** 2 months after surgery. Significant differences were observed between autograft and Matrigel-engrafted group, and autograft and MPC-engrafted group, but not between Matrigel-engrafted and MPC-engrafted groups at 2 months after transplantation. Bars represent mean ± S.D. ** indicates significant difference (p<0.01; n=6 for each group). **(D)** 2 months after surgery, gastrocnemius muscle wet weight was measured and compared between injured hindlimb and contralateral normal hindlimb of a rat. There were no significant differences between all groups for muscle mass measurement at 2 months after surgery. Bars represent mean ± S.D. (n=6 for each group).

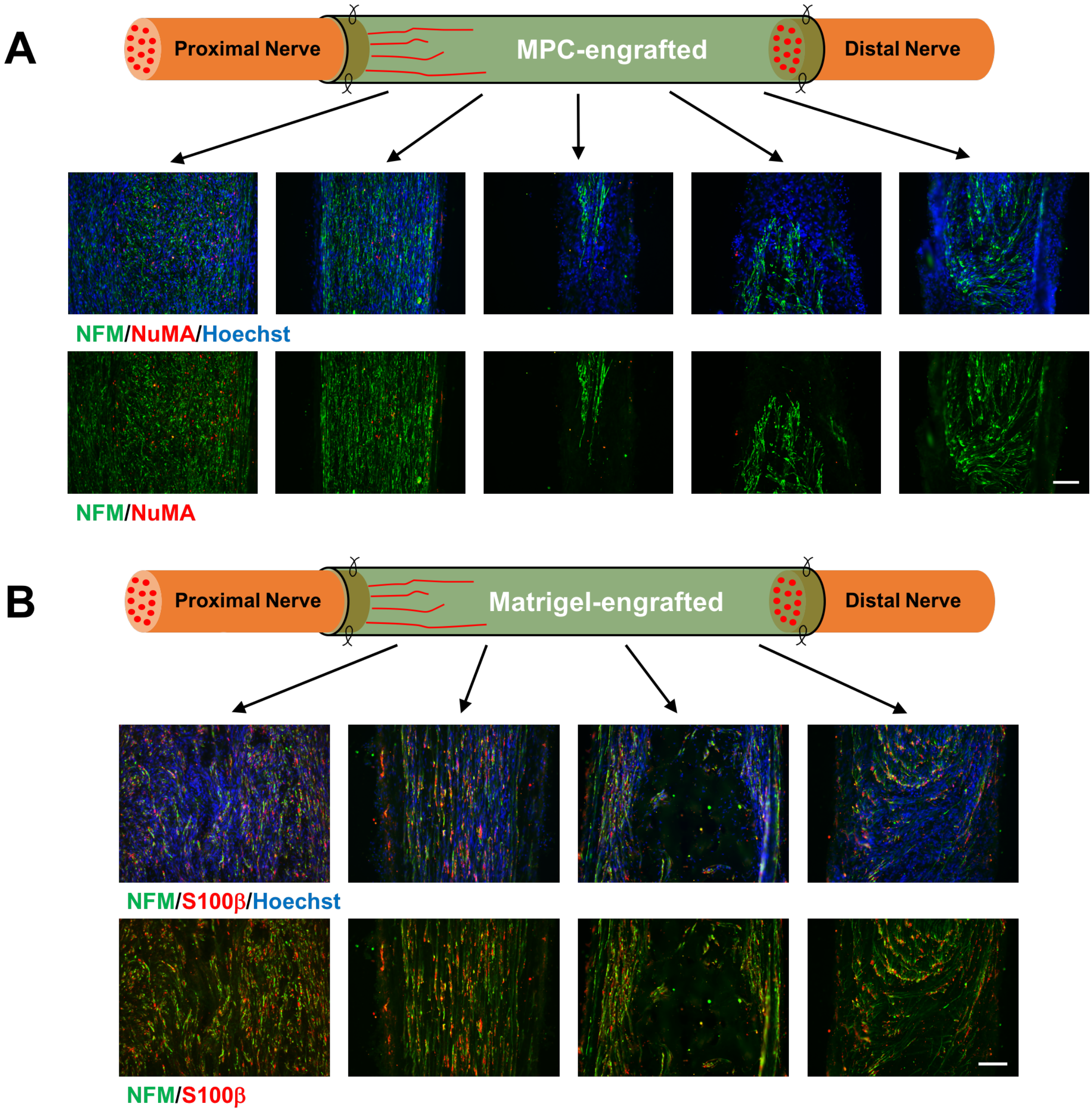

Figure 3.6. Distribution of transplanted MPCs in nerve conduit during nerve regeneration. (A) Immunofluorescence staining of axon marker NFM and human nuclei antigen NuMA was performed in longitudinally cryosectioned nerve conduits of MPC-engrafted group at 2-month after surgery. **(B)** Immunostaining of axon marker NFM with Schwann cell marker S100β was performed in cryosectioned samples of Matrigel-engrafted group. Immunostaining images showed that peripheral nerve tissues did not grow across the nerve conduits in the MPC-engrafted group, but partially grew across the nerve conduits in the Matrigel-engrafted group. There were no NuMA+ cells co-localized with NFM+ axons observed throughout the entire nerve conduit. The NFM staining also revealed that the peripheral nerve grew organizedly in the proximal end of nerve conduits, but grew disorderly near the distal end of nerve conduits in both Matrigel-engrafted group and MPC-engrafted group at 2 months of transplantation. Scale bar = 100 μm.

3.3.4 Differentiation and Distribution of Mesenchymal Stem Cells *In Vivo*

To elucidate the mechanisms of nerve regeneration and the distribution of transplanted cells, histological analysis was performed to examine the cell fate of the MPCs after two months of nerve recovery. Immunostaining of the longitudinally cryosectioned samples revealed that peripheral nerve tissues did not grow across the nerve conduits in the MPC-engrafted group (Figure 3.6A), but partially grew across the nerve conduits in the Matrigel-engrafted group (Figure 3.6B). We then examined the fate of transplanted MPCs in the nerve conduits to determine whether MPCs contribute to the myelination of axons or the regeneration of peripheral nerves. Human NuMA was used to identify the transplanted MPCs in immunofluorescence staining. Longitudinal sections of the nerve conduits were stained with NuMA and the neuronal marker NFM. Positive NuMA staining was observed in MPC-engrafted nerve conduits. The majority of NuMA+ cells were found in the proximal end of nerve conduits, and only a few NuMA+ cells were observed in the middle and the distal end of nerve conduits (Figure 3.6A). The NFM staining showed that peripheral nerves grew in an organized manner with aligned nerve fibers in the proximal end of nerve conduits, but grew in a disorderly fashion near the distal end of nerve conduits in both Matrigel-engrafted and MPC-engrafted groups two months after transplantation (Figure 3.6).

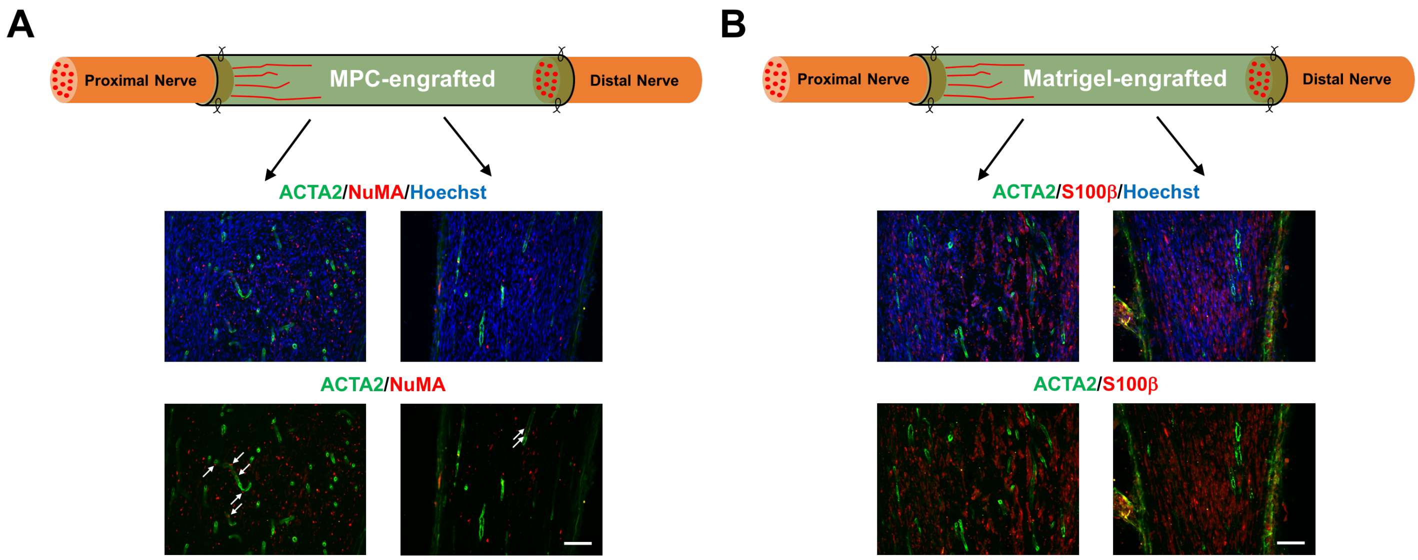

Figure 3.7. Differentiation of transplanted MPCs in nerve conduit *in vivo*. (A) Immunofluorescence staining of myofibroblast/SMC marker ACTA2 and human nuclei antigen NuMA was performed in longitudinally cryosectioned nerve conduits of MPC-engrafted group at 2 months after surgery. **(B)** Immunostaining of ACTA2 with Schwann cell marker S100β was performed in sections of Matrigel-engrafted group. Immunostaining images showed that ACTA2+ microvessels were found in the nerve conduits, and there were a few NuMA+ cells co-localized with ACTA2+ microvessels in newly growing nerve tissues *in vivo*. White arrows pointed the co-localization of NuMA+ cells with ACTA2+ microvessels. Scale bar = 100 μm.

The cell fate of transplanted MPCs was determined by immunostaining for neuronal marker NFM and myofibroblast/smooth muscle cell marker ACTA2 with double staining of human NuMA in longitudinal sections of 2-month nerve conduits. NuMA+ cells were found but were not co-localized with NFM+ neurons in MPC-engrafted nerve conduits (Figure 3.6A). The results suggested that the MPCs may not differentiate into neurons to regenerate the newly-growing peripheral nerves. Additionally, microvessel-like structures with positive for ACTA2 were found throughout the entire length of nerve conduits in both MPC-engrafted and Matrigel-engrafted groups. There were a few NuMA+ cells co-localized with ACTA2 found in whole nerve conduits (Figure 3.7A), however, indicating that the MPCs can differentiate into myofibroblasts or SMCs to form microvessels in newly-growing nerve tissues *in vivo*. Combined together, these results demonstrated that the transplanted MPCs were able to survive in nerve conduits and were involved in microvessel formation, but could not contribute to the myelination of axons or the regeneration of peripheral nerves by differentiating into appropriate neural cell types.

3.4 Discussion

Functional nerve recovery by conducting tissue engineering is a complicated process that is determined by several essential factors including cell source, carrier hydrogel and specific nerve conduits. Previous studies have shown that transplantation of stem cells has the potential to promote nerve regeneration and myelination [30, 48, 49, 61-67]. However, the essential factors that guide these cells to differentiate into specific types of cells or to control the communication between cells are not fully understood. Because MPCs have been studied to express the neurotrophic factors to aid in nerve regeneration [52], we used the MPCs as a cell source and delivered with Matrigel into the nanofibrous PLCL nerve conduits to investigate if MPCs could repair injured nerve tissues and enhance functional recovery *in vivo*.

MPCs have been reported to have similar marker expression to that of adult bone marrow MSCs, and can differentiate into osteoblasts, adipocytes and chondrocytes [54, 56]. In addition, MPCs exhibit pro-angiogenic and immunoregulatory functions that promote tissue regeneration, which are also critical characteristics of MSCs [56]. It has previously been shown that MPCs appeared to be involved in the wound healing response to muscle injury, and secreted specific neurotrophic factors to reduce scar formation and promote tissue regeneration [68]. These MPCs not only expressed the characteristics of MSCs, however, but also exhibited the similar marker expression to that of NCSCs [28, 30] and multipotent vascular stem cells (MVSCs) [60]. Based on the immunostaining results of this study, MPCs expressed the NCSC markers SOX10, AP2, p75 and Vimentin, and the MVSC markers SOX17 and S100β, but did not express the SMC markers CNN1 and SM-MHC. We also noticed that SMC marker ACTA2 was expressed by MPCs with diffused staining rather than typical filamentous structures, indicating that MPCs may be associated with pericytes, which surrounded microvascular endothelial cells in blood microvessels throughout the body. Furthermore, MPCs possess multipotency, being able to differentiate into neural lineages such as neurons and Schwann cells, and mesenchymal lineages including osteoblasts, adipocytes and smooth muscle cells *in vitro*. This resembles the multipotency of NCSCs and MVSCs as described previously [54, 56]. Overall, MPCs possess characteristics similar to those of MSCs and NCSCs, such as stem cell marker expression and multipotent differentiation of MSCs and NCSCs, and are able to secrete specific neurotrophic factors that could aid in nerve regeneration, making them a promising cell source for improving nerve repair in peripheral nerve injuries.

To evaluate functional nerve recovery, electrophysiology testing was performed two weeks, one month and two months after transplantation. Two weeks after transplantation, CMAPs in five out of six rats were detected in operated hindlimbs of MPC-engrafted nerve conduit group, whereas CMAPs were detected in only three out of seven rats and two out of six rats within the Matrigel-engrafted and autograft groups, respectively. These findings revealed that MPCs had better ability to improve nerve regeneration in the early stage of nerve injury. One month after surgery, however, CMAPs were observed in all the animals in the autograft group were observed, whereas CMAPs were observed in only two out of six rats in both the MPC-engrafted and Matrigel-engrafted groups. Two months after transplantation, CMAPs were detected in all the animals in both the autograft and Matrigel-engrafted groups, whereas CMAPs were detectable in four out of six rats within the MPC-engrafted group, implying that MPCs may not be able to facilitate nerve repair for long-term tissue regeneration. In addition, NCSCs were able to enhance early functional nerve recovery, and CMAPs were detected in the NCSC-engrafted nerve conduits one month after surgery [30]. These results suggest that MPCs were capable of improving early nerve repair, but they may not be helpful for long-term nerve regeneration from peripheral nerve injuries.

In MPC-engrafted nerve conduits, transplanted cells were mainly located around the newly-growing axons in the proximal end of nerve conduits, implying that the transplanted MPCs were involved in axon growth and their distinct survival rates between newly-growing nerve tissues. Double-staining with human NuMA and NFM showed that there were no NuMA+ cells co-localized with NFM+ axons, indicating that transplanted MPCs failed to give rise to peripheral neurons in newly-growing nerve tissues. In addition, some NuMA+ MPCs co-localized with the myofibroblast/SMC marker ACTA2+ microvessels throughout the entire nerve conduits, suggesting that MPCs could differentiate into SMCs, which are involved in microvessel formation after nerve injuries. Interestingly, these MPCs were positive for the SMC marker ACTA2 *in vitro*, but after transplantation, only a few MPCs were detected expressing ACTA2 *in vivo*. These findings indicated that the MPCs may undergo cell differentiation into other types of cells rather than neurons, Schwann cells or SMCs, and may lose their stemness during nerve regeneration in the injured sciatic nerve microenvironment.

Neurotrophic factors are important for promoting nerve regeneration and reducing scar formation, and it has been reported that injured muscle tissue can express high levels of neurotrophic factors to encourage axonal growth and Schwann cell migration to the injured site [69-71]. MPCs derived from traumatized muscle tissue were able to secrete necessary neurotrophic factors such as NGF, BDNF, CNTF and NT-3 *in vitro* [52], and all of which have critical functions in promoting the growth of axons and guiding Schwann cells to migrate into the site of injury during the process of peripheral nerve regeneration [57-59]. Our findings showed that MPCs can facilitate nerve recovery in the early stage of nerve repair, but are not helpful for long-term nerve recovery, which may be due to low viability of MPCs in nerve conduits and lack of paracrine signaling by MPCs themselves to support their survival and differentiation, resulting in a difference in peripheral nerve regeneration in comparison to MSCs and NCSCs. In summary, this study demonstrated that the MPC is not an appropriate cell type and cell source for nerve tissue repair. In regenerating nerves, MPCs cannot differentiate into peripheral neurons to facilitate nerve regrowth and enhance tissue repair. Differences in the expression of neurotrophic factors by MPCs *in vitro* and *in vivo* would be an important issue to understand in depth before clinical use of MPCs for stem cell therapies in tissue engineering and regenerative medicine.

Chapter 4: SOX10+ Cells Contribute to Vascular Diseases

4.1 Introduction

4.1.1 Smooth Muscle Cells in Blood Vessels and Vascular Diseases

Vascular disease, such as atherosclerosis, is a chronic and complicated process of cell proliferation, migration, differentiation and inflammatory reaction [72-75]. Studies conducted by many laboratories over the past few decades have shown that vascular smooth muscle cells (SMCs) are the major cell source contributing to the differentiated vascular cells accumulated within atherosclerotic lesions of blood vessels [76-82]. It is generally accepted that these mature SMCs in the tunica media of vessels have remarkable plasticity and can phenotypically de-differentiate into proliferative and synthetic SMCs, subsequently giving rise to various types of cells in the lesions [83-85]. Since the mature SMC is a cell type that is not terminally differentiated, the plasticity of SMCs is likely dependent on various factors, such as environmental matrix, extracellular signals sensed by the cell and growth factors secreted by other cells during the progression of vascular diseases. In addition, there are several previous studies have reported that other cell types, such as hematopoietic origin cells, can undergo a transition from circulating cell to SMC-like cell [86-89], and then repopulate in the lesions, which eventually leads to advanced atherosclerosis. Overall, it is likely that different SMC-related cells may be involved in the complex process of vascular diseases. A rigorous and reliable method is required for identifying the origins and cellular composition of these differentiated vascular cells within the lesions, which can help us to explore the detailed mechanisms of the development of vascular disease.

4.1.2 Resident Stem Cells in Blood Vessels and Vascular Diseases

Although numerous reports have shown that phenotypically modulated SMCs can contribute to vascular diseases and remodeling, resident stem cells in blood vessel walls and other types of stem cells exhibit their plasticity and contribution to vascular pathogenesis. Based on previous studies, MSC-like cells in the tunica media possess multipotency towards osteogenic and chondrogenic differentiation [90, 91]. In addition, CD146+ perivascular MSC-like cells have been found to possess multilineage potential for osteogenic, chondrogenic and adipogenic differentiation [92]. Furthermore, it has been shown that vascular endothelial cells can be converted into multipotent MSC-like cells and then differentiate into desired cells [93]. Moreover, previous reports have revealed that adventitial Sca-1+ stem cells can actively participate in the pathogenesis of vascular disease via differentiation into SMCs in vein grafts [94, 95]. Accumulated studies also indicate that pericytes and pericyte-like cells in arterial blood vessels can be involved in the development of atherosclerotic lesions from the early stages of disease under pathological conditions [96, 97]. Based on the above studies, the origins of cellular composition in atherosclerotic lesions are complicated and various types of cells can be involved in the development of vascular disease.

A recent study conducted by our laboratory [60] showed in a SM-MHC-Cre/LoxP-EGFP mouse model that multipotent vascular stem cells (MVSCs) isolated from the tunica media of normal and diseased blood vessels are not of SMC origin. The MVSCs can be isolated from blood vessels by explant culture, and differentiate into neural lineages and mesenchymal lineages *in vitro*. Furthermore, these MVSCs can be activated and then proliferate in tunica media and the lesions of neointima *in vivo* after vascular injury and remodeling. In this study, we collect human arteries to isolate vascular stem cells (VSCs) and also identify the existence of VSCs in both normal and diseased blood vessels. Importantly, we provide strong evidence that SOX10+ VSCs can indeed differentiate into multiple lesional vascular cells that contribute to atherosclerotic lesions *in vitro* and *in vivo*. Notably, the origins of these vascular cells accumulated within lesions are identified via the ISPCR-PLA lineage tracing method, and the results show that the majority of atherosclerotic cells are SMC-related cells that may be derived from SMCs or VSCs, whereas the existence of the population of non-SMC origin SOX10+ VSCs is mighty identified. These findings indicate that VSCs can contribute to vascular diseases after injury and provide a promising model to elucidate the mechanisms of vascular pathogenesis.

4.2 Materials and Methods

4.2.1 Explant Culture of Vascular Stem Cells from Human Blood Vessels

Cell isolation and culture from human blood vessels.

Human aortas and carotid arteries were obtained from National Disease Research Interchange (Philadelphia, PA) and Department of Surgery, University of California, Davis (Sacramento, CA). The cells were isolated from human arteries and maintained as previously described [60]. Briefly, the tissue segments were washed with 1% penicillin/streptomycin-containing PBS for three times. To obtain the clear tunica media layer from human blood vessels for explant culture, the perivascular connective and fat tissues, and adventitial layer were peeled off under a dissecting microscope and endothelial layer was removed by scraping off the cell layer on the luminal surface with a sterile scalpel blade. The tunica media was further cut into pieces with size of 5mm x 5mm and placed onto tissue culture plate in MSC growth medium (Lonza). After 5 days of explant culture, cells migrating out (passage 0, P0) from tissue pieces was observed. The tissues were then removed and cells were detached with Accutase (Life Technologies). The cells were pelleted and plated onto tissue culture plate in MSC growth medium for several passages to obtain homogeneous cell populations until further analysis.

For comparison of maintaining stemness of VSCs under different cell culture media, DMEM supplemented with 10% FBS and 1% P/S (10% FBS medium) and mTeSR^{TM}1 medium were used to maintain homogeneous SOX10+ cells (passage 4, P4) isolated from human blood vessels. Cell culture medium was replenished every other day until cell differentiation and cell fixation.

4.2.2 Characterization and Differentiation of Vascular Stem Cells *In Vitro*

Characterization of human vascular stem cells.

To characterize the cells, immunostaining was performed to examine marker expression. Cells were fixed with 4% paraformaldehyde for 15 minutes, permeabilized with 0.5% Triton X-100 for 10 minutes, and blocked with 4% goat serum/PBS for 30 minutes. For the immunostaining of stem cell markers, cells were incubated with specific primary antibodies for 1 hour at room temperature, washed with PBST for 3 times, and incubated with corresponding secondary antibodies for 1 hour. Nuclei were stained with Hoechst 33342. Fluorescence images were collected using a Zeiss Axio Observer.A1 inverted microscope. All image analyses were performed by Zeiss ZEN or Photoshop software.

Lineage-specific differentiation of human MPCs.

To evaluate the differentiation ability of cells, multipotent differentiation towards mesenchymal lineage (osteogenic, adipogenic cells and SMCs) and neural lineage (peripheral neurons and Schwann cells) was performed according to the protocol described previously [30, 60]. For peripheral neuron differentiation, cells were cultured in N2 medium supplemented with 10 ng/mL BDNF, 10 ng/mL NGF, 10 ng/mL GDNF, and 500 μg/mL dbcAMP for 2 weeks. The differentiated cells were then immunostained with peripheral neuron markers TUJ1. For Schwann cell differentiation, cells were cultured in N2 medium supplemented with 10 ng/mL CNTF, 10 ng/mL bFGF, 500 μg/mL dbcAMP and 20 ng/mL NRG for 2 weeks. The cells were then fixed and immunostained with Schwann cell markers S100β. For osteogenic differentiation, cells were seeded at a low density (10^3 cells/cm^2) and grown for 4 weeks in the presence of 10 mM β-glycerol phosphate, 0.1 μm dexamethasone and 200 μm ascorbic acid. Then cells were fixed and stained with Alizarin red for calcified matrix and osteoblast marker alkaline phosphatase (ALP). For adipogenic differentiation, confluent cells were treated with 10 μg/mL insulin, 1 μM dexamethasone and 0.5 mM isobutylmethylxanthine for 4 weeks. The differentiated cells were stained with Oil red for lipid droplet and fat deposited by the cells and adipocyte marker PPAR gamma (PPARγ). For SMC differentiation, confluent cells were cultured in the presence of 10 ng/mL TGFβ1 for 3 weeks, and cells were then immunostained with SMC markers ACTA2 and CNN1.

4.2.3 Histological Analysis and Immunohistochemistry

Human tissues and analysis of atherosclerosis.

Aorta and carotid artery specimens from patient (*n*=16) were collected during autopsy. These specimens were fixed in 4% paraformaldehyde, and cryoprotection was carried out with 30% sucrose solution at 4°C overnight. The tissues were then embedded in OCT compound and serially cryosectioned into 10-μm sections. Frozen sections were used for organic dye staining, immunohistochemistry, and *in situ* polymerase chain reaction (*in situ* PCR) assay in this study.

To assess the progression of atherosclerosis of aorta and carotid artery specimens, organic dye staining including Alizarin red and Oil red staining was performed to determine vascular calcification and lipid deposition. For Alizarin red staining, frozen sections were post-fixed with 4% paraformaldehyde and washed with distilled water for 3 times. Alizarin red staining solution was applied to samples and incubated in the dark for 30 minutes. Mineralized osteoblasts with extracellular calcium deposits within atherosclerotic lesions appeared bright orange/red color. For Oil red staining, slides were post-fixed with 4% paraformaldehyde and washed with distilled water for 3 times. Samples were incubated in 60% isopropanol solution and then Oil red staining solution in the dark for 15 minutes. Lipid droplets produced from adipocytes within atherosclerotic lesions showed bright red color. Images were collected by a Zeiss Axio Observer.A1 microscope.

Immunohistochemical Staining.

For immunostaining, frozen sections of blood vessels were fixed with 4% paraformaldehyde, permeabilized with 0.5% Triton X-100 solution, and blocked with 4% goat serum or donkey serum. For the staining of specific cell markers, samples were incubated with specific primary antibodies at 4°C overnight, washed with PBST for 3 times, and then incubated with corresponding secondary antibodies for 1 hour at room temperature. Nuclei were stained with Hoechst 33342. Fluorescence images were acquired with a Zeiss Axio Observer.A1 microscope and Zeiss ZEN software. All image analysis was performed with Zeiss ZEN or Photoshop software.

4.2.4 Lineage Tracing of Smooth Muscle Cells in Histological Sections

In situ polymerase chain reaction proximity ligation assay (ISPCR-PLA).

The protocol of ISPCR-PLA was modified and performed as previously described [78]. Briefly, frozen sections from human blood vessels were fixed with 4% paraformaldehyde, and treated with RNase A solution for 1 hour at 37°C, then rinsed in 10 mM HCl solution. Samples were incubated in 0.5% pepsin solution at 37°C for 20 minutes, then post-fixed with 4% paraformaldehyde for 10 minutes. After fixation, slides were rinsed in distilled water and air-dried completely at room temperature. PCR primers targeted to the proximal 2 kb of human *MYH11* promoter were generated (Table 4.1). Primers and melting temperature were determined by conducting genomic PCR in human dermal fibroblasts as a positive control. PCR was carried out by applying PCR cocktail solution (1X PCR buffer, *Taq* polymerase, primers, Biotin-labeled dNTP mix) to the air-dried slides, then PCR underwent temperature program in corresponding heat blocks. To remove residual primers and dNTPs, *in situ* PCR was followed by multiple washes in 0.1% NP-40/2X SSC buffer. Sections were blocked with 4% donkey serum, and then incubated with the combination of mouse H3K4me2, rabbit biotin, goat SOX10 or rat SM-MHC antibodies at 4°C overnight. After primary antibody incubation, samples were washed, then incubated with secondary antibodies conjugated with PLA probes at 37°C for 1 hour. Directly after immunostaining, Proximity ligation assay (PLA) was performed according to manufacturer's instructions (Duolink In Situ Starter Kit). PLA Ligation was performed at 37°C for 30 minutes, followed by incubation with Amplification solution at 37°C for 100 minutes. Nuclei were stained with Hoechst 33342. Fluorescence images were acquired with a Zeiss LSM700 confocal microscope or Zeiss Axio Observer.A1 microscope. All image analysis was performed with Zeiss ZEN or Photoshop software.

Statistical analysis.

The data were reported as mean ± S.D., unless otherwise described. All experiments were performed by at least three independent repeats. Comparisons among values for groups greater than two were performed by one-way analysis of variance (ANOVA), and differences between groups were then determined using a Tukey's *post hoc* test. For two groups analysis, a two-tailed, unpaired Student's *t*-test was used for the analysis of differences. For all experiments, a value of $p < 0.05$ was considered statistically significant. GraphPad Prism and SigmaPlot software were used for all statistical analyses.

Promoter	Forward Primer	Reverse Primer
*MYH11*_1	AGCCTGGGGAAGAGAGAGAG	AGTCTGCGAGTTCCCTTCAA
*MYH11*_2	CCTGGGCATTTCCCTTTAAT	ACGCAGGCCCTTAGTCTACA
*MYH11*_3	CACACCCACTTTCTCCTTGG	CCTAGAGAAAGGGGGTCGAG

Table 4.1. Forward and reverse primers used for ISPCR-PLA.

4.3 Results

4.3.1 Characterization of Vascular Stem Cells from Human Blood Vessels

Human aortas and carotid arteries were collected (Figure 4.1A) to isolate cells that were maintained in appropriate conditions, as described previously [60]. To obtain the tunica media from human arteries for explant culture, the adventitial connective tissues were peeled off and the endothelial layer was removed. The tunica media was further cut into small pieces and placed onto tissue culture plates in MSC growth medium. With the tissue explant culture method, which relies on cell migration, only migratory and proliferative cells can be harvested from explant tunica media. The cells migrating out from tunica media showed elongated spindle-shaped fibroblast-like cell morphology (Figure 4.1B) and expressed the NCSC marker SOX10 and the proliferation marker Ki67 (Figure 4.1D), but did not express the SMC marker ACTA2 (Figure 4.1C). Further extensive cell marker expression was performed by immunofluorescence staining. This detailed characterization showed that the cells expressed low levels of ACTA2 and CNN1 but no SM-MHC and Smoothelin, and exhibited the NCSC markers SOX10, p75 and Vimentin, but did not express the leukocyte marker CD45 and macrophage marker CD68 (Figure 4.2A). These results indicate that the cells migrating out from explant vessels share the characteristics of NCSCs, and are distinct from mature SMCs and circulating leukocytes.

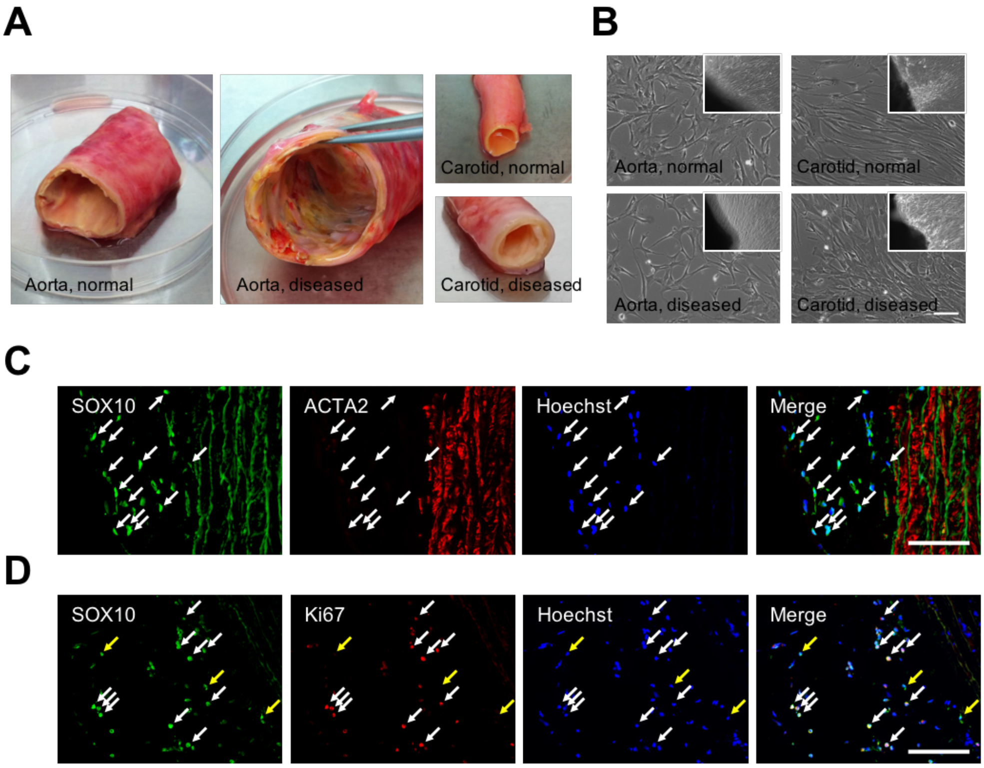

Figure 4.1. Primary culture of vascular stem cells isolated from human blood vessels. (A) Human aorta and carotid artery samples collected from NDRI and UC Davis. **(B)** Primary cultured cells showed spindle-shaped cell morphology. **(C)** Cells migrating out from explant tissue expressed the NCSC marker SOX10 but not the SMC marker ACTA2. **(D)** Migrating SOX10+ cells were proliferative with the expression of Ki67. Scale bar = 100 μm.

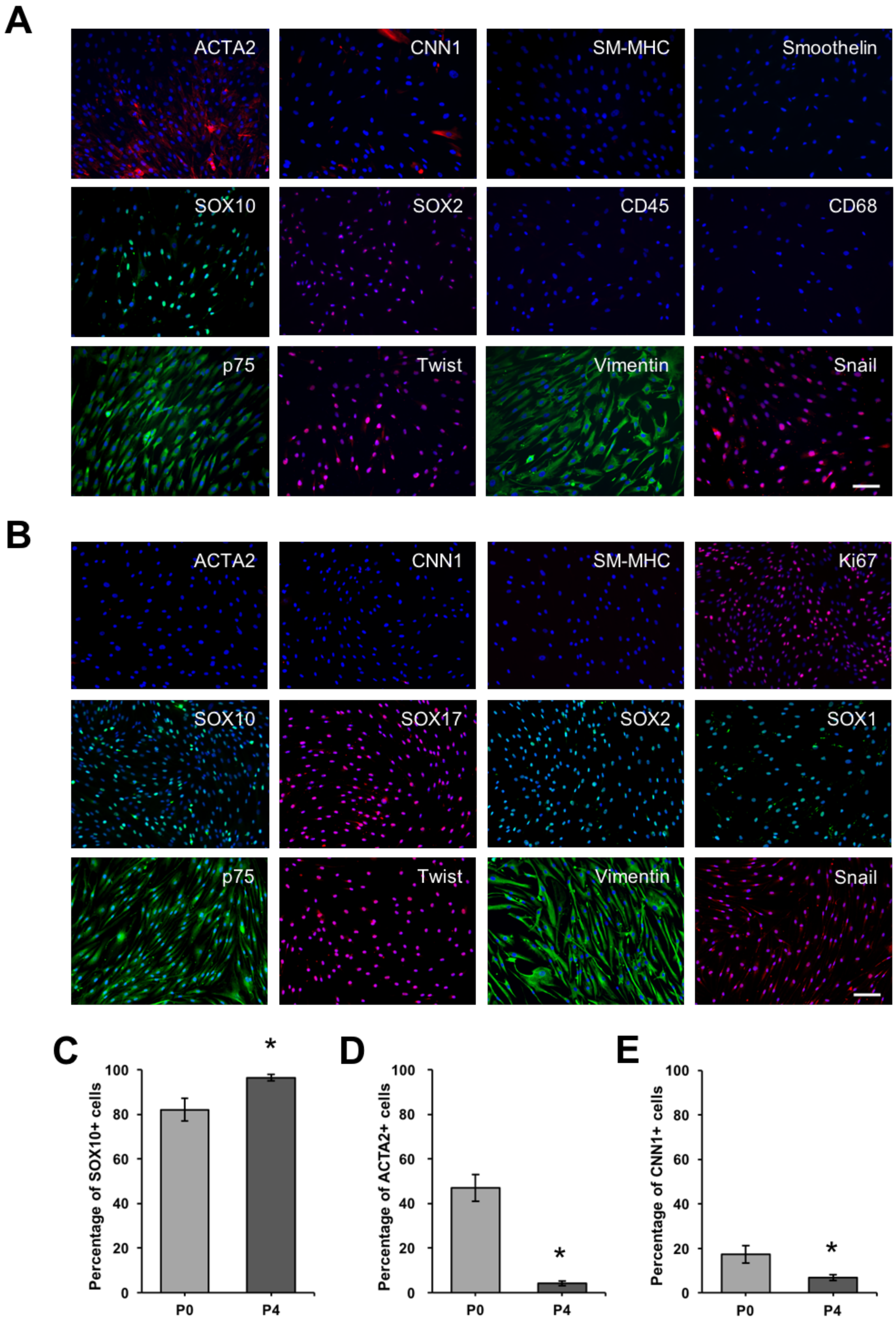
A
ACTA2
CNN1
SM-MHC
Smoothelin
SOX10
SOX2
CD45
CD68
p75
Twist
Vimentin
Snail
B
ACTA2
CNN1
SM-MHC
Ki67
SOX10
SOX17
SOX2
SOX1
p75
Twist
Vimentin
Snail
C
Percentage of SOX10+ cells
0
20
40
60
80
100
P0
P4
*
D
Percentage of ACTA2+ cells
0
20
40
60
80
100
P0
P4
*
E
Percentage of CNN1+ cells
0
20
40
60
80
100
P0
P4
*

Figure 4.2. Characterization of primary vascular stem cells and high-passage vascular stem cells isolated from human blood vessels. (A) Primary cultured cells expressed the NCSC markers SOX10, p75, Twist and Vimentin, with low-level expression of SMC markers ACTA2 and CNN1, and undetectable for mature SMC markers SM-MHC and Smoothelin as well as inflammatory markers CD45 and CD68. **(B)** High-passage cultured cells uniformly expressed SOX10, SOX17, SOX2, SOX1, p75, Twist and Vimentin, without the expression of ACTA2, CNN1 and SM-MHC. Percentage of total cells with the expression of **(C)** SOX10, **(D)** ACTA2 and **(E)** CNN1 were counted. Scale bar = 100 μm.

After culturing in MSC growth medium for several passages, we then obtained more homogeneous cell populations and examined these cells by immunostaining. As shown in Figure 4.2B, these cells (passage 4, P4) uniformly expressed the NCSC markers SOX10, SOX17, p75, and Vimentin, as well as neural stem cell markers SOX2 and SOX1, and were negative for SMC markers ACTA2, CNN1 and SM-MHC. In addition, these cells isolated from different donors and conditions exhibited similar cell doubling time and proliferation rates. The cells derived from the older donor had longer cell doubling time than those from the younger donor, indicating that the cell proliferation and growth may be age-dependent, instead of condition-dependent (healthy or diseased). On the other hand, based on quantitative analysis of cell populations, we observed that the SOX10+ cells increased significantly over several passages (Figure 4.2C), accompanied by a decrease of ACTA2+ cells (Figure 4.2D) and CNN1+ cells (Figure 4.2E). These results suggest that SOX10+ stem cells expand and proliferate faster than ACTA2+ and CNN1+ cells, and eventually dominate the culture and form homogeneous cell populations.

4.3.2 Multipotent Differentiation of Vascular Stem Cells *In Vitro*

In vitro differentiation of the SOX10+ stem cells was further examined by treating cells with specific differentiation induction media as previously described [30, 60]. After several weeks of treatment with the corresponding induction medium, the cells were capable of differentiating into peripheral neurons (positive for TUJ1), Schwann cells (positive for S100β), adipocytes (positive for PPARγ and Oil red staining), osteoblasts (positive for ALP and Alizarin red staining) and SMCs (positive for ACTA2 and CNN1) *in vitro* (Figure 4.3A). These results reveal that the SOX10+ stem cells isolated from the tunica media, but not from the adventitial layer, endothelium or fat tissue surrounding blood vessels, possess multipotent differentiation abilities.

In addition to cell differentiation, we also examined maintenance of the SOX10+ cell phenotype under different conditions by performing screening for maintenance medium. Media for pluripotent stem cell culture (mTeSR1), fibroblast culture (DMEM supplemented with 10% FBS) and SOX10+ cell culture (MSC growth medium) were used to compare the cell morphology and stem cell marker expression of the SOX10+ cells (passage 5, P5). Cultured in mTeSR1 medium for seven days, the SOX10+ cells spread out and showed stretching morphology, and only few cells expressed the proliferation marker Ki67 and the NSC marker SOX2, accompanied with an increased expression of ACTA2 and CNN1 (Figure 4.3C, D, F, G). Additionally, the expression of SOX10 decreased in comparison to the cells cultured in MSC medium (Figure 4.3E). In contrast, the SOX10+ cells cultured in 10% FBS medium for seven days showed slight stretching morphology and elongated arms, and exhibited the decreased expression of Ki67, SOX10 and SOX2 compared to the cells maintained in MSC medium (Figure 4.3B, D, E, F). In addition, these cells showed slightly increased expression of ACTA2 and CNN1 when compared to cells cultured in MSC medium, but the expressions of ACTA2 and CNN1 were much lower than those maintained in mTeSR1 medium (Figure 4.3G). These results indicate that cells cultured in mTeSR1 and 10% FBS media may lose their capability of proliferation, fail to maintain the expression of stem cell markers and undergo the spontaneous differentiation into SMCs.

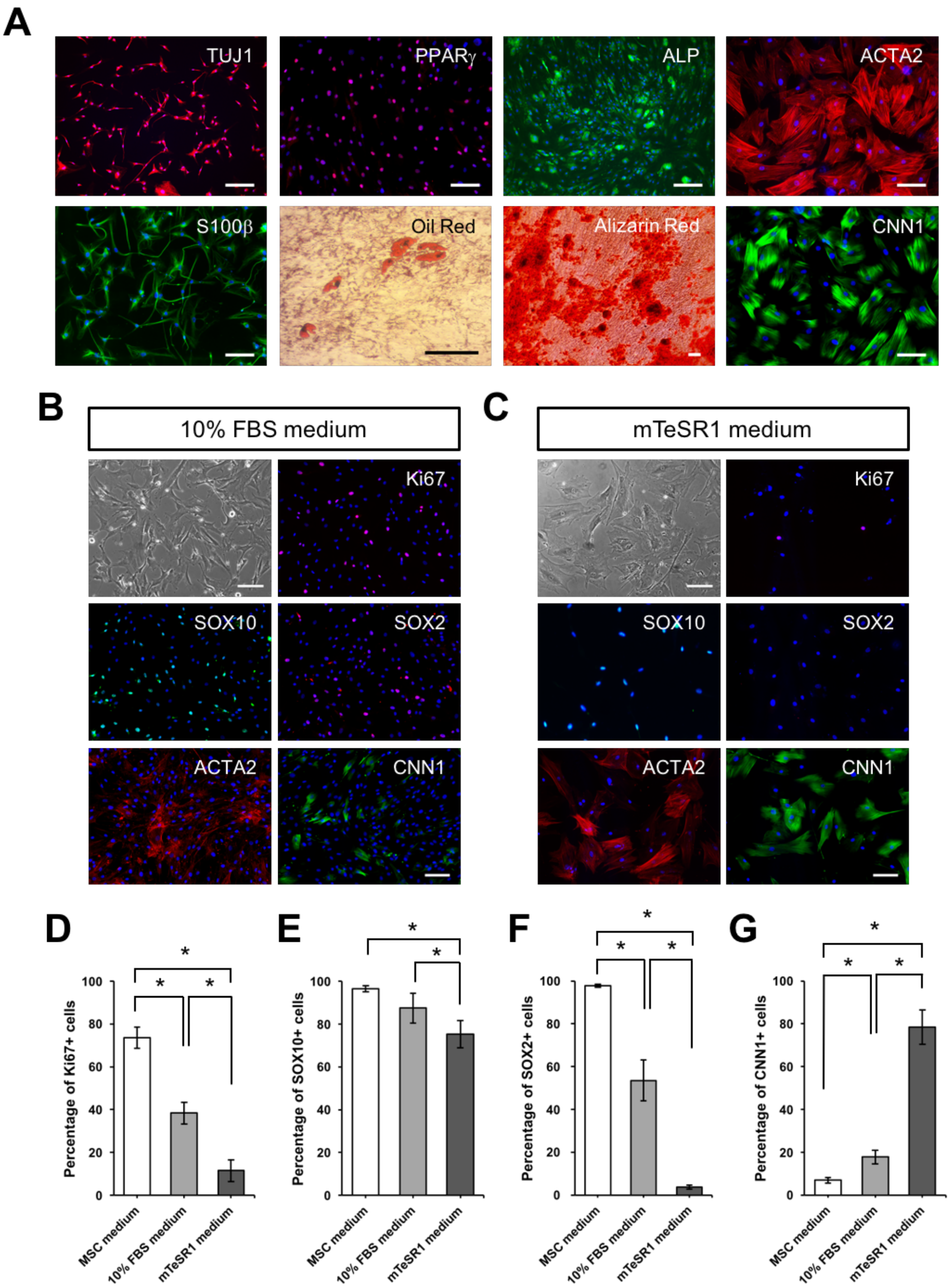

Figure 4.3. Lineage-specific and spontaneous differentiation of SOX10+ vascular stem cells in differentiation induction medium and cell culture medium *in vitro*. (A) Differentiation of SOX10+ cells into neural lineages such as peripheral neurons (TUJ1), Schwann cells (S100β), SMCs (ACTA2 and CNN1), adipocytes (PPARγ and Oil red) and osteoblasts (ALP and Alizarin red). **(B)** SOX10+ cells cultured in 10% FBS medium exhibited a little stretching morphology and expressed Ki67, SOX10, SOX2, ACTA2 and CNN1. **(C)** SOX10+ cells cultured in mTeSR1 medium exhibited stretching cell morphology and expressed low levels of Ki67, SOX10, SOX2 and high levels of ACTA2 and CNN1. Percentage of total cells with the expression of **(D)** Ki67, **(E)** SOX10, **(F)** SOX2 and **(G)** CNN1 were counted. Scale bar = 100 μm.

4.3.3 Identification of SOX10+ Vascular Stem Cell in Blood Vessels

To verify the existence of SOX10+ stem cells in the tunica media of human blood vessels, immunofluorescence staining was performed to examine cryosections from different donors. First, we conducted Alizarin red staining and Oil red staining to evaluate the status of blood vessels from each donor. Figure 4.4A showed that the diseased arteries had strong calcification in the tunica media, partially in the tunica intima, by using Alizarin red staining, whereas the healthy arteries had clear staining. In contrast, the diseased blood vessels revealed large amount of lipid deposition in the tunica intima by Oil red staining, and there was no positive Oil red staining in healthy arteries.

Immunofluorescence images of tissue cryosections confirmed that the SOX10+ cells existed in both normal and diseased blood vessel walls. The SOX10+ cells were only found in the tunica media of normal blood vessels, and not in the tunica intima (Figure 4.4B). These SOX10+ cells did not express the SMC marker CNN1, and there were no CNN1+ SMCs co-localized with the expression of SOX10 (Figure 4.4B). In addition, more SOX10+ cells were observed in the atherosclerotic lesions of the tunica intima and on the border between the tunica media and tunica adventitia of diseased carotid artery (Figure 4.4C) and diseased aorta (Figure 4.4D). Similar to the SOX10+ cells in normal blood vessels, no SOX10+ cells in diseased arteries were found to express CNN1 (Figure 4.4C, D). These results suggest that SOX10+ cells may be activated from quiescent resident cells and proliferate in response to vascular injury and remodeling.

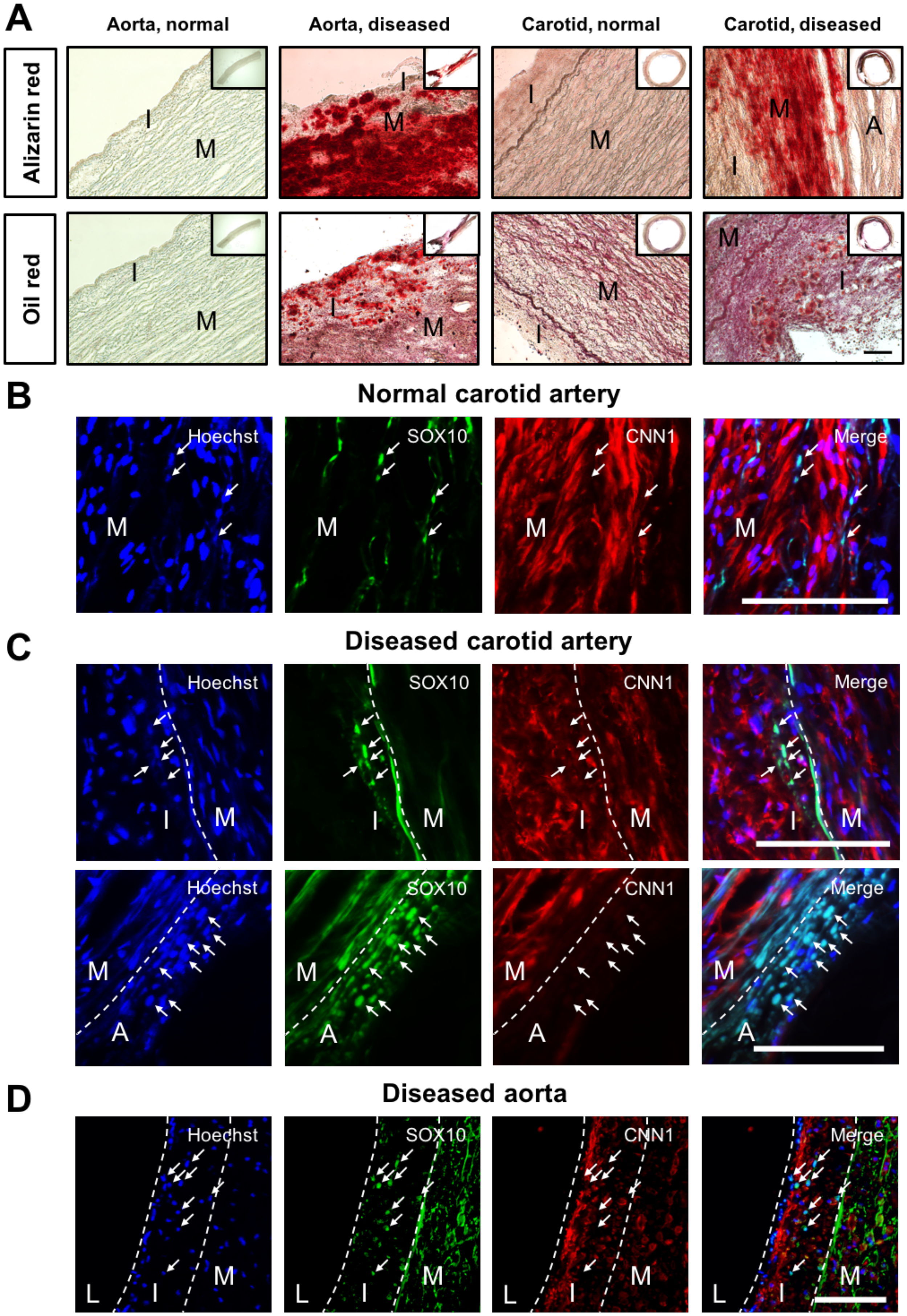
A
Aorta, normal
Aorta, diseased
Carotid, normal
Carotid, diseased
Alizarin red
Oil red
I
M
A
B
Normal carotid artery
Hoechst
SOX10
CNN1
Merge
C
Diseased carotid artery
D
Diseased aorta
L

Figure 4.4. Identification of SOX10+ cell populations in healthy and diseased blood vessels. (A) Evaluation of blood vessels was performed by Alizarin red and Oil red staining. **(B)** Immunofluorescence staining showed that SOX10+ cells were found in tunica media, and without the expression of SMC marker CNN1. **(C)** SOX10+ cells without the expression of CNN1 were observed in the lesions of tunica intima and the border between tunica media and tunica adventitia of diseased carotid artery. **(D)** SOX10+ cells were found within the lesions of diseased aorta, but did not express CNN1. Scale bar = 100 μm.

4.3.4 *In Vivo* Differentiation of SOX10+ Vascular Stem Cells in Blood Vessels

To understand cellular composition within the lesions after vascular injury, we first performed hematoxylin and eosin (H&E) staining to recognize various tissue types of diseased blood vessels. Based on the H&E staining, different cell types and tissue structures were observed within the lesions, such as cartilage-like, bone-like, and smooth muscle-like tissues (Figure 4.5A). These results showed that various types of differentiated cells are involved in atherosclerotic lesions during the progression of vascular diseases. We have shown that SOX10+ cells are able to differentiate into different types of cells *in vitro*. To further investigate whether or not these cells can differentiate into the cells found within the lesions under pathological conditions, immunostaining with SOX10 and the differentiation markers (adipocyte: PPARγ, osteoblast: Osterix, chondrocyte: SOX9) was performed to identify the detailed cellular composition in the lesions following vascular injury. Immunofluorescence staining showed that some vascular cells were double-positive for SOX10 and the adipocyte marker PPARγ, and a portion of these cells formed aggregate-like structures to express SOX10 and PPARγ within the lesions in the tunica intima (Figure 4.5B). Similar to the adipogenic differentiation of the SOX10+ cells *in vivo*, the double-positive cells with SOX10 and the osteoblast marker Osterix (Figure 4.5C), and SOX10 with the chondrocyte marker SOX9 (Figure 4.5D) were also found in the lesions of diseased blood vessels, some of which were observed to form cell aggregate-like structures. These results indicate that the SOX10+ cells are capable of differentiating into various types of cells accumulated within the atherosclerotic lesions following vascular injury and remodeling.

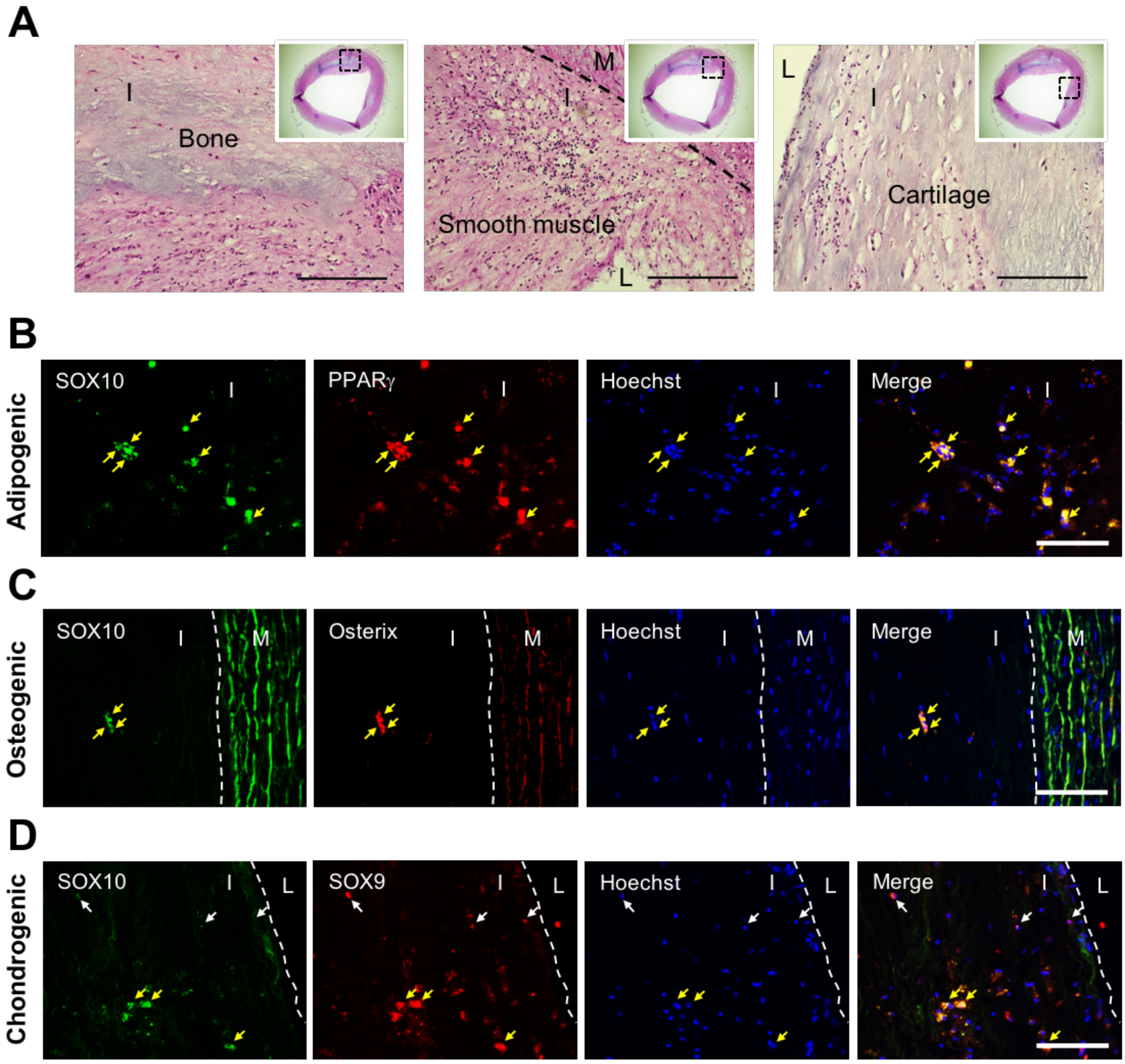

Figure 4.5. *In vivo* differentiation of SOX10+ cells in the lesions of diseased blood vessels. (A) H&E staining of diseased carotid artery showed various tissue structures such as cartilage-like, bone-like and smooth muscle-like tissues in the lesions. Differentiated SOX10+ cells were found within the lesions positive for **(B)** adipogenic marker (PPARγ), **(C)** osteogenic marker (Osterix) and **(D)** chondrogenic marker (SOX9). Scale bar = 100 μm.

4.3.5 Expression of SOX10 in Inflammatory Cells in Blood Vessels

We noticed that some SOX10+ cells were found in the lumen of blood vessels, raising the question whether some inflammatory cells could express SOX10. It has been reported that leukocytes and/or inflammatory cells can contribute to arterial atherosclerotic lesions [86, 88]. To investigate the relationship of inflammatory cells and SOX10+ cells involved in vascular diseases, immunofluorescence staining with inflammatory cell markers (leukocyte: CD45, macrophage: LGALS3, foam cell: LIGHT) was performed to examine the cells associated with the expression of SOX10 within lesions of diseased blood vessels. Based on the immunostaining results, cells double-positive for the leukocyte marker CD45 and SOX10 were detected within the lesions, whereas some cells were positive for SOX10 alone or CD45 alone (Figure 4.6A). In addition, cells expressing SOX10 and the macrophage marker LGALS3 were found in the lesion areas where SOX10+ cells without the expression of LGALS3 were also observed (Figure 4.6B). SOX10+ cells were found co-localized with the foam cell marker LIGHT within the lesions were found, and some cells positive for SOX10 alone were observed there as well (Figure 4.6C). We also noticed, however, that there were many LIGHT+ cells mainly located in the tunica media of diseased blood vessels (Figure 4.6C), indicating that the migration of mature foam cells towards the medial layer. These results suggest that not only are the SOX10+ stem cells involved in the development of atherosclerosis, but also inflammatory cells such as leukocytes, macrophages, and foam cells can express SOX10 and contribute to atherosclerotic lesions.

Furthermore, to understand if these inflammatory cells transdifferentiate into SMCs, immunofluorescence staining with inflammatory markers (CD45, LGALS3 and LIGHT) and the SMC marker ACTA2 was conducted to detect the marker expressions of these cells. Interestingly, there were no CD45+, LGALS3+ or LIGHT+ cells were found to express ACTA2 within the lesions of diseased blood vessels (Figure 4.6D, E, F). Conversely, the differentiation of these inflammatory cells (CD45+ cells) was examined by double-staining for CD45 and the differentiated markers (PPARγ, Osterix and Aggrecan), which showed that the CD45+ cells can differentiate into adipocytes and osteoblasts double-positive for CD45/PPARγ (Figure 4.7A) and CD45/Osterix (Figure 4.7B), respectively, but not into chondrocytes *in vivo* (Figure 4.7C). Combined together, these results indicate that the inflammatory cells involved in atherosclerotic lesions can express SOX10 and differentiate into adipocytes and osteoblasts *in vivo.*

4.3.6 Identification of SOX10+ Cells Around Microvessels

In addition to the existence of SOX10+ cells in the tunica media and the lesion areas of tunica intima, we found a number of SOX10+ cells around the microvessels in the adventitial layer. We first used NG2, a marker for pericytes, to investigate the role of SOX10+ cells around microvessels and the cellular interaction with pericytes. Immunostaining showed that some cells double-positive for SOX10 and NG2 were found around microvessels in the tunica adventitia, whereas there were some NG2+ only cells in the tunica media (Figure 4.8D), indicating that the SOX10+ cells around microvessels are a part of pericytes. To further determine whether these SOX10+ cells lining microvessels were related to SMCs and microvascular endothelial cells, immunostaining was performed, and the results showed that none of SOX10+ cells expressed CNN1 (Figure 4.8A) and CD31, a marker of microvascular endothelial cells (Figure 4.8B). In addition, a previous study has shown that S100β is a marker of SOX10+ vascular stem cells *in vitro* and *in vivo* [60]. Interestingly, cells double-positive for SOX10 and S100β were found around microvessels, whereas some cells were only SOX10+, there were no cells only positive for S100β (Figure 4.8C).

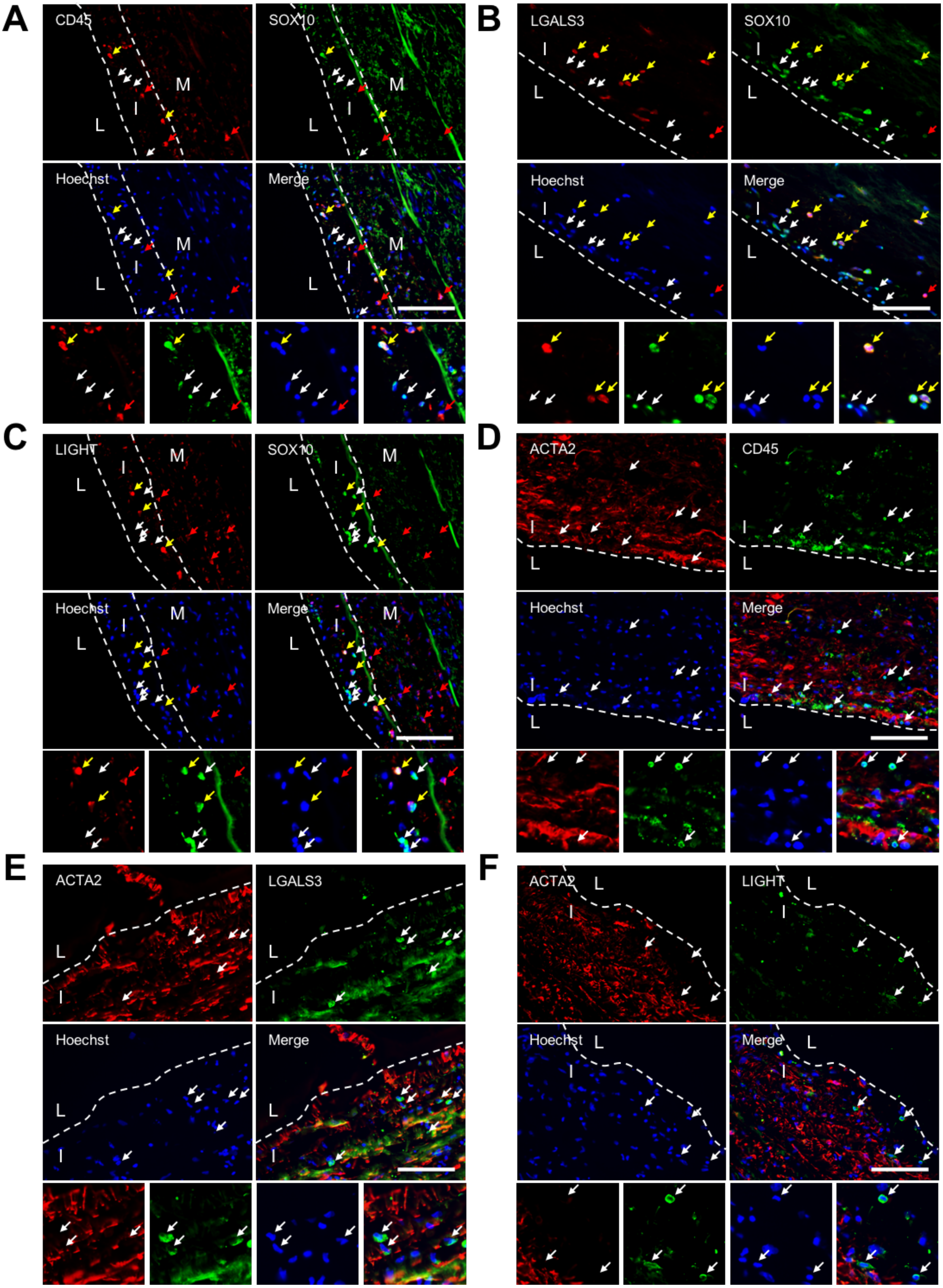
A
CD45
SOX10
Hoechst
Merge
M
I
L
B
LGALS3
SOX10
Hoechst
Merge
I
L
C
LIGHT
SOX10
Hoechst
Merge
M
I
L
D
ACTA2
CD45
Hoechst
Merge
I
L
E
ACTA2
LGALS3
Hoechst
Merge
L
I
F
ACTA2
LIGHT
Hoechst
Merge
L
I

Figure 4.6. Identification of inflammatory cells expressing SOX10, but not SMC marker in the lesions of diseased blood vessels. Immunofluorescence staining showed that **(A)** CD45+ leukocytes, **(B)** LGALS3+ macrophages and **(C)** LIGHT+ foam cells could express SOX10 within the lesions. Immunostaining revealed that SMC marker ACTA2 was not expressed in **(D)** CD45+ leukocytes, **(E)** LGALS3+ macrophages and **(F)** LIGHT+ foam cells. Yellow arrows pointed cells double-positive for SOX10 and inflammatory markers, white arrows indicated cells expressed SOX10 alone, and red arrows pointed cells expressed inflammatory markers alone in **(A-C)**. White arrows pointed cells expressed inflammatory markers alone in **(D-F)**. Scale bar = 100 μm.

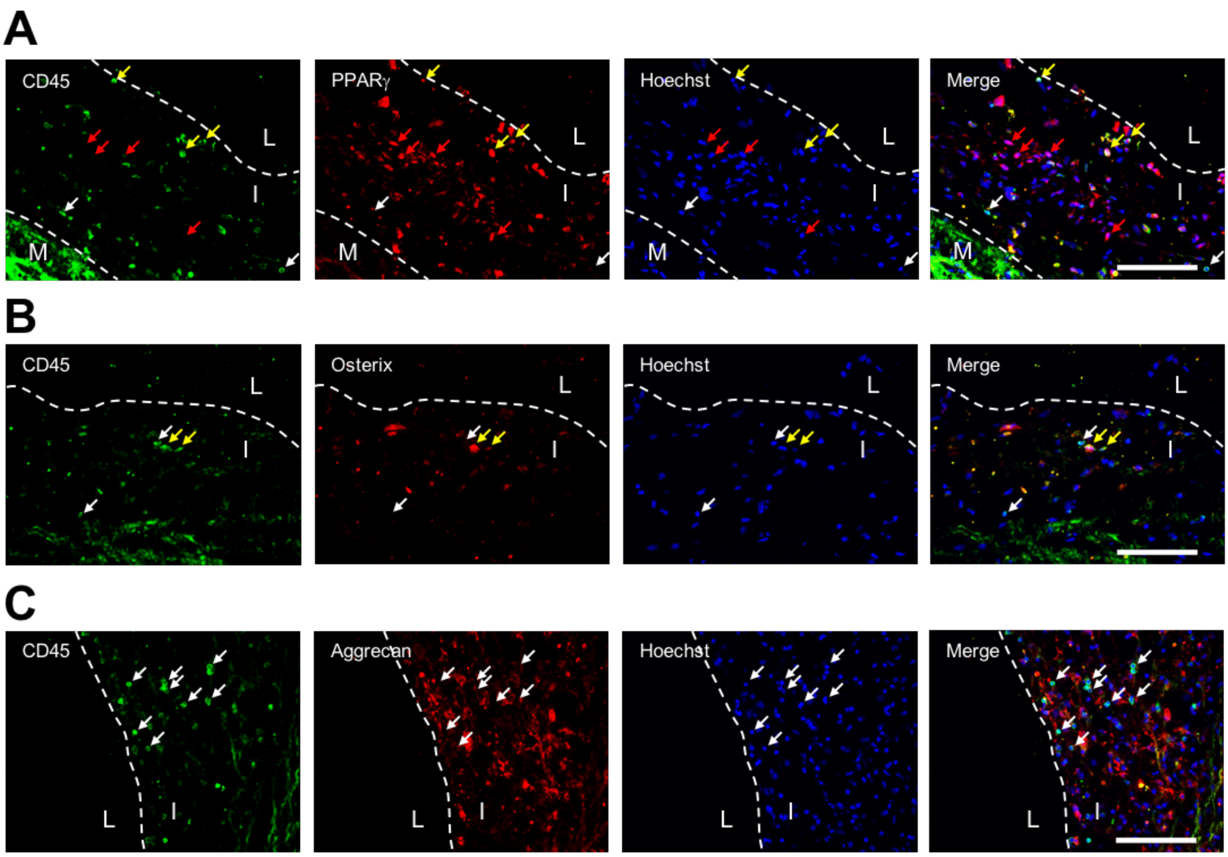

Figure 4.7. *In vivo* transdifferentiation of CD45+ leukocytes/inflammatory cells in the lesions of diseased blood vessels. Immunofluorescence staining showed that CD45+ leukocytes positive for **(A)** adipogenic marker (PPARγ), **(B)** osteogenic marker (Osterix), but not **(C)** chondrogenic marker (Aggrecan) within the lesions. Yellow arrows pointed cells double-positive for CD45 and differentiated markers, white arrows indicated cells expressed CD45 alone, and red arrows pointed cells expressed differentiated markers alone in **(A-C)**. Scale bar = 100 μm.

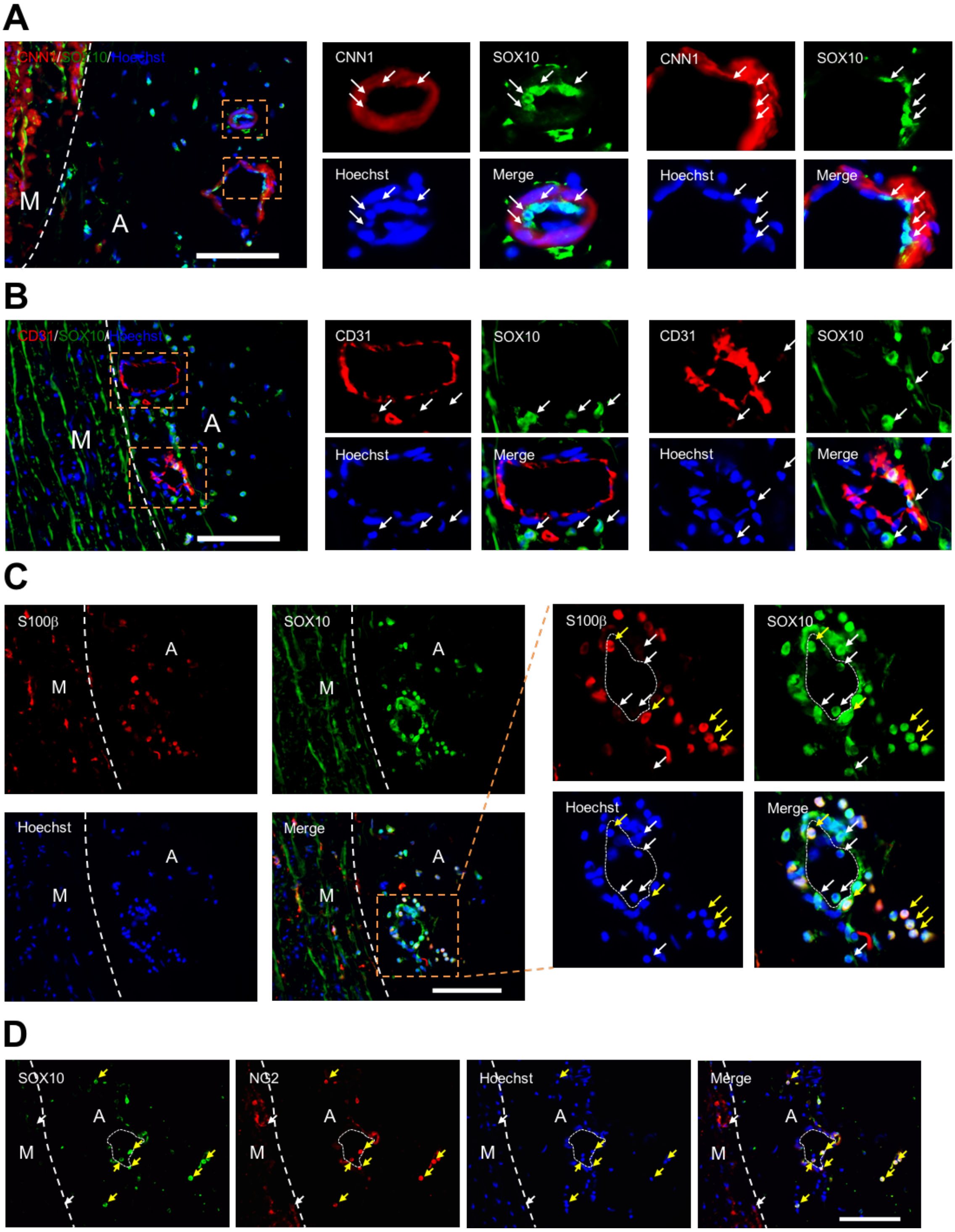

Figure 4.8. Identification of SOX10+ stem cells around microvessels in tunica adventitia of diseased vessels. (A) SOX10+ cells without the expression of CNN1 were found lining on the inner surface of microvessel. **(B)** SOX10+ cells did not express microvascular endothelial cell marker CD31. **(C)** Double-positive for S100β and SOX10 cells were detected. **(D)** SOX10+ cells expressed the pericyte marker NG2. White arrows pointed cells expressed SOX10 alone in **(A-C)** and NG2 alone in **(D)**, yellow arrows indicated cells double-positive for SOX10 and S100β in **(C)**, and NG2 in **(D)**. Dashed lines indicated microvessel in **(C)** and **(D)**. Scale bar = 100 μm.

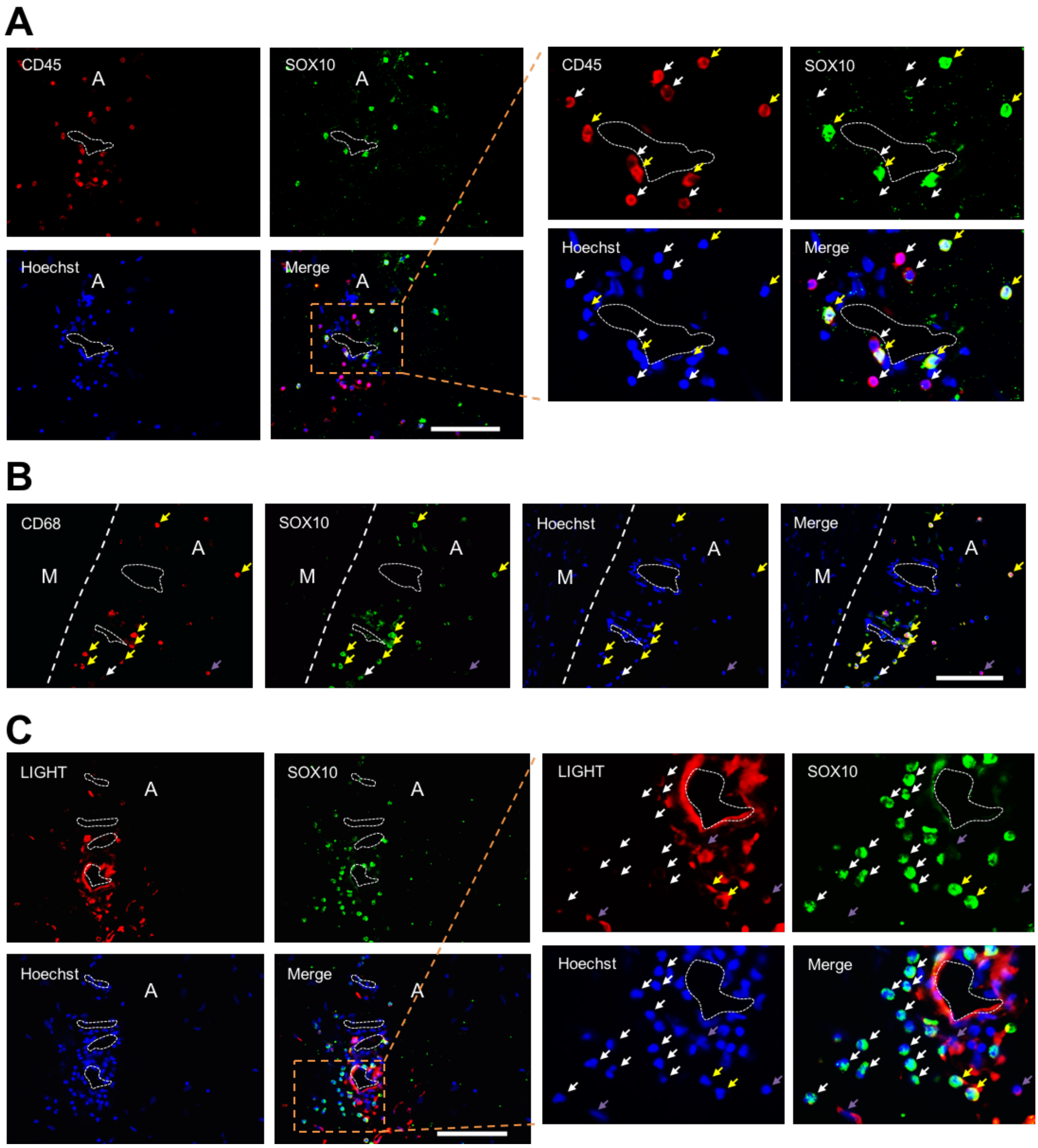

Figure 4.9. Identification of inflammatory cells expressing SOX10 around microvessels in tunica adventitia of diseased vessels. Immunofluorescence staining showed that **(A)** CD45+ leukocytes, **(B)** CD68+ macrophages and **(C)** LIGHT+ foam cells could express SOX10 around microvessels of tunica adventitia. Yellow arrows pointed cells double-positive for SOX10 and inflammatory markers, white arrows indicated cells expressed inflammatory marker CD45 alone in **(A)**, and SOX10 alone in **(B-C)**, and purple arrows pointed cells expressed inflammatory markers CD68 alone in **(B)** and LIGHT alone in **(C)**. Dashed lines illustrated microvessel in **(A)**, **(B)** and **(C)**. Scale bar = 100 μm.

As mentioned previously, inflammatory cells can express SOX10 during the development of vascular disease. Various types of inflammatory cells were detected to be expressing SOX10 around microvessels in the tunica adventitia as well. To further determine the cellular composition of these cells around microvessels, immunofluorescence staining for inflammatory markers (CD45, CD68 and LIGHT) and SOX10 was performed. Around adventitial microvessels, the expression of SOX10 was detected in CD45+ leukocytes (Figure 4.9A), as well as in CD68+ macrophages (Figure 4.9B) and LIGHT+ foam cells (Figure 4.9C), suggesting that the circulating leukocytes entering into the diseased blood vessels through microvessels could express SOX10, and subsequently differentiated into macrophages and foam cells *in vivo* during the progression of vascular disease. Taken together, these results suggest that SOX10+ cells around adventitial microvessels may be derived from pericytes or circulating leukocytes, and participated in the remodeling of vessel wall.

4.3.7 Determination of the Relationship between SMCs and SOX10+ Cells by Lineage Tracing

The origins of the differentiated vascular cells accumulated within the atherosclerotic lesions are not fully understood and remain a crucial issue to be addressed. In this study, we have shown the existence of SOX10+ stem cells in the tunica media, tunica adventitia and lesions in the tunica intima. Furthermore, these cells were capable of differentiating into different types of cells to contribute to vascular disease *in vivo* after vascular injury. The origins of these SOX10+ cells remain ambiguous, however; they might be derived from resident stem cells in blood vessel walls or from SMCs via a phenotypically de-differentiation transition. To determine whether SMCs may de-differentiate into SOX10+ cells, we performed an *in situ* polymerase chain reaction proximity ligation assay (ISPCR-PLA) that was modified with a recently developed method from another laboratory (Figure 4.10B) [78]. This technique allows lineage-specific epigenetic signatures to persist in cells based on the detection of histone modifications in specific gene promoters. In this study, the detection of the histone modification H3K4me2 in the *MYH11* promoter was used and permitted us to exclusively label the cell populations of SMC-derived cells and SMCs (Figure 4.10A), even though they failed to express the SMC markers such as ACTA2, CNN1 and SM-MHC.

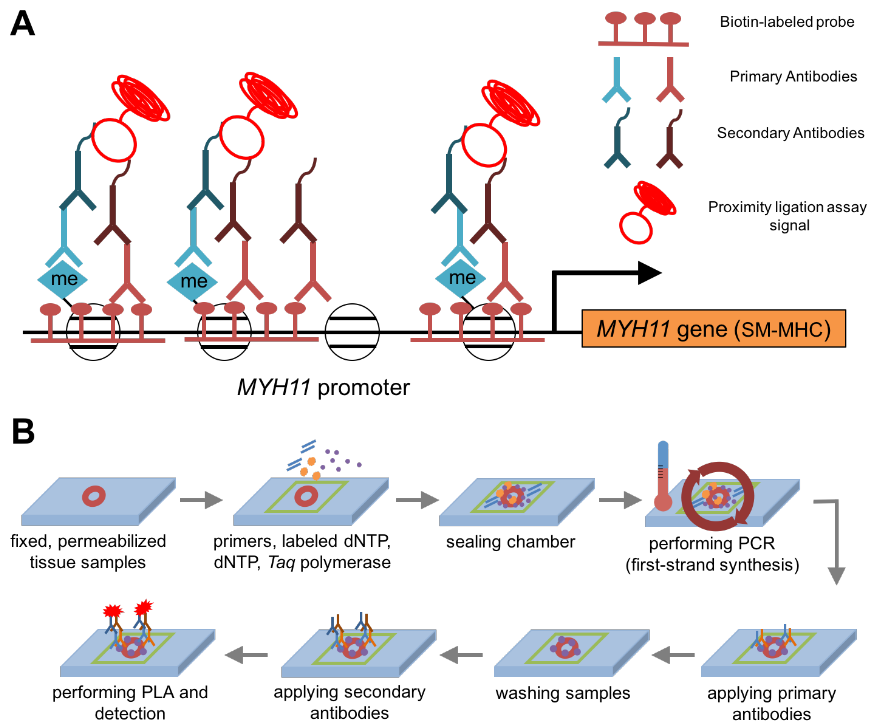

Figure 4.10. Lineage tracing of SMCs and SMC-derived cells by ISPCR-PLA method. (A) Schematic outline of the detection of histone modification H3K4me2 in the *MYH11* promoter in tissue sections. **(B)** Schematic protocol of ISPCR-PLA for detecting SMCs and SMC-derived cells.

To determine the relationship between SMCs and SOX10+ cells, immunofluorescence staining for SOX10 and the detection of ISPCR-PLA were performed to label SMC-lineage cells within atherosclerotic lesions from different arterial sections. In the lesion areas, ~84% of the cells were PLA+ (SMCs or SMC-derived cells), whereas ~54% of the cells expressed SOX10. Based on the immunostaining and PLA labeling, three distinct cell populations were identified within the lesions (Figure 4.11B): ~42% PLA+SOX10- cells (Figure 4.11A, D, F), ~42% PLA+SOX10+ cells (Figure 4.11A, D, E, F) and ~12% PLA-SOX10+ cells (Figure 4.11A, D, E).

We then further analyzed the cellular composition of these lesional cells and found that 77% of SOX10+ cells co-expressed the SMC-specific epigenetic signature PLA (PLA+SOX10+ cells, 42% of total cell population within the lesions, Figure 4.11B, C). These cells may be of SMC origin and then phenotypically changed to express SOX10, or may have been SOX10-positive cells that spontaneously differentiated into SMCs, but which process occurred first was unidentified. In addition, we found that 23% of SOX10+ cells were negative for PLA labeling (PLA-SOX10+ cells, 12% of total cell population within the lesions, Figure 4.11B, C), demonstrating that these cells were derived from resident stem cells or inflammatory cell-derived cells, and were not of SMC origin.

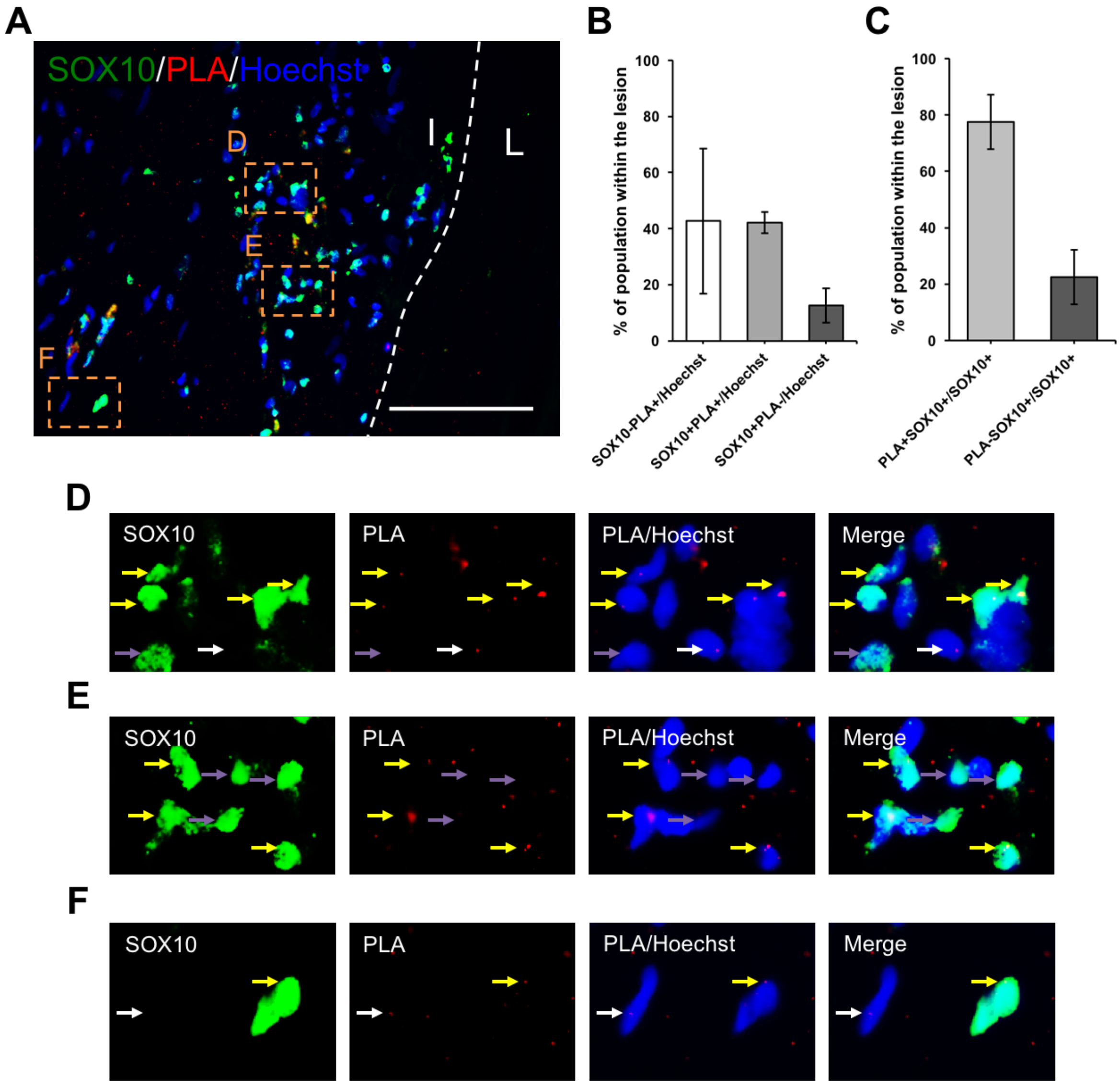

Figure 4.11. Relationship of SMCs and SOX10+ cells in the lesions by ISPCR-PLA. (A) Immunofluorescence staining combined with ISPCR-PLA for the detection of SOX10 and epigenetic modification H3K4me2 in *MYH11*. Three distinct cell populations were identified as shown at higher magnification in **(D)**, **(E)** and **(F)**, and indicated with different arrows. **(B)** Quantitative analysis of these three cell populations within the lesions with correction for the efficiency of PLA labeling. Yellow arrows pointed cells double-positive for SOX10 and PLA (PLA+SOX10+), white arrows indicated cells labeled with PLA alone (PLA+SOX10-), and purple arrows pointed cells positive for SOX10 alone (PLA-SOX10+). Scale bar = 100 μm.

4.4 Discussion

The development of vascular disease is a long-term and complicated process that includes that cell migration, proliferation, differentiation, accumulation and extracellular matrix production. Each of these factors can affect the extent of vascular disease. It has been reported that various types of cells, such as SMCs [78, 79, 98], hematopoietic cells [86-88], MSC-like cells [90, 91] and adventitial progenitor cells [94, 95], can differentiate into various types of cells repopulated in the lesions and then result in vascular disease. In addition, a previous study has shown that MVSCs isolated from the tunica media are able to differentiate into mesenchymal cells *in vitro* and *in vivo*, and contribute to vascular diseases in a rat model. In this study, we took advantage of the methods described previously [60, 78] to ascertain whether vascular stem cells, rather than SMCs, are involved in the progression of vascular disease.

The identification of SOX10+ stem cells *in vitro* shows that there is indeed a population of cells exhibits the characteristics of NCSCs, which can be isolated from the tunica media by explant culture. In primary culture, some of these SOX10+ cells expressed low levels of the SMC markers ACTA2 and CNN1, but not the mature SMC marker SM-MHC. In addition, SOX10+ cells were not positive for inflammatory cell markers CD45 and CD68, suggesting that these primary SOX10+ cells are not SMCs and inflammatory cells. After being cultured for several passages, these cells homogeneously expressed SOX10 without the expression of ACTA2, CNN1 and SM-MHC, demonstrating that the SOX10+ cells rapidly proliferate and eventually dominate the cell culture, which is consistent with a previous study [60]. Conventional explant culture methods show that cells migrating out from tissue pieces express SMC markers and can be considered as synthetic/proliferative SMCs [99, 100]. However, these explant cultures are under high-levels of serum-containing medium, which may cause the cells inside explant tissues to spontaneously differentiate into immature SMCs and migrate out simultaneously. Our *in vitro* medium screening results support the evidence that SOX10+ cells undergo differentiation when cultured in 10% FBS medium, which may explain the apparent discrepancy of immature SMCs or SMCs, rather than VSCs, that are obtained by using conventional explant culture methods. On the other hand, the multipotency of the SOX10+ cells, allowing differentiation into SMCs, chondrocytes, adipocytes and osteoblasts provides a reasonable explanation for the complex cellular composition in the lesions of diseased blood vessels.

In addition to SOX10+ cells isolated from the tunica media *in vitro*, the existence of SOX10+ cells in both normal and diseased blood vessels was verified in this study. SOX10+ cells were only found in the tunica media of normal blood vessels, but were observed in the tunica intima lesions and on the border between the tunica media and tunica adventitia of diseased vessels, accompanied by an increase of SOX10+ cells. Moreover, all of these SOX10+ cells in normal or diseased vessels did not express the SMC marker CNN1, which means that these cells were not mature SMCs. Overall, it is possible that these SOX10+ cells may be derived from a small population of dormant stem cells, instead of from SMCs in blood vessels, and activated to proliferate or differentiate in response to vascular injury and remodeling. Similar to the differentiation potentials of SOX10+ cells *in vitro*, these cells showed multipotent differentiation into chondrocytes, adipocytes and osteoblasts within the lesions of diseased vessels *in vivo*. These findings support the direct evidence that the activation, expansion and differentiation of SOX10+ cells may contribute to fat deposition, cartilage formation, vascular calcification and extracellular matrix remodeling during vascular disease.

The origins of differentiated vascular cells accumulated in the lesions have attracted much interest and could unveil the mechanisms of vascular pathogenesis. Lineage tracing is a powerful and well-established approach to identify the origins of lesional cells; however, it is nearly impossible to apply to human beings due to ethical concerns. Recent studies by the Owens laboratory [78] established a technique that allows lineage-specific epigenetic signatures to persist in desired cells permanently via detection of histone modifications in the lineage-specific gene promoter, even though these cells fail to express the lineage-specific markers. Based on this method, we were able to label the cells of SMC-lineage in histological sections, and then determine that there were three distinct cell populations within the atherosclerotic lesions: SMCs/SMC-derived cells (PLA+SOX10-), SMC marker-expressing SOX10+ stem cells (PLA+SOX10+) and non-SMC origin SOX10+ stem cells (PLA-SOX10+). It is clear that PLA-SOX10+ cells are stem cell-derived or inflammatory cell-derived cell populations and not of SMC origin. In contrast, for the PLA+SOX10+ cell population, there are two possible explanations. First, these cells may be entirely or partially derived from SOX10+ stem cells that then differentiated into SMC-lineage cells. Second, they may instead be derived from mature SMCs that then phenotypically de-differentiated into SOX10-expressing stem cells. Which process occurred first is unknown. Similar to the PLA+SOX10+ cells, the PLA+SOX10- cells may also be derived from SOX10+ stem cells that subsequently lost stemness and differentiated into SMC-lineage cells. However, we cannot exclude the possibility that these cells are of SMC origin and then differentiated into various types of cells accumulated within the lesions. Since the development of human vascular diseases is a chronic process involving in cell proliferation, migration and differentiation, a detailed lineage tracing method is required for deciphering the fate and dynamics of cells at different stages during vascular pathogenesis.

In addition to the SOX10+ cells that were found in the tunica media and lesions in the tunica intima, the existence of these cells around microvessels of the tunica adventitia was also observed. These cells were able to co-express SOX10 and inflammatory cell markers such as CD45, CD68, LGALS3 and LIGHT, indicating that circulating leukocytes can enter the adventitial layer from microvessels, and then be activated to express SOX10 and differentiate into different types of vascular cells, as well as migrating towards the luminal side of the blood vessel in response to pathophysiological cues, which is consistent with previously studies [101, 102]. We also found that S100β, a MVSC marker, was expressed in SOX10+ cells around microvessels, but not all of SOX10+ cells were positive for S100β, suggesting that S100β may be a marker of partially differentiated SOX10+ stem cells in human blood vessels. Another finding was that the SOX10+ cells around microvessels were not derived from CD31+ microvascular endothelial cells and were able to express NG2, a marker of pericytes, which implies that these cells may be associated with pericytes and may participate in microvascular formation and remodeling.

In summary, this study provides evidence that aberrant activation and differentiation of SOX10+ cells may play a crucial role in the development of vascular disease, resulting in proliferative and differentiated cells accumulated in lesions in blood vessel walls. In addition, the identification of the origins of these cells provides a novel insight into the role of stem cells in vascular disease and remodeling, and has significant implications in clinical vascular biology. Overall, these results show SOX10+ stem cells to be a promising model to unravel the mechanisms of vascular pathogenesis and a potential therapeutic target of vascular disease.

Chapter 5: Conclusion

5.1 Dissertation Conclusions and Broader Implications

The focus of my research is to investigate the role of stem cells in tissue regeneration of the peripheral nerve system and in the development of vascular disease. As we know, stem cells have self-renewal ability and great plasticity that can give rise to desired cell types under the appropriate conditions. Different environmental cues, such as secreted growth factors, cell-cell interactions and cell-extracellular matrix interactions, can dramatically impact genetic expression and cellular behavior of stem cells, subsequently affecting tissue formation and disease development. In this dissertation, we performed several types of cells, such as NCSCs, NCSC-SCs and MPCs, combined with different carrier hydrogels in nanofibrous PLCL nerve conduits to connect transected sciatic nerves in a well-established peripheral nerve repair rat model. Based on this experiment, the selection of the appropriate stem cell type to facilitate nerve recovery is an important key for cell therapy in regenerative medicine. In addition, the role of stem cells involved in the development of vascular disease and the mechanisms of stem cell differentiation and proliferation is also explored via a lineage tracing technique.

In **Chapter 2**, we established a reliable protocol to derive NCSCs from human integration-free iPSCs, and these NCSCs exhibited great multipotency towards cells of neural lineages and mesenchymal lineages. Moreover, to investigate the therapeutic effect of differentiation stage of stem cells, we utilized NCSCs and NCSC-SCs with nanofibrous PLCL nerve conduits for peripheral nerve tissue engineering in a rat model. The results showed that transplantation of NCSCs had better motor nerve recovery in both early-stage and long-term muscle innervation recovery than that of NCSC-SCs. When exploring the cellular composition of NCSC differentiation in nerve conduits, we observed that NCSCs mainly differentiated into Schwann cells, which can effectively promote nerve repair through the myelination of injured nerve tissues. In addition, we elucidate the mechanism of NCSC-promoted nerve regeneration in detail. The secretion of essential neurotrophic factors by paracrine signaling may help NCSCs to differentiate into functional Schwann cells and then successfully integrate into newly-growing host axons, leading to a superior therapeutic effect in peripheral nerve regeneration.

In **Chapter 3**, we showed that MPCs possess multipotent differentiation ability *in vitro* as described previously, making them a promising cell source for cell therapy in nerve regeneration. In this study, we combined MPCs with Matrigel in a nanofibrous PLCL nerve conduit to bridge transected sciatic nerves in a peripheral nerve regeneration rat model to investigate whether MPCs can promote nerve repair at early and long-term stages. Based on the results, however, the recovery of the conduction of electrical signal and the neuromuscular innervation of sciatic nerve was relative low compared to the autograft group, and it is likely that MPCs cannot facilitate nerve regeneration for long-term recovery. Furthermore, we observed that these MPCs not only cannot differentiate into Schwann cells for myelination and peripheral neurons for nerve regrowth, but these cells also have a low survival rate in nerve conduits, which results in the failure of nerve regeneration *in vivo*.

In **Chapter 4**, we isolated VSCs from human normal and diseased blood vessels, and showed that these cells possess multilineage differentiation potential *in vitro*. Based on our explant culture results, we also clarified the mechanism by which cells migrate out from explant tissues, which demonstrated that SOX10+ cells are found to proliferate and migrate simultaneously inside explant vessels. On the other hand, we identified the existence of SOX10+ cells without the expression of SMC markers in the tunica media and in lesions of normal and diseased vessels, which indicates that these cells are not mature SMCs and can be activated to proliferate *in vivo* after vascular injury. In addition, we also provided vigorous evidence that SOX10+ cells can differentiate into various cell types and contribute to atherosclerotic lesions *in vivo*, which shows that vascular diseases are attributed to the aberrant stem cell proliferation and differentiation. Importantly, based on the ISPCR-PLA lineage tracing technique, we successfully identified the existence of a population of SOX10+ cells within the lesions, which are indeed resident stem cells that did not originate from SMCs.

In summary, this dissertation demonstrated that the stem cell differentiation stage and paracrine signaling are extremely crucial for cell fate and tissue recovery, which may result in discrepancies in peripheral nerve regeneration, as well as in other tissues. This work therefore has important implications for the selection of suitable stem cells for cell therapy and for the mechanism of tissue regeneration. In addition, my study of vascular stem cells shows strong evidence that aberrant proliferation and differentiation of SOX10+ cells may play a critical role in the development of vascular disease, and provides a novel insight into the mechanisms of vascular pathogenesis and potential therapeutic targets of vascular disease.

References

[1] K. Takahashi, K. Tanabe, M. Ohnuki, M. Narita, T. Ichisaka, K. Tomoda, S. Yamanaka, Induction of pluripotent stem cells from adult human fibroblasts by defined factors, Cell 131(5) (2007) 861-72.

[2] J. Yu, M.A. Vodyanik, K. Smuga-Otto, J. Antosiewicz-Bourget, J.L. Frane, S. Tian, J. Nie, G.A. Jonsdottir, V. Ruotti, R. Stewart, Slukvin, II, J.A. Thomson, Induced pluripotent stem cell lines derived from human somatic cells, Science 318(5858) (2007) 1917-20.

[3] M. Wernig, A. Meissner, R. Foreman, T. Brambrink, M. Ku, K. Hochedlinger, B.E. Bernstein, R. Jaenisch, In vitro reprogramming of fibroblasts into a pluripotent ES-cell-like state, Nature 448(7151) (2007) 318-24.

[4] D. Huangfu, K. Osafune, R. Maehr, W. Guo, A. Eijkelenboom, S. Chen, W. Muhlestein, D.A. Melton, Induction of pluripotent stem cells from primary human fibroblasts with only Oct4 and Sox2, Nat Biotechnol 26(11) (2008) 1269-75.

[5] I.H. Park, R. Zhao, J.A. West, A. Yabuuchi, H. Huo, T.A. Ince, P.H. Lerou, M.W. Lensch, G.Q. Daley, Reprogramming of human somatic cells to pluripotency with defined factors, Nature 451(7175) (2008) 141-6.

[6] J.B. Kim, H. Zaehres, G. Wu, L. Gentile, K. Ko, V. Sebastiano, M.J. Arauzo-Bravo, D. Ruau, D.W. Han, M. Zenke, H.R. Scholer, Pluripotent stem cells induced from adult neural stem cells by reprogramming with two factors, Nature 454(7204) (2008) 646-50.

[7] J.B. Kim, V. Sebastiano, G. Wu, M.J. Arauzo-Bravo, P. Sasse, L. Gentile, K. Ko, D. Ruau, M. Ehrich, D. van den Boom, J. Meyer, K. Hubner, C. Bernemann, C. Ortmeier, M. Zenke, B.K. Fleischmann, H. Zaehres, H.R. Scholer, Oct4-induced pluripotency in adult neural stem cells, Cell 136(3) (2009) 411-9.

[8] C.W. Chang, Y.S. Lai, K.M. Pawlik, K. Liu, C.W. Sun, C. Li, T.R. Schoeb, T.M. Townes, Polycistronic lentiviral vector for "hit and run" reprogramming of adult skin

fibroblasts to induced pluripotent stem cells, Stem Cells 27(5) (2009) 1042-9.

[9] K. Kaji, K. Norrby, A. Paca, M. Mileikovsky, P. Mohseni, K. Woltjen, Virus-free induction of pluripotency and subsequent excision of reprogramming factors, Nature 458(7239) (2009) 771-5.

[10] D. Kim, C.H. Kim, J.I. Moon, Y.G. Chung, M.Y. Chang, B.S. Han, S. Ko, E. Yang, K.Y. Cha, R. Lanza, K.S. Kim, Generation of human induced pluripotent stem cells by direct delivery of reprogramming proteins, Cell Stem Cell 4(6) (2009) 472-6.

[11] K. Okita, M. Nakagawa, H. Hyenjong, T. Ichisaka, S. Yamanaka, Generation of mouse induced pluripotent stem cells without viral vectors, Science 322(5903) (2008) 949-53.

[12] M. Stadtfeld, M. Nagaya, J. Utikal, G. Weir, K. Hochedlinger, Induced pluripotent stem cells generated without viral integration, Science 322(5903) (2008) 945-9.

[13] K. Woltjen, I.P. Michael, P. Mohseni, R. Desai, M. Mileikovsky, R. Hamalainen, R. Cowling, W. Wang, P. Liu, M. Gertsenstein, K. Kaji, H.K. Sung, A. Nagy, piggyBac transposition reprograms fibroblasts to induced pluripotent stem cells, Nature 458(7239) (2009) 766-70.

[14] J. Yu, K. Hu, K. Smuga-Otto, S. Tian, R. Stewart, Slukvin, II, J.A. Thomson, Human induced pluripotent stem cells free of vector and transgene sequences, Science 324(5928) (2009) 797-801.

[15] H. Zhou, S. Wu, J.Y. Joo, S. Zhu, D.W. Han, T. Lin, S. Trauger, G. Bien, S. Yao, Y. Zhu, G. Siuzdak, H.R. Scholer, L. Duan, S. Ding, Generation of induced pluripotent stem cells using recombinant proteins, Cell Stem Cell 4(5) (2009) 381-4.

[16] L. Warren, P.D. Manos, T. Ahfeldt, Y.H. Loh, H. Li, F. Lau, W. Ebina, P.K. Mandal, Z.D. Smith, A. Meissner, G.Q. Daley, A.S. Brack, J.J. Collins, C. Cowan, T.M. Schlaeger, D.J. Rossi, Highly efficient reprogramming to pluripotency and directed differentiation of human cells with synthetic modified mRNA, Cell Stem Cell 7(5) (2010) 618-30.

[17] J.S. Belkas, M.S. Shoichet, R. Midha, Peripheral nerve regeneration through guidance tubes, Neurol Res 26(2) (2004) 151-60.

[18] C.E. Schmidt, J.B. Leach, Neural tissue engineering: strategies for repair and regeneration, Annu Rev Biomed Eng 5 (2003) 293-347.

[19] S.Y. Fu, T. Gordon, The cellular and molecular basis of peripheral nerve regeneration, Mol Neurobiol 14(1-2) (1997) 67-116.

[20] T. Hadlock, C. Sundback, D. Hunter, M. Cheney, J.P. Vacanti, A polymer foam conduit seeded with Schwann cells promotes guided peripheral nerve regeneration, Tissue Eng 6(2) (2000) 119-27.

[21] C. Miller, S. Jeftinija, S. Mallapragada, Micropatterned Schwann cell-seeded biodegradable polymer substrates significantly enhance neurite alignment and outgrowth, Tissue Eng 7(6) (2001) 705-15.

[22] D.M. Thompson, H.M. Buettner, Neurite outgrowth is directed by schwann cell alignment in the absence of other guidance cues, Ann Biomed Eng 34(1) (2006) 161-8.

[23] D.L. Stemple, D.J. Anderson, Isolation of a stem cell for neurons and glia from the mammalian neural crest, Cell 71(6) (1992) 973-85.

[24] K.R. Jessen, R. Mirsky, The origin and development of glial cells in peripheral nerves, Nat Rev Neurosci 6(9) (2005) 671-82.

[25] A. Woodhoo, L. Sommer, Development of the Schwann cell lineage: from the neural crest to the myelinated nerve, Glia 56(14) (2008) 1481-90.

[26] J.F. Crane, P.A. Trainor, Neural crest stem and progenitor cells, Annu Rev Cell Dev Biol 22 (2006) 267-86.

[27] G. Lee, H. Kim, Y. Elkabetz, G. Al Shamy, G. Panagiotakos, T. Barberi, V. Tabar,

L. Studer, Isolation and directed differentiation of neural crest stem cells derived from human embryonic stem cells, Nat Biotechnol 25(12) (2007) 1468-75.

[28] G. Lee, S.M. Chambers, M.J. Tomishima, L. Studer, Derivation of neural crest cells from human pluripotent stem cells, Nat Protoc 5(4) (2010) 688-701.

[29] L. Menendez, M.J. Kulik, A.T. Page, S.S. Park, J.D. Lauderdale, M.L. Cunningham, S. Dalton, Directed differentiation of human pluripotent cells to neural crest stem cells, Nat Protoc 8(1) (2013) 203-12.

[30] A. Wang, Z. Tang, I.H. Park, Y. Zhu, S. Patel, G.Q. Daley, S. Li, Induced pluripotent stem cells for neural tissue engineering, Biomaterials 32(22) (2011) 5023-32.

[31] F. Stang, H. Fansa, G. Wolf, M. Reppin, G. Keilhoff, Structural parameters of collagen nerve grafts influence peripheral nerve regeneration, Biomaterials 26(16) (2005) 3083-91.

[32] S. Patel, K. Kurpinski, R. Quigley, H. Gao, B.S. Hsiao, M.M. Poo, S. Li, Bioactive nanofibers: synergistic effects of nanotopography and chemical signaling on cell guidance, Nano Lett 7(7) (2007) 2122-8.

[33] Y.T. Kim, V.K. Haftel, S. Kumar, R.V. Bellamkonda, The role of aligned polymer fiber-based constructs in the bridging of long peripheral nerve gaps, Biomaterials 29(21) (2008) 3117-27.

[34] Y. Lei, S. Gojgini, J. Lam, T. Segura, The spreading, migration and proliferation of mouse mesenchymal stem cells cultured inside hyaluronic acid hydrogels, Biomaterials 32(1) (2011) 39-47.

[35] J. Jin, M. Park, A. Rengarajan, Q. Zhang, S. Limburg, S.K. Joshi, S. Patel, H.T. Kim, A.C. Kuo, Functional motor recovery after peripheral nerve repair with an aligned nanofiber tubular conduit in a rat model, Regen Med 7(6) (2012) 799-806.

[36] J. Jin, S. Limburg, S.K. Joshi, R. Landman, M. Park, Q. Zhang, H.T. Kim, A.C.

Kuo, Peripheral nerve repair in rats using composite hydrogel-filled aligned nanofiber conduits with incorporated nerve growth factor, Tissue Eng Part A 19(19-20) (2013) 2138-46.

[37] Y. Zhu, A. Wang, S. Patel, K. Kurpinski, E. Diao, X. Bao, G. Kwong, W.L. Young, S. Li, Engineering bi-layer nanofibrous conduits for peripheral nerve regeneration, Tissue Eng Part C Methods 17(7) (2011) 705-15.

[38] C.A. Heath, G.E. Rutkowski, The development of bioartificial nerve grafts for peripheral-nerve regeneration, Trends Biotechnol 16(4) (1998) 163-8.

[39] S. Parrinello, I. Napoli, S. Ribeiro, P. Wingfield Digby, M. Fedorova, D.B. Parkinson, R.D. Doddrell, M. Nakayama, R.H. Adams, A.C. Lloyd, EphB signaling directs peripheral nerve regeneration through Sox2-dependent Schwann cell sorting, Cell 143(1) (2010) 145-55.

[40] X. Ke, Q. Li, L. Xu, Y. Zhang, D. Li, J. Ma, X. Mao, Netrin-1 overexpression in bone marrow mesenchymal stem cells promotes functional recovery in a rat model of peripheral nerve injury, J Biomed Res 29(5) (2015) 380-9.

[41] A. Kishino, Y. Ishige, T. Tatsuno, C. Nakayama, H. Noguchi, BDNF prevents and reverses adult rat motor neuron degeneration and induces axonal outgrowth, Exp Neurol 144(2) (1997) 273-86.

[42] N.I. Bamber, H. Li, X. Lu, M. Oudega, P. Aebischer, X.M. Xu, Neurotrophins BDNF and NT-3 promote axonal re-entry into the distal host spinal cord through Schwann cell-seeded mini-channels, Eur J Neurosci 13(2) (2001) 257-68.

[43] C. Bucci, P. Alifano, L. Cogli, The role of rab proteins in neuronal cells and in the trafficking of neurotrophin receptors, Membranes (Basel) 4(4) (2014) 642-77.

[44] L.A. Greene, D.R. Kaplan, Early events in neurotrophin signalling via Trk and p75 receptors, Curr Opin Neurobiol 5(5) (1995) 579-87.

[45] B.D. Carter, C. Kaltschmidt, B. Kaltschmidt, N. Offenhauser, R. Bohm-Matthaei,

P.A. Baeuerle, Y.A. Barde, Selective activation of NF-kappa B by nerve growth factor through the neurotrophin receptor p75, Science 272(5261) (1996) 542-5.

[46] D.L. Shelton, J. Sutherland, J. Gripp, T. Camerato, M.P. Armanini, H.S. Phillips, K. Carroll, S.D. Spencer, A.D. Levinson, Human trks: molecular cloning, tissue distribution, and expression of extracellular domain immunoadhesins, J Neurosci 15(1 Pt 2) (1995) 477-91.

[47] S. Walsh, R. Midha, Practical considerations concerning the use of stem cells for peripheral nerve repair, Neurosurg Focus 26(2) (2009) E2.

[48] F.J. Rodriguez, E. Verdu, D. Ceballos, X. Navarro, Nerve guides seeded with autologous schwann cells improve nerve regeneration, Exp Neurol 161(2) (2000) 571-84.

[49] M. Tohill, G. Terenghi, Stem-cell plasticity and therapy for injuries of the peripheral nervous system, Biotechnol Appl Biochem 40(Pt 1) (2004) 17-24.

[50] S.K. Lee, S.W. Wolfe, Peripheral nerve injury and repair, J Am Acad Orthop Surg 8(4) (2000) 243-52.

[51] J.S. Taylor, E.T. Bampton, Factors secreted by Schwann cells stimulate the regeneration of neonatal retinal ganglion cells, J Anat 204(1) (2004) 25-31.

[52] J.D. Bulken-Hoover, W.M. Jackson, Y. Ji, J.A. Volger, R.S. Tuan, L.J. Nesti, Inducible expression of neurotrophic factors by mesenchymal progenitor cells derived from traumatically injured human muscle, Mol Biotechnol 51(2) (2012) 128-36.

[53] W.M. Jackson, P.G. Alexander, J.D. Bulken-Hoover, J.A. Vogler, Y. Ji, P. McKay, L.J. Nesti, R.S. Tuan, Mesenchymal progenitor cells derived from traumatized muscle enhance neurite growth, J Tissue Eng Regen Med 7(6) (2013) 443-51.

[54] W.M. Jackson, A.B. Aragon, F. Djouad, Y. Song, S.M. Koehler, L.J. Nesti, R.S. Tuan, Mesenchymal progenitor cells derived from traumatized human muscle, J Tissue Eng Regen Med 3(2) (2009) 129-38.

[55] L.J. Nesti, W.M. Jackson, R.M. Shanti, S.M. Koehler, A.B. Aragon, J.R. Bailey, M.K. Sracic, B.A. Freedman, J.R. Giuliani, R.S. Tuan, Differentiation potential of multipotent progenitor cells derived from war-traumatized muscle tissue, J Bone Joint Surg Am 90(11) (2008) 2390-8.

[56] W.M. Jackson, T.P. Lozito, F. Djouad, N.Z. Kuhn, L.J. Nesti, R.S. Tuan, Differentiation and regeneration potential of mesenchymal progenitor cells derived from traumatized muscle tissue, J Cell Mol Med 15(11) (2011) 2377-88.

[57] T. Gordon, The role of neurotrophic factors in nerve regeneration, Neurosurg Focus 26(2) (2009) E3.

[58] T. Gordon, K.M. Chan, O.A. Sulaiman, E. Udina, N. Amirjani, T.M. Brushart, Accelerating axon growth to overcome limitations in functional recovery after peripheral nerve injury, Neurosurgery 65(4 Suppl) (2009) A132-44.

[59] J. Xiao, T.J. Kilpatrick, S.S. Murray, The role of neurotrophins in the regulation of myelin development, Neurosignals 17(4) (2009) 265-76.

[60] Z. Tang, A. Wang, F. Yuan, Z. Yan, B. Liu, J.S. Chu, J.A. Helms, S. Li, Differentiation of multipotent vascular stem cells contributes to vascular diseases, Nat Commun 3 (2012) 875.

[61] G. Keilhoff, F. Stang, A. Goihl, G. Wolf, H. Fansa, Transdifferentiated mesenchymal stem cells as alternative therapy in supporting nerve regeneration and myelination, Cell Mol Neurobiol 26(7-8) (2006) 1235-52.

[62] V.T. Ribeiro-Resende, P.M. Pimentel-Coelho, L.A. Mesentier-Louro, R.M. Mendez, J.P. Mello-Silva, M.C. Cabral-da-Silva, F.G. de Mello, R.A. de Melo Reis, R. Mendez-Otero, Trophic activity derived from bone marrow mononuclear cells increases peripheral nerve regeneration by acting on both neuronal and glial cell populations, Neuroscience 159(2) (2009) 540-9.

[63] H.C. Pan, F.C. Cheng, C.J. Chen, S.Z. Lai, C.W. Lee, D.Y. Yang, M.H. Chang,

S.P. Ho, Post-injury regeneration in rat sciatic nerve facilitated by neurotrophic factors secreted by amniotic fluid mesenchymal stem cells, J Clin Neurosci 14(11) (2007) 1089-98.

[64] P. Bossolasco, L. Cova, C. Calzarossa, S.G. Rimoldi, C. Borsotti, G.L. Deliliers, V. Silani, D. Soligo, E. Polli, Neuro-glial differentiation of human bone marrow stem cells in vitro, Exp Neurol 193(2) (2005) 312-25.

[65] M. Brohlin, D. Mahay, L.N. Novikov, G. Terenghi, M. Wiberg, S.G. Shawcross, L.N. Novikova, Characterisation of human mesenchymal stem cells following differentiation into Schwann cell-like cells, Neurosci Res 64(1) (2009) 41-9.

[66] D. Mahay, G. Terenghi, S.G. Shawcross, Growth factors in mesenchymal stem cells following glial-cell differentiation, Biotechnol Appl Biochem 51(Pt 4) (2008) 167-76.

[67] M.W. Amoroso, G.F. Croft, D.J. Williams, S. O'Keeffe, M.A. Carrasco, A.R. Davis, L. Roybon, D.H. Oakley, T. Maniatis, C.E. Henderson, H. Wichterle, Accelerated high-yield generation of limb-innervating motor neurons from human stem cells, J Neurosci 33(2) (2013) 574-86.

[68] W.M. Jackson, A.B. Aragon, J.D. Bulken-Hoover, L.J. Nesti, R.S. Tuan, Putative heterotopic ossification progenitor cells derived from traumatized muscle, J Orthop Res 27(12) (2009) 1645-51.

[69] Y.L. Tang, Q. Zhao, Y.C. Zhang, L. Cheng, M. Liu, J. Shi, Y.Z. Yang, C. Pan, J. Ge, M.I. Phillips, Autologous mesenchymal stem cell transplantation induce VEGF and neovascularization in ischemic myocardium, Regul Pept 117(1) (2004) 3-10.

[70] M. Nagano, H. Suzuki, Quantitative analyses of expression of GDNF and neurotrophins during postnatal development in rat skeletal muscles, Neurosci Res 45(4) (2003) 391-9.

[71] A.J. Geddes, H.E. Angka, K.A. Davies, B. Kablar, Subpopulations of motor and sensory neurons respond differently to brain-derived neurotrophic factor depending

on the presence of the skeletal muscle, Dev Dyn 235(8) (2006) 2175-84.

[72] G.K. Hansson, Inflammation, atherosclerosis, and coronary artery disease, N Engl J Med 352(16) (2005) 1685-95.

[73] P. Libby, Inflammation in atherosclerosis, Nature 420(6917) (2002) 868-74.

[74] R. Ross, Atherosclerosis--an inflammatory disease, N Engl J Med 340(2) (1999) 115-26.

[75] P.L. Weissberg, G.J. Clesham, M.R. Bennett, Is vascular smooth muscle cell proliferation beneficial?, Lancet 347(8997) (1996) 305-7.

[76] R. Ross, The pathogenesis of atherosclerosis--an update, N Engl J Med 314(8) (1986) 488-500.

[77] J.H. Campbell, G.R. Campbell, The role of smooth muscle cells in atherosclerosis, Curr Opin Lipidol 5(5) (1994) 323-30.

[78] D. Gomez, L.S. Shankman, A.T. Nguyen, G.K. Owens, Detection of histone modifications at specific gene loci in single cells in histological sections, Nat Methods 10(2) (2013) 171-7.

[79] L.S. Shankman, D. Gomez, O.A. Cherepanova, M. Salmon, G.F. Alencar, R.M. Haskins, P. Swiatlowska, A.A. Newman, E.S. Greene, A.C. Straub, B. Isakson, G.J. Randolph, G.K. Owens, KLF4-dependent phenotypic modulation of smooth muscle cells has a key role in atherosclerotic plaque pathogenesis, Nat Med 21(6) (2015) 628-37.

[80] M. Aikawa, P.N. Sivam, M. Kuro-o, K. Kimura, K. Nakahara, S. Takewaki, M. Ueda, H. Yamaguchi, Y. Yazaki, M. Periasamy, et al., Human smooth muscle myosin heavy chain isoforms as molecular markers for vascular development and atherosclerosis, Circ Res 73(6) (1993) 1000-12.

[81] P. Lacolley, V. Regnault, A. Nicoletti, Z. Li, J.B. Michel, The vascular smooth

muscle cell in arterial pathology: a cell that can take on multiple roles, Cardiovasc Res 95(2) (2012) 194-204.

[82] D. Gomez, G.K. Owens, Smooth muscle cell phenotypic switching in atherosclerosis, Cardiovasc Res 95(2) (2012) 156-64.

[83] R.R. Pauly, A. Passaniti, M. Crow, J.L. Kinsella, N. Papadopoulos, R. Monticone, E.G. Lakatta, G.R. Martin, Experimental models that mimic the differentiation and dedifferentiation of vascular cells, Circulation 86(6 Suppl) (1992) III68-73.

[84] S.S. Rensen, P.A. Doevendans, G.J. van Eys, Regulation and characteristics of vascular smooth muscle cell phenotypic diversity, Neth Heart J 15(3) (2007) 100-8.

[85] T. Yoshida, G.K. Owens, Molecular determinants of vascular smooth muscle cell diversity, Circ Res 96(3) (2005) 280-91.

[86] N.M. Caplice, T.J. Bunch, P.G. Stalboerger, S. Wang, D. Simper, D.V. Miller, S.J. Russell, M.R. Litzow, W.D. Edwards, Smooth muscle cells in human coronary atherosclerosis can originate from cells administered at marrow transplantation, Proc Natl Acad Sci U S A 100(8) (2003) 4754-9.

[87] J.F. Bentzon, C. Weile, C.S. Sondergaard, J. Hindkjaer, M. Kassem, E. Falk, Smooth muscle cells in atherosclerosis originate from the local vessel wall and not circulating progenitor cells in ApoE knockout mice, Arterioscler Thromb Vasc Biol 26(12) (2006) 2696-702.

[88] H. Iwata, I. Manabe, K. Fujiu, T. Yamamoto, N. Takeda, K. Eguchi, A. Furuya, M. Kuro-o, M. Sata, R. Nagai, Bone marrow-derived cells contribute to vascular inflammation but do not differentiate into smooth muscle cell lineages, Circulation 122(20) (2010) 2048-57.

[89] M. Sata, A. Saiura, A. Kunisato, A. Tojo, S. Okada, T. Tokuhisa, H. Hirai, M. Makuuchi, Y. Hirata, R. Nagai, Hematopoietic stem cells differentiate into vascular cells that participate in the pathogenesis of atherosclerosis, Nat Med 8(4) (2002) 403-9.

[90] Y. Tintut, Z. Alfonso, T. Saini, K. Radcliff, K. Watson, K. Bostrom, L.L. Demer, Multilineage potential of cells from the artery wall, Circulation 108(20) (2003) 2505-10.

[91] M.Y. Speer, H.Y. Yang, T. Brabb, E. Leaf, A. Look, W.L. Lin, A. Frutkin, D. Dichek, C.M. Giachelli, Smooth muscle cells give rise to osteochondrogenic precursors and chondrocytes in calcifying arteries, Circ Res 104(6) (2009) 733-41.

[92] M. Crisan, S. Yap, L. Casteilla, C.W. Chen, M. Corselli, T.S. Park, G. Andriolo, B. Sun, B. Zheng, L. Zhang, C. Norotte, P.N. Teng, J. Traas, R. Schugar, B.M. Deasy, S. Badylak, H.J. Buhring, J.P. Giacobino, L. Lazzari, J. Huard, B. Peault, A perivascular origin for mesenchymal stem cells in multiple human organs, Cell Stem Cell 3(3) (2008) 301-13.

[93] D. Medici, E.M. Shore, V.Y. Lounev, F.S. Kaplan, R. Kalluri, B.R. Olsen, Conversion of vascular endothelial cells into multipotent stem-like cells, Nat Med 16(12) (2010) 1400-6.

[94] Y. Hu, Z. Zhang, E. Torsney, A.R. Afzal, F. Davison, B. Metzler, Q. Xu, Abundant progenitor cells in the adventitia contribute to atherosclerosis of vein grafts in ApoE-deficient mice, J Clin Invest 113(9) (2004) 1258-65.

[95] Y. Chen, M.M. Wong, P. Campagnolo, R. Simpson, B. Winkler, A. Margariti, Y. Hu, Q. Xu, Adventitial stem cells in vein grafts display multilineage potential that contributes to neointimal formation, Arterioscler Thromb Vasc Biol 33(8) (2013) 1844-51.

[96] A.N. Orekhov, Karpova, II, V.V. Tertov, S.A. Rudchenko, E.R. Andreeva, A.V. Krushinsky, V.N. Smirnov, Cellular composition of atherosclerotic and uninvolved human aortic subendothelial intima. Light-microscopic study of dissociated aortic cells, Am J Pathol 115(1) (1984) 17-24.

[97] A.N. Orekhov, E.R. Andreeva, A.V. Krushinsky, I.D. Novikov, V.V. Tertov, G.V. Nestaiko, A. Khashimov Kh, V.S. Repin, V.N. Smirnov, Intimal cells and

atherosclerosis. Relationship between the number of intimal cells and major manifestations of atherosclerosis in the human aorta, Am J Pathol 125(2) (1986) 402-15.

[98] E.R. Andreeva, I.M. Pugach, A.N. Orekhov, Subendothelial smooth muscle cells of human aorta express macrophage antigen in situ and in vitro, Atherosclerosis 135(1) (1997) 19-27.

[99] O.A. Cherepanova, D. Gomez, L.S. Shankman, P. Swiatlowska, J. Williams, O.F. Sarmento, G.F. Alencar, D.L. Hess, M.H. Bevard, E.S. Greene, M. Murgai, S.D. Turner, Y.J. Geng, S. Bekiranov, J.J. Connelly, A. Tomilin, G.K. Owens, Activation of the pluripotency factor OCT4 in smooth muscle cells is atheroprotective, Nat Med 22(6) (2016) 657-65.

[100] A.A. Geisterfer, M.J. Peach, G.K. Owens, Angiotensin II induces hypertrophy, not hyperplasia, of cultured rat aortic smooth muscle cells, Circ Res 62(4) (1988) 749-56.

[101] G. Li, S.J. Chen, S. Oparil, Y.F. Chen, J.A. Thompson, Direct in vivo evidence demonstrating neointimal migration of adventitial fibroblasts after balloon injury of rat carotid arteries, Circulation 101(12) (2000) 1362-5.

[102] H. De Leon, J.D. Ollerenshaw, K.K. Griendling, J.N. Wilcox, Adventitial cells do not contribute to neointimal mass after balloon angioplasty of the rat common carotid artery, Circulation 104(14) (2001) 1591-3.